



Study Report

SR360 [2018]

Vertical external fire spread from flames extending out of an opening

Kevin Frank, Haejun Park, Greg Baker and Colleen Wade





1222 Moonshine Rd
RD1, Porirua 5381
Private Bag 50 908
Porirua 5240
New Zealand
branz.nz



The work reported here was funded by BRANZ from the
Building Research Levy.

© BRANZ 2018
ISSN: 1179-6197



Preface

This report has been prepared as part of a research project on limiting fire spread by design where the subproject investigates the basis of external fire spread due to flames projecting out of a wall opening in an enclosure.

Vertical external fire spread from flames extending out of an opening

BRANZ Study Report SR360

Authors

Kevin Frank, Haejun Park, Greg Baker and Colleen Wade

Reference

Frank, K., Park, H., Baker, G. & Wade, C. (2018). *Vertical external fire spread from flames extending out of an opening*. BRANZ Study Report SR460. Judgeford, New Zealand: BRANZ Ltd.

Abstract

A series of reduced-scale fire experiments have been conducted to better understand the phenomena of flames projected from a single compartment opening, which can lead to vertical fire spread up a building exterior. Although there are several correlations and experimental data available to predict the projected flame heights, there exist some differences in the predicted flame heights. Correlations to estimate the heat fluxes above the opening are relatively limited.

In the current study, using heptane and wood cribs as fire fuels, the effects of variables such as opening location, fuel location, fuel type and fuel surface area on the projected flame phenomena are investigated. Correlations to calculate the projected flame heights and heat flux on the wall above the opening are developed, and recommendations are made for design practices. Relevant aspects of the C/VM2 Verification Method and New Zealand Acceptable Solutions are evaluated using the New Zealand Building Code heat flux criteria.

Keywords

Combustion, vertical fire spread, projected flame height, incident heat flux, external walls, façades, fire experiments.

Contents

| | | |
|-----------|---|-----------|
| 1. | INTRODUCTION | 1 |
| 2. | RELEVANCE TO FIRE SAFETY DESIGN | 3 |
| 2.1 | Building Code clauses | 3 |
| 2.2 | C/ASx Acceptable Solutions | 4 |
| 2.3 | C/VM2 Verification Method | 4 |
| 2.3.1 | Fire spread up façade surfaces..... | 4 |
| 2.3.2 | External fire spread via openings and unprotected areas..... | 4 |
| 2.4 | Modelling external fire plume characteristics | 5 |
| 3. | LITERATURE REVIEW | 6 |
| 3.1 | Ventilation-limited burning and pyrolysis in a compartment..... | 6 |
| 3.1.1 | Bullen and Thomas | 7 |
| 3.1.2 | Law | 7 |
| 3.1.3 | Drysdale | 9 |
| 3.2 | Projected flame height..... | 9 |
| 3.2.1 | Yokoi | 10 |
| 3.2.2 | Thomas | 11 |
| 3.2.3 | Law | 14 |
| 3.2.4 | Quintiere and Cleary | 14 |
| 3.2.5 | Ohmiya et al. | 15 |
| 3.2.6 | Delichatsios et al. | 16 |
| 3.2.7 | Summary of simple flame height correlations | 18 |
| 3.2.8 | Mizuno and Kawagoe | 19 |
| 3.3 | Heat flux from external flame..... | 21 |
| 3.3.1 | NRCC façade experiments | 21 |
| 3.3.2 | Delichatsios et al. | 22 |
| 3.3.3 | Yoshioka et al..... | 23 |
| 3.3.4 | Back et al..... | 24 |
| 3.3.5 | Law | 26 |
| 3.3.6 | Abecassis Empis | 28 |
| 4. | MODELLING HEAT TRANSFER FROM FLAMES WITH FDS | 29 |
| 4.1 | Heat release rate, flame height and flame profile | 29 |
| 4.2 | Heat flux to targets | 31 |
| 4.3 | Heat flux on walls from adjacent flames | 32 |
| 4.4 | Heat flux on external walls from flames projecting from openings | 32 |
| 4.5 | Effects of aprons on heat flux on external walls from flames projecting from openings | 34 |
| 5. | EXPERIMENTAL STUDY | 35 |
| 5.1 | Compartment configuration and instrumentation..... | 35 |
| 5.2 | Experimental program | 38 |
| 5.2.1 | Opening location in the front panel | 38 |
| 5.2.2 | Fuel..... | 38 |
| 5.2.3 | Test matrix | 41 |
| 5.3 | Flame height measurement..... | 41 |

| | |
|---|-----------|
| 5.4 Incident heat flux measurement | 41 |
| 6. EXPERIMENTAL RESULTS..... | 44 |
| 6.1 Heat release and mass loss rates..... | 44 |
| 6.1.1 Comparison to free-burning heat release rate..... | 45 |
| 6.1.2 Comparison to the theoretical ventilation-limited heat release rate | 45 |
| 6.2 External flame heights | 48 |
| 6.2.1 Opening and fire location | 48 |
| 6.2.2 Opening configuration and size | 48 |
| 6.3 Heat flux on the external vertical wall above the opening | 48 |
| 6.4 Apron experiments | 50 |
| 7. MODELLING RADIATION TO EXTERNAL WALLS FROM EXPERIMENTAL WALL OPENING FIRE PLUMES USING FDS..... | 53 |
| 7.1 FDS modelling of reduced-scale experiments | 53 |
| 7.2 Additional FDS comparisons based on NRCC façade data | 57 |
| 7.2.1 Heat release rates..... | 57 |
| 7.2.2 Flame heights..... | 58 |
| 7.2.3 Heat flux to the external wall..... | 58 |
| 7.2.4 NRCC façade experiments with aprons | 58 |
| 8. BENCHMARKING EXISTING TOOLS WITH EXPERIMENTAL DATA | 59 |
| 8.1 Heat release rate..... | 59 |
| 8.1.1 Comparison of the C/VM2 heat release rate design fire criteria to experimental results..... | 59 |
| 8.1.2 Ability of FDS to model heat release rate | 59 |
| 8.2 Flame height..... | 59 |
| 8.2.1 Correlation comparisons to reduced-scale experiments | 60 |
| 8.2.2 Correlation comparisons to NRCC façade experimental data | 62 |
| 8.2.3 FDS comparisons to NRCC façade experimental data | 63 |
| 8.3 Estimation of incident heat flux on the vertical wall | 63 |
| 8.3.1 Back et al. and Delichatsios et al. correlations comparison to reduced-scale experiments (no apron)..... | 63 |
| 8.3.2 Back et al., Delichatsios et al. and Law peak heat flux predictions. | 65 |
| 8.3.3 Abecassis Empis correlation comparison to reduced-scale experiments | 68 |
| 8.3.4 Back et al. and Delichatsios et al. correlations comparison to NRCC façade experiments..... | 70 |
| 8.3.5 Abecassis Empis correlation comparison to NRCC façade experiments | 70 |
| 8.4 Apron heat flux comparison..... | 71 |
| 8.4.1 Heat flux correlation comparison to reduced-scale apron experiments | 71 |
| 8.4.2 NRCC façade apron experiments FDS heat flux comparison | 71 |
| 9. EXTERNAL FLAME PROJECTION DESIGN GUIDELINES | 73 |
| 9.1 Design fire heat release rate input | 73 |
| 9.2 Openings..... | 73 |
| 9.3 Estimating projected flame height..... | 73 |

| | |
|---|------------|
| 9.4 Estimating maximum heat flux incident on a wall above a projected flame | 73 |
| 9.5 Evaluation of Acceptable Solution spandrel and apron requirements | 74 |
| 10. CONCLUSIONS | 77 |
| 11. FUTURE WORK | 79 |
| REFERENCES | 80 |
| APPENDIX A: HEAT FLUX METER CALIBRATION..... | 83 |
| APPENDIX B: INCIDENT HEAT FLUX MEASUREMENT | 88 |
| APPENDIX C: MASS FLOW RATE CALCULATION | 90 |
| APPENDIX D: HEAT RELEASE RATES AND FLAME HEIGHTS..... | 92 |
| APPENDIX E: EXTERNAL WALL HEAT FLUX | 95 |
| APPENDIX F: COMPARTMENT TEMPERATURES..... | 98 |
| APPENDIX G: COMPARTMENT HEAT FLUX | 105 |
| APPENDIX H: NEUTRAL PLANE HEIGHTS..... | 108 |
| APPENDIX I: TEMPERATURES AT THE OPENING..... | 111 |
| APPENDIX J: FLAME HEIGHT ESTIMATION | 114 |

Figures

| | |
|---|----|
| Figure 1. Flames projecting from a window during the 2005 Bracken Court fire in Dunedin. | 1 |
| Figure 2. Data used to develop Law and O'Brien's correlation for maximum ventilation-limited burning rate (Law, 1978). | 8 |
| Figure 3. Ratio of the maximum heat release rate from Law (1978) to the ventilation-controlled heat release rate from Kawagoe (1958). | 9 |
| Figure 4. Schematic diagram of flame height. | 9 |
| Figure 5. Correlation reproduced from Yokoi's (1960) experimental results..... | 11 |
| Figure 6. Data and correlation for flame height (Ohmiya et al., 2000, p. 382)..... | 16 |
| Figure 7. Flame height for dimensionless heat release rate < 1.3 (Lee et al., 2008)... | 17 |
| Figure 8. Flame height for dimensionless heat release rate ≥ 1.3 (Lee et al., 2008)... | 17 |
| Figure 9. Section view of the projected flame and opening. | 19 |
| Figure 10. Heat flux data for various apron depths. Data is relative to readings at 1 m above opening with no projection (Oleszkiewicz, 1991). | 22 |
| Figure 11. Heat flux on an opposing wall above an opening (Lee et al., 2009)..... | 22 |
| Figure 12. Incident heat flux profile for 2.6 MW heptane fire..... | 24 |
| Figure 13. Measured incident heat fluxes (Back et al., 1994)..... | 26 |
| Figure 14. Flame geometry from Law (1978): no through draft, single opening. | 28 |
| Figure 15. FDS heat release rate verification for 1 m x 1 m propane fires (McGrattan et al., 2016). | 30 |
| Figure 16. Comparison of flame heights from FDS to several correlations (McGrattan et al., 2016). | 30 |
| Figure 17. Comparison of FDS flame profile to experimental data (McGrattan et al., 2016)..... | 31 |
| Figure 18. Selected results from FDS heat flux comparisons to Fleury's experimental data (McGrattan et al., 2016)..... | 31 |

Figure 19. Scatterplot of FDS predicted heat flux values to targets compared to experimental measurements (McGrattan et al., 2016).32

Figure 20. Selections from FDS heat flux comparisons to experimentally measured wall heat flux by NRL/HAI (Back et al.) (McGrattan et al., 2016).32

Figure 21. Selected comparisons of FDS results to the NRCC façade experimental data (McGrattan et al., 2016).33

Figure 22. Scatterplot of FDS predicted heat flux to walls, ceilings and floors compared to experimental measurements including NRL/HAI (Back et al.) and NRCC façade data (McGrattan et al., 2016).33

Figure 23. Compartment configuration and instrumentation.35

Figure 24. Heat flux meter locations (front elevation view).36

Figure 25. Section view of the fuel bed.37

Figure 26. Plan view of the compartment.37

Figure 27. Location of opening in front wall.38

Figure 28. Section view of a heptane pan and a retention pan.39

Figure 29. Free-burning heat release rate of a 2L heptane fire in a 300 mm by 300 mm pan. 39

Figure 30. Wood crib configuration.40

Figure 31. Free-burning heat release rate of the wood crib shown in Figure 30.40

Figure 32. Flame region identification.43

Figure 33. A side view of the plate heat flux meter.....43

Figure 34. Flame height and heat release rate for experiment H-500-214-B-3L.....44

Figure 35. Flame height and heat release rate compared for experiments: (a) H-M-F-2L; (b) W-M-F.....45

Figure 36. The flame height and heat release rate compared for experiments where the maximum HRR-O2 exceeded 150% of the ventilation-limited heat release rate.46

Figure 37. The flame height and heat release rate compared for heptane pool experiments where the maximum heat release rate did not exceed 150% of the ventilation-limited heat release rate and comparative small heptane pool experiments.47

Figure 38. External wall heat flux levels for experiments without projected flames on the vertical panel.49

Figure 39. External wall heat flux levels for experiment W-T-B. A small external flame was observed for a short period of time just before 1000 s.....49

Figure 40. External wall heat flux levels for experiments using the 300 mm square opening with large projected flames on the vertical panel.....49

Figure 41. The flame height and heat release rate compared between the non-apron and apron experiments.....50

Figure 42. Representative flame images from maximum flame heights.51

Figure 43. External wall heat fluxes measured in the apron and no-apron experiments.52

Figure 44. Initial FDS computational domain for simulating the experiments in this study.53

Figure 45. Comparison of the heat release rate from the H-M-F-2L experiment with the FDS simulation.....54

Figure 46. Comparison of the heat release rate from a free-burning 300 mm by 300 mm heptane pool experiment with the FDS simulation.54

Figure 47. Comparison of heat release rate output from FDS with an input ramp HRRPUA based on the heat release rate measured experimentally by the calorimeter.55

Figure 48. Comparison of FDS heat release rate output with a specified HRRPUA ramp with and without a compartment to experimental results.....55

Figure 49. Reduced computational domain.56

Figure 50. Comparison of FDS output for a constant 150 kW HRRPUA fire specification to the experimental heat release rate.57

Figure 51. FDS heat release rate output for four coarse grid simulations of the NRCC façade experiment using the third window configuration and a nominal heat release rate of 6.9 MW.58

Figure 52. Comparison of estimated and measured maximum flame height for reduced-scale experiments (linear scale).....60

Figure 53. Comparison of estimated and measured maximum flame height for reduced-scale experiments (log-log scale). Equality and $\pm 25\%$ lines are shown.60

Figure 54. Comparison of flame heights for the H-M-F-2L and W-T-F experiment.61

Figure 55. Linear scale comparison of estimated and measured average flame height for NRCC façade experiments using simple correlations. Equality and $\pm 25\%$ lines are shown.....62

Figure 56. Log-log scale comparison of estimated and measured average flame height for NRCC façade experiments using simple correlations. Equality and $\pm 25\%$ lines are shown.....62

Figure 57. Comparison of estimated and measured average flame height for NRCC façade experiments using FDS. Equality and $\pm 25\%$ lines are shown.63

Figure 58. Comparison of Back et al. and Delichatsios et al. correlations to reduced-scale experiments with significant flaming and no aprons.64

Figure 59. Reduced-scale experimental comparisons to Back et al. and Delichatsios et al. for experiments, split by heat flux slope above flame tip.64

Figure 60. Peak heat flux experimental data and modified Back et al. correlation.....65

Figure 61. Comparison of modified Back et al., Delichatsios et al. and Law peak heat flux correlation predictions for the reduced-scale and NRCC façade experimental data (no aprons).66

Figure 62. Comparison of modified Back et al., Delichatsios et al. and Law peak heat flux correlation predictions for the reduced-scale and NRCC façade experimental data (no aprons, log-log scale).66

Figure 63. Back et al. and Delichatsios et al. correlation comparisons to reduced-scale data (no aprons) using 10-second interval measured heat release rates and flame heights.....67

Figure 64. Back et al. and Delichatsios et al. heat flux profile comparisons to reduced-scale data (no aprons) using the modified Back et al. peak heat flux correlation.....68

Figure 65. Comparison of Abecassis Empis correlation to average heat flux from reduced-scale experiments (no aprons).....69

Figure 66. Comparison of Abecassis Empis correlation to maximum heat flux from reduced-scale experiments (no aprons).....69

Figure 67. Abecassis Empis heat flux profile correlation compared to reduced-scale experimental data (no aprons).69

Figure 68. Comparison of Back et al. correlation to NRCC façade experiments.70

Figure 69. Comparison of Abecassis Empis correlation to NRCC façade experiments...70

Figure 70. Back et al. and Delichatsios et al. comparison to reduced-scale experimental data where aprons were used.71

Figure 71. FDS heat flux results comparisons to NRCC façade experiments with aprons.72

Figure 72. Cone and heat flux meter configuration.83

Figure 73. Section view of plate thermometer heat flux meter.....84

Figure 74. Conceptual discretisation of the ceramic fibre board.85

Figure 75. Energy balance of insulation surface node in contact with the Inconel plate.86

Figure 76. Incident radiative heat flux comparison with calculated heat flux components and estimated incident heat flux based on cone heater temperature.87

Figure 77. Various configurations of the plate heat flux meters in the test.....89

Figure 78. Vent flows (Karlsson & Quintiere, 2000).90

Figure 79. Heat release rates and flame heights for heptane fires with the standard 300 mm x 300 mm opening.....92

Figure 80. Heat release rates and flame heights for wood crib fires.93

Figure 81. Heat release rates and flame heights for heptane fires with non-standard opening sizes.....94

Figure 82. External wall heat flux for heptane fires with the standard 300 mm x 300 mm opening.95

Figure 83. External heat flux for wood crib fires.96

Figure 84. External heat flux for heptane fires with non-standard opening sizes.97

Figure 85. Front compartment temperatures for heptane fires with the standard 300 mm x 300 mm opening.....98

Figure 86. Front compartment temperatures for wood crib fires.99

Figure 87. Front compartment temperatures for heptane fires with non-standard opening sizes..... 100

Figure 88. Rear compartment temperatures for heptane fires with the standard 300 mm x 300 mm opening..... 101

Figure 89. Rear compartment temperatures for wood crib fires. 102

Figure 90. Rear compartment temperatures for heptane fires with non-standard opening sizes..... 103

Figure 91. Average room temperature with the top opening. 103

Figure 92. Average room temperature with the middle opening (heptane fires). 104

Figure 93. Average room temperature with the middle opening (wood crib fires)..... 104

Figure 94. Compartment heat flux for heptane fires with the standard 300 mm x 300 mm opening. 105

Figure 95. Compartment heat flux for wood crib fires. 106

Figure 96. Compartment heat flux for heptane fires with non-standard opening sizes. 107

Figure 97. Neutral plane heights for heptane fires with the standard 300 mm x 300 mm opening..... 108

Figure 98. Neutral plane heights for wood crib fires. 109

Figure 99. Neutral plane heights for heptane fires with non-standard opening sizes. 110

Figure 100. Opening temperatures for heptane fires with the standard 300 mm x 300 mm opening. 111

Figure 101. Opening temperatures for wood crib fires. 112

Figure 102. Opening temperatures for heptane fires with non-standard opening sizes. 113

Figure 103. Flame height estimation (heptane). 114

Figure 104. Flame height estimation (wood crib). 115

Figure 105. Flame height estimation for heptane fires with non-standard opening sizes. 116

Tables

Table 1. Summary of flame height correlations. 18

Table 2. NRCC façade experiment summarised data (Oleszkiewicz, 1989) and experimental flame heights reported by Quintiere and Cleary (1994). 21

Table 3. Heat flux values (kW/m²) at various locations above the opening. 23

Table 4. Test conditions and flame heights from Back et al. (1994). 25

Table 5. Physical and thermal properties of compartment materials. 35

Table 6. Thermal properties of heptane and wood cribs. 38

Table 7. Test matrix. 42

Table 8. Ratio of maximum heat release rate (measured by calorimetry) to the ventilation-limited heat release rate for reduced-scale experiments. 46

Table 9. Summary of qualitative comparisons between experimental flames and correlation estimates. 61

Table 10. Evaluation of New Zealand Acceptable Solution spandrel criteria using the Abecassis Empis correlation. 74

Table 11. Evaluation of New Zealand Acceptable Solution spandrel criteria using the 150% ventilation-limited heat release rate criteria and recommended flame height and heat flux correlations. 75

Table 12. Fire sizes predicted to cause heat flux criteria to be reached at the New Zealand Acceptable Solution spandrel criteria (1.5 m) using recommended flame height and heat flux correlations. 75

Table 13. Evaluation of New Zealand Acceptable Solution apron criteria using the 150% ventilation-limited heat release rate criteria and recommended flame height and heat flux correlations. 76

1. Introduction

Compartment fires in buildings have the potential to breach unprotected openings in the building exterior and cause fire to spread up the outside of the building. There are two mechanisms for external vertical fire spread: flame spread on the exterior following ignition of the building exterior cladding surface by the buoyant fire products and the fire igniting materials in the building interior on an upper level through an unprotected opening. An example of flames projecting from a window during the 2005 Bracken Court fire in Dunedin is shown in Figure 1.



Reproduced with permission from 111 Emergency www.111emergency.co.nz.

Figure 1. Flames projecting from a window during the 2005 Bracken Court fire in Dunedin.

Current building fire safety design requirements take the risk of exterior vertical fire spread from internal fires into consideration through prescriptive requirements for the exterior surface specification and geometry, active fire suppression systems or by calculating the effect of radiation from fire plumes projected from openings in the building. Justification for the prescriptive requirements is unclear, and methods and inputs for fire plume radiation estimation are not clarified. This report examines methods and inputs for estimating radiation from fire plumes projected from wall openings and the prescriptive requirements for preventing exterior vertical fire spread.

The current study focuses on the flame projection phenomena through a wall opening in an enclosure. Projected flame heights and heat flux levels on a wall above the opening are discussed with an emphasis on the potential for fire to spread to upper levels in a building. Only no-through-draft conditions are considered, with a single compartment and a single exterior opening. Through-draft or forced-draft conditions are not included.

Previous research at BRANZ includes a literature review aimed at developing an understanding of the factors influencing external thermal exposures and the potential

for external horizontal and vertical fire spread (Collier, 2015). This report gives a more detailed description and analysis of existing correlations in the literature for determining the height of external flames. It also describes a series of intermediate-scale fire experiments using non-gas burner fuels so that projected flame heights could be compared to the existing correlations. The data from these experiments is intended to be used for:

- improving current correlations for external flame height for engineering purposes
- validation and benchmarking of a fire model for predicting the combustion environment within and external to an enclosure.

2. Relevance to fire safety design

Vertical and horizontal external fire spread is addressed in the New Zealand building regulations in the C/ASx Acceptable Solutions (where x is a number from 1 to 6, with each document relating to specific occupancies) and the C/VM2 Verification Method.

2.1 Building Code clauses

Building Code clauses C3.2 and C3.3 provide the functional requirements to address vertical fire spread to upper floors where sleeping occupancies and other property are located.

Clause C3.2 states:

Buildings with a building height greater than 10 m where upper floors contain sleeping uses or other property must be designed and constructed so that there is a low probability of external vertical fire spread to upper floors in the building.

Clause C3.3 states:

Buildings must be designed and constructed so that there is a low probability of fire spread to other property vertically or horizontally across a relevant boundary.

Clause C3.5 addresses vertical fire spread over the external façade and states:

Buildings must be designed and constructed so that fire does not spread more than 3.5 m vertically from the fire source over the external cladding of multi-level buildings.

There are no other performance criteria clauses in the Building Code that directly address the mechanism of fire spread to upper floors of a building. While they do not address vertical fire spread specifically, the requirements of clauses C3.6 and C3.7 are useful for identifying acceptable levels of heat flux on external walls.

Clause 3.6 describes the amount of radiation that is acceptable to be incident on surfaces both on and 1 metre beyond the relevant property boundary. It states that:

... buildings must be designed and constructed so that in the event of fire in the building the received radiation at the relevant boundary of the property does not exceed 30 kW/m² and at a distance of 1 m beyond the relevant boundary of the property does not exceed 16 kW/m².

Additionally, clause 3.7 provides requirements for the external wall materials when they are within 1 metre of the relevant property boundary. If external walls fall within this criterion, they can either be of non-combustible construction or their materials must not ignite when subjected to a radiant flux of 30 kW/m² for 30 minutes for importance level 3 and 4 buildings or 15 minutes for importance level 1 and 2 buildings.

The C/VM2 commentary provides additional explanation that C3.7 does not "restrict the ignitability" of external wall materials "beyond 1.0 m across the relevant

boundary". It notes that, while some materials may ignite below 16 kW/m^2 , it is anticipated that Fire Service intervention will assist in preventing fire spread.

2.2 C/ASx Acceptable Solutions

Section 5.7 of the C/ASx Acceptable Solutions addresses vertical fire spread. The C/ASx Acceptable Solutions for fire address external vertical fire spread through unprotected areas for the following cases: unsprinklered firecells containing sleeping risk groups or exitways with an escape height of 4.0 m or more or where firecells with other property are located one above the other.

External vertical fire spread through unprotected areas is managed by specifying either aprons, spandrels, or a checkerboard pattern for the arrangement of openings. Acceptable combinations of apron projection and spandrel heights are given, as discussed in Collier (2015). Aprons and spandrels are required to have fire resistance ratings no less than the floor separating upper and lower firecells, with spandrels being rated from both sides and aprons only being rated from the underside.

Vertical flame spread involving combustible exterior surfaces is addressed in section 5.8 of the C/ASx documents by one of two methods:

- Specifying the allowable maximum heat release rate and maximum total heat release of the cladding material.
- Cladding systems comprised of only materials that are individually classified as non-combustible.

Thin surface finishes 1 mm or less applied to a non-combustible substrate are also acceptable.

2.3 C/VM2 Verification Method

Vertical fire spread requirements of C/VM2 are covered in Design Scenario VS (Vertical Spread). They can be satisfied using the methods in the C/ASx Acceptable Solutions, and the Verification Method also allows for more fundamental analysis-based approaches.

2.3.1 Fire spread up façade surfaces

A design fire radiant flux is specified for fire spread up façade surfaces for multi-level buildings greater than 10 m in height with upper floors containing sleeping uses or other property. The design radiant flux, evaluated at the façade surface, is either 50 kW/m^2 for importance level 2 and 3 buildings or 90 kW/m^2 for importance level 4 buildings. The design radiant flux duration is 15 minutes.

The effects of the design fire are evaluated by either limiting the maximum heat release rate contribution from the cladding materials using a small-scale fire test or limiting the extent of vertical flame spread to less than 3.5 m above the fire source using a large-scale fire test. Cladding systems comprised of only materials that are individually classified as non-combustible are also acceptable.

2.3.2 External fire spread via openings and unprotected areas

For external vertical fire spread via openings and unprotected areas, C/VM2 states that the:

... design fire exposure is a fire plume projecting from openings or unprotected areas in the external wall, with characteristics determined from the design fire as described in Part 2 for the applicable occupancy”

The intention is stated as preventing:

... fire spread in unsprinklered buildings from projecting fire plumes to unprotected areas on upper floors where they are within 1.5 m vertically of a projecting plume fire source.

The intention can be achieved by either sprinklering or placing fire-rated construction on the external building surface to prevent a building opening fire plume from “re-entering the building via an opening or unprotected area at a higher level”.

Methods of achieving this outcome include following the C/ASx required construction features (apron, spandrels and/or checkerboard pattern) or calculating:

... the effect of radiation from fire plumes projected from openings. Fire plume characteristics and geometry shall be derived from the design fires as described in Part 2 for the applicable geometry.

C/VM2 considers five cases for fires once the end of the growth phase is reached:

1. A fuel-limited fire that does not reach flashover (deemed to occur when the upper layer temperature reaches 500°C).
2. A sprinkler-controlled fire.
3. Flashover is achieved (the heat release rate is ramped up to peak over 15 s), but there is sufficient ventilation in the compartment to allow free burning in the compartment at the peak heat release rate.
4. Flashover is achieved, and the fire is ventilation limited (not enough air in the compartment to allow the fuel to fully combust at the peak heat release rate).
5. The fire is ventilation limited before flashover is achieved.

Cases 1, 2 and 3 are not likely to result in significant external flaming since there is enough air in the compartment to allow the fuel to combust within the compartment. For cases 4 and 5, the heat release rate is ramped up to 1.5 times the ventilation limit based on compartment geometry. This means that at least one-third of the total heat release rate burns when it is mixed with air outside of the compartment.

The fire is allowed to continue until the energy content of the room based on the fire load energy density (FLED) is consumed.

2.4 Modelling external fire plume characteristics

C/VM2 does not provide guidance on characterising the fire plumes projected from openings as discussed above. The goal of this research is to provide such guidance. Ultimately, the thermal conditions on the exterior of the building features above and adjacent to the external flaming is the desired outcome, which would then be used to look at either ignition of the exterior surface or degradation over time of fire-rated exterior walls. In order to achieve this outcome, intermediate parameters such as the heat release rate inside and outside of ventilation-limited compartments and the resulting fire plume geometry and characteristics are likely required.

Several attempts have been made and documented in existing literature to address these aspects and are reviewed in the following chapter.

3. Literature review

External flame extension from a compartment opening has been studied for more than 50 years. In the 1960s, Thomas (1961), Seigel (1969) and Yokoi (1960) conducted various experiments exploring the temperature profile and height of external flames. Subsequently, Thomas and Law (1972) developed a simple correlation that could estimate the external flame height for a given compartment and opening configuration. Due to simplicity, the Thomas and Law correlation has been widely used, but several fire incidents such as the fire incident at Bouwkunde, The Netherlands, have occurred where significantly taller external flames were observed (Park, Meacham, Dembsey & Goulthorpe, 2014). Since 2000, this topic has been revisited by various researchers mainly in the UK and Japan in association with the development of ISO 13785-1:2002 *Reaction-to-fire tests for façades – Part 1: Intermediate-scale test*. In this more recent research, external flames were treated independently like an imaginary fire source outside the compartment. Complicated phenomena such as fuel pyrolysis and combustion in the fire compartment were assumed to be obtained separately. Examples of previous research outcomes are reviewed and compared briefly below.

3.1 Ventilation-limited burning and pyrolysis in a compartment

External flames (or the visible fuel vapour-air combustion reaction zone) from a compartment opening are observed when there is insufficient air, fuel-air mixing and/or reacting mixture transport time within the compartment for the visible combustion reaction to take place fully within the compartment. The common term for the first case is ventilation-limited burning, which, for typical solid or liquid fuels, occurs when there is an excess of fuel vapour created through either pyrolysis or vaporisation, respectively, than can burn given the amount of oxidiser (air) entering the compartment through openings. Work done by Kawagoe (1958) empirically determined a ventilation factor that described the amount of air that can enter an opening in a compartment in fire conditions under natural fire flows:

$$\dot{m}_{air} = 0.5A_o\sqrt{H_o} \quad \text{Eqn. 1}$$

Where:

A_o = opening area, m²

H_o = opening height, m

This result has also been confirmed through derivation from the Bernoulli equation (Drysdale, 1998), albeit with many simplifying assumptions made. It has been noted that combustion energy produced is 3 MJ/kg of air (13.1 MJ/kg of O₂) (Thornton, 1917) and is nearly constant for hydrocarbon-based fuel sources. Combining this with the ventilation factor for airflow into the compartment yields the following equation for estimating the maximum heat release rate inside a compartment when a fire has reached steady burning conditions:

$$\dot{Q}_{vent} = 1500 A_o\sqrt{H_o} \quad \text{Eqn. 2}$$

In Eqn. 2, \dot{Q}_{vent} is the ventilation-limited heat release rate in kW. The total heat release rate will depend on the total amount of fuel vapour being created (pyrolysed or vaporised) and whether the reaction continues outside of the compartment. For

example, Lee et. al. (2008) noted a plateau in measured heat release rate at \dot{Q}_{vent} using oxygen calorimetry and gaseous hydrocarbon fires when increasing the fuel flow rate. Continued increases of the fuel flow rate eventually caused flames to appear outside of the compartment, and the measured heat release rate caught up with the fuel flow rate.

3.1.1 Bullen and Thomas

Bullen and Thomas (1979) defined an excess fuel factor as:

$$f_{ex} = 1 - \frac{\dot{m}_{air}}{r} \cdot \frac{1}{\dot{m}} \quad \text{Eqn. 3}$$

Where:

f_{ex} = excess fuel factor

\dot{m}_{air} = mass flow rate of air entering the compartment, kg/s

r = stoichiometric air/fuel ratio, kg air/kg fuel

\dot{m} = fuel burning rate, kg/s

This can be compared to the C/VM2 specification of 1.5 times the ventilation-limited heat release rate as follows:

$$f_{ex} = 1 - \frac{\dot{Q}_{vent}}{\dot{Q}} = 1 - \frac{\dot{Q}_{vent}}{1.5 \cdot \dot{Q}_{vent}} = 1 - \frac{1}{1.5} = 0.333 \quad \text{Eqn. 4}$$

Bullen and Thomas found excess fuel factors up to 0.63 ($\dot{Q} = 2.7 \cdot \dot{Q}_{vent}$), 0.48 ($\dot{Q} = 1.9 \cdot \dot{Q}_{vent}$) and 0.45 ($\dot{Q} = 1.8 \cdot \dot{Q}_{vent}$) for ethanol, polyethylene (PE) and polymethacrylate (PMMA) fires, respectively, using a compartment of dimensions 2 m × 1 m × 1 m.

3.1.2 Law

Law (1978) provided the following equation for the maximum burning rate for cellulosic fuels in a compartment under restricted ventilation:

$$R = A_o \sqrt{H_o} \left(\frac{W}{D} \right)^{\frac{1}{2}} (0.18) (1 - e^{-0.036\eta}), \eta = \frac{A_T}{A_o \sqrt{H_o}} \quad \text{Eqn. 5}$$

Where:

R = maximum burning rate, kg/s

W = width of wall containing window, m

D = depth of compartment, m

A_T = total area of floor, ceiling and walls excluding opening area, m²

This correlation and the data used to develop it are shown in Figure 2.

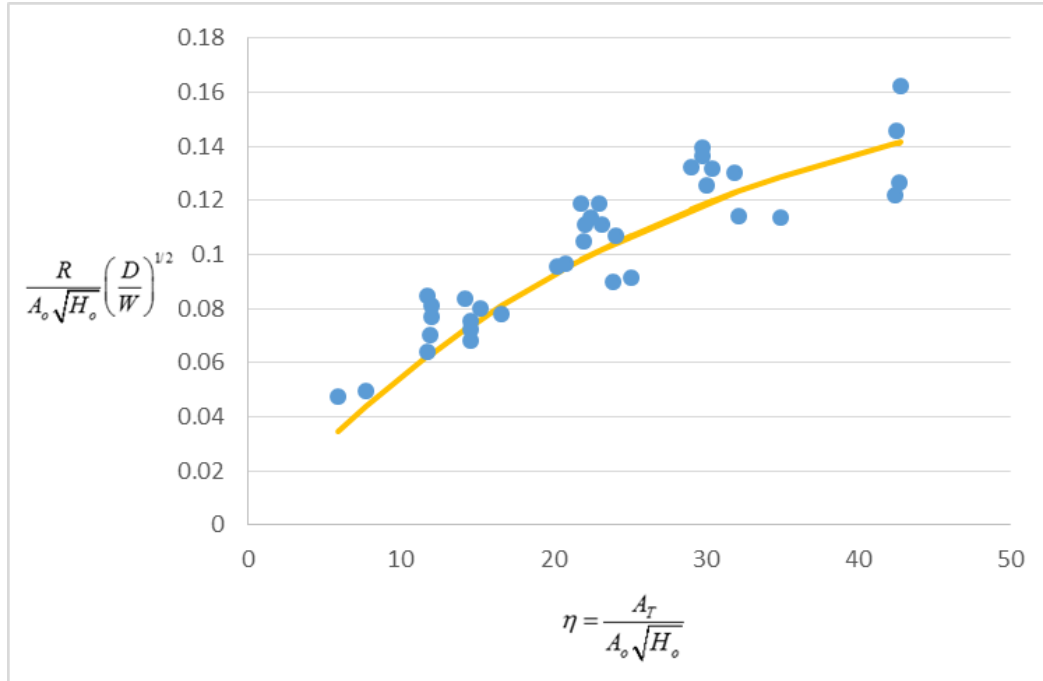


Figure 2. Data used to develop Law and O’Brien’s correlation for maximum ventilation-limited burning rate (Law, 1978).

A similar correlation is also used in EN 1991-1-2 *Eurocode 1: Actions on structures – Part 1-2: General actions – Actions on structures exposed to fire*:

$$\dot{Q} = 3.15 (1 - e^{-0.036/O}) A_o \sqrt{\frac{H_o}{D/W}}, O = \frac{A_o \sqrt{H_o}}{A_t} \quad \text{Eqn. 6}$$

In this equation, \dot{Q} is in MW. The difference between the constants of 0.18 and 3.15 for maximum burning rate R and heat release rate \dot{Q} respectively corresponds to a heat of combustion of 17.5 MJ/kg.

The definition of A_t used in Eqn. 6 differs from A_T in Eqn. 5 because it includes the area of openings. Including the area of openings in A_t causes the opening factor O to be reduced, which increases the predicted value of \dot{Q} in Eqn. 6.

By dividing Eqn. 6 by Eqn. 2, the following equation can be obtained:

$$\frac{\dot{Q}}{\dot{Q}_{vent}} = \frac{2.1 (1 - e^{-0.036/O})}{\sqrt{D/W}} \quad \text{Eqn. 7}$$

This equation provides a dimensionless heat release rate ratio that is only a function of the opening factor O and the depth-to-width ratio of the compartment and is plotted for a range of compartment depth-to-width ratios in Figure 3. Shallow compartments (relative to the opening side) with small openings are predicted to have over four times the heat release rate predicted by the ventilation factor, while deep compartments are closer to unity.

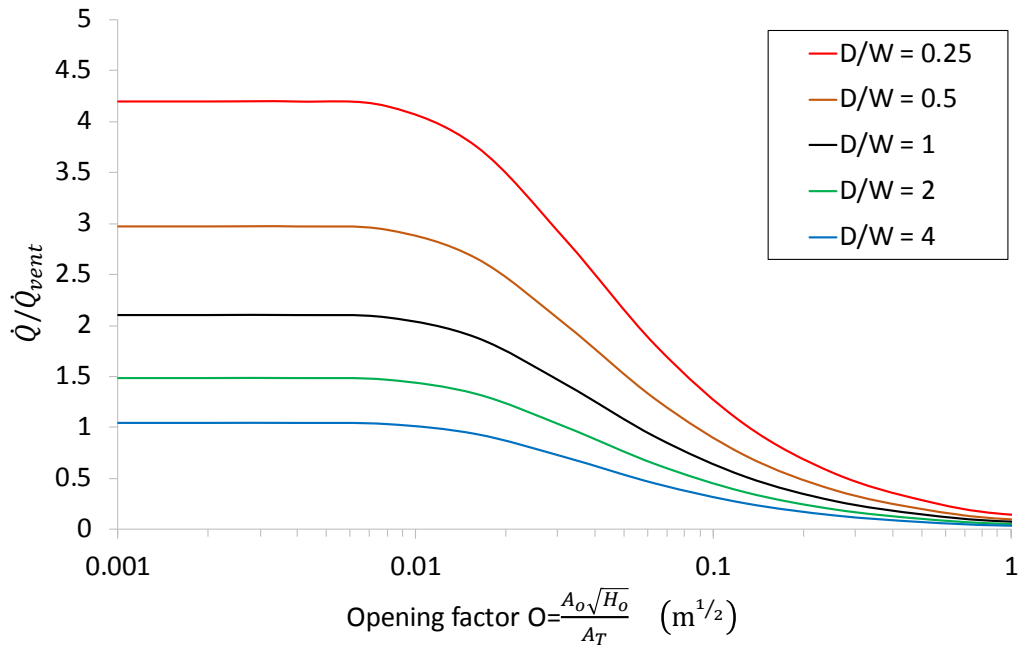


Figure 3. Ratio of the maximum heat release rate from Law (1978) to the ventilation-controlled heat release rate from Kawagoe (1958).

3.1.3 Drysdale

Drysdale (1998) noted that a large excess fuel factor can result from a combination of a large fuel bed surface area and non-cellulosic fuel with a low heat of gasification. He postulated that the combination of the low heat of gasification with the higher air requirement for non-cellulosic hydrocarbon-based (including thermoplastic) fuels would have more significant external flaming than cellulosic fuels (such as wood).

3.2 Projected flame height

Projected flame heights are typically measured either from the bottom of flame shown outside the opening or from the top of an opening. In this study, the latter option is used as it can exclude the variations of flame heights due to opening heights. A schematic diagram is shown in Figure 4.

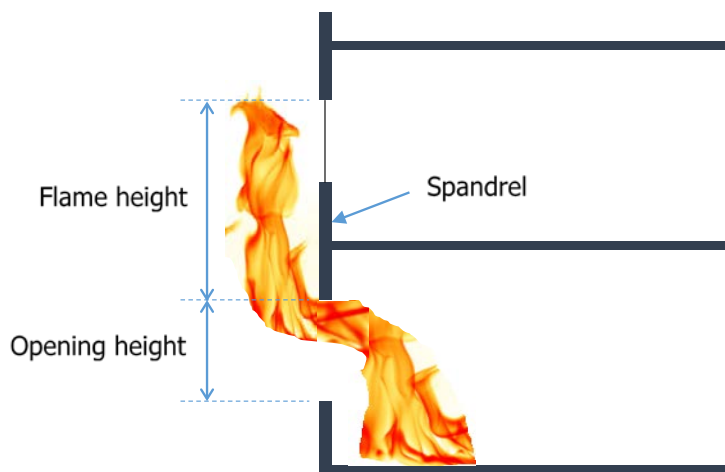


Figure 4. Schematic diagram of flame height.

3.2.1 Yokoi

Yokoi (1960) conducted small-scale fire tests with alcohol fuel for two compartment sizes (30 cm square by 25 cm high and 40 cm square by 20 cm high) and different window sizes investigating the thermal environment near a plume exiting an opening. Yokoi's objective was to determine the length of spandrel necessary to prevent fire spread to upper levels of concrete buildings through windows.

Yokoi's correlation for the temperature data is shown below:

$$\Theta = \frac{\Delta\theta r_o^{5/3}}{\sqrt[3]{\frac{\dot{Q}^2 \theta_0}{c_p^2 \rho^2 g}}} \quad \text{Eqn. 8}$$

In which:

$$r_o = \sqrt{\frac{H_o W_o}{2\pi}} \quad \text{Eqn. 9}$$

And:

$$\Delta\theta = \theta - \theta_0 \quad \text{Eqn. 10}$$

Where:

r_o = equivalent opening radius, m

Θ = non-dimensional quantity representing the temperature rise on the external plume centreline

\dot{Q} = heat energy released at the opening per unit time, kJ/s

θ = temperature, K

θ_0 = ambient temperature, K

ρ = density of the gases in the plume, kg/m³

c_p = constant pressure specific heat capacity of the plume gases, kJ/(kg K)

g = acceleration due to gravity, m/s²

The term r_o is an equivalent radius of the opening based on an approximation for the area of the opening occupied by the exiting flame plume as being the full width and the upper half of the height (Yokoi, 1960, p. 95), and the term n is proportional to the aspect ratio of the window:

$$n = \frac{2W_o}{H_o} \quad \text{Eqn. 11}$$

In Figure 5, the parameter z is the distance above the opening where $\Delta\theta$ is achieved.

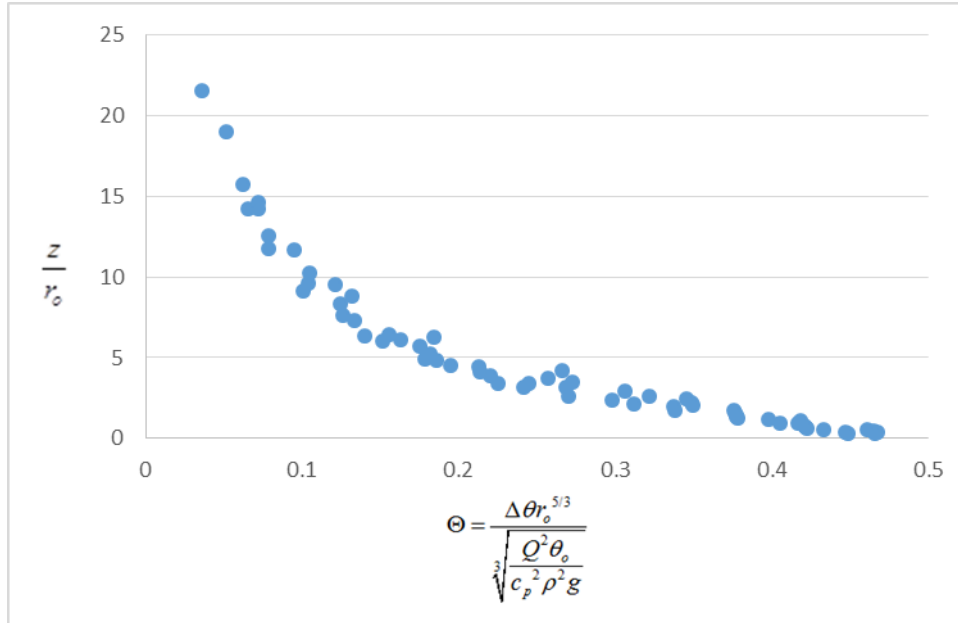


Figure 5. Correlation reproduced from Yokoi's (1960) experimental results.

Yokoi used a temperature rise of $\Delta\theta = 500^\circ\text{C}$ as the criteria for the maximum height above the window where a window can be broken. It is not made explicit in Yokoi's report that this temperature rise was observed at the flame tip. Yokoi noted that the correlations from his experiments were based on the case where there was no limit on ventilation within the room and on the assumption that the fuel burns perfectly in the room.

Yokoi compared his correlations to four full-scale experiments with timber as the primary fuel source. Three different concrete buildings were used, with experiments 3 and 4 in the same building. Experiments 1, 2 and 3 used non-combustible interior linings, while experiment 4 included a combustible plywood interior lining. A necessary spandrel height (the height of the wall above the window where a temperature rise of 500°C was found near the wall surface) of 1.33 m was determined for the second full-scale experiment and 0.88 m for the third and fourth experiments. A necessary spandrel height was not reported for experiment 1.

3.2.2 Thomas

A dimensional analysis by Thomas (1960) for the height of a buoyant diffusion flame from a gaseous fuel orifice jet found the following relationship:

$$\frac{L}{D} = f\left(\frac{v^2}{gD}\right) = f\left(\frac{Q^2}{gD^5}\right) \quad \text{Eqn. 12}$$

Where:

L = flame height, m

D = orifice diameter, m

v = orifice velocity, m/s

Q = orifice volume flow rate, m^3/s

Subsequently, Thomas (1961) revisited this relationship for flames from the open side of a cube and fit the following relation to data from Webster and Raftery (1959):

$$\frac{L}{D} = 400 \left(\frac{R^2}{D^5} \right)^{1/3} \quad \text{Eqn. 13}$$

Where:

L = flame height from base of cube

D = side dimension of cube

R = burning rate

The burning rate R is based on the wood-equivalent burning rate with a heat of combustion value of $h_c = 16,800$ kJ/kg. By multiplying both sides by D and changing the units to kilograms and metres, Thomas and Law (1972) established the following relationship for flame height from a window:

$$L = z + H_o = 18.6 \left(\frac{R}{W_o} \right)^{2/3} \quad \text{Eqn. 14}$$

Where:

L = total flame height, m

z = flame height above the top of the window, m

H_o = height of the window, m

W_o = width of the window, m

Thomas (1961) compared this correlation to that developed by Yokoi and noted that:

Yokoi's analysis does not refer explicitly to flames, though he does define an equivalent flame height at the point where the temperature is 500°C on the argument that the radiation has largely ceased by the time the temperature falls to this value.

The relationship between z/r_o and θ from Yokoi's data for no wall above the window was given by Thomas and Law (1972) as:

$$\frac{z}{r_o} = \frac{A}{\theta} \text{ for } \frac{z}{r_o} \gg 1 \quad \text{Eqn. 15}$$

and where A depends on the width-to-height ratio of the window. Further, Thomas found a good correlation to Yokoi's data by setting:

$$A = \left(\frac{H_o}{2W_o} \right)^{1/3} = \frac{1}{\eta^{1/3}} \quad \text{Eqn. 16}$$

Where:

$$\eta = \frac{2W_o}{H_o}$$

Substituting Eqn. 16 into Eqn. 15 results in:

$$\eta^{1/3} \frac{z}{r_o} = \frac{1}{\Theta} \quad \text{Eqn. 17}$$

Noting the similarities, Thomas's equation based on Webster's data was rewritten as follows, using the relationship:

$$\dot{Q} = h_c R$$

Where:

\dot{Q} = heat release rate

h_c = heat of combustion

R = burning rate

As follows:

$$L = z + H_o = 18.6 \left(\frac{R}{W_o} \right)^{2/3} \quad \text{Eqn. 18}$$

$$L = 18.6 \left(\frac{\dot{Q}}{h_c W_o} \right)^{2/3} \quad \text{Eqn. 19}$$

$$\left(\frac{\eta^{1/3}}{r_o} \right) L = \left(\frac{\eta^{1/3}}{r_o} \right) 18.6 \left(\frac{\dot{Q}}{h_c W_o} \right)^{2/3} \quad \text{Eqn. 20}$$

$$\left(\frac{\eta^{1/3}}{r_o} \right) L = 18.6 \frac{\dot{Q}^{2/3}}{\pi^{1/3} h_c^{2/3} r_o^{5/3}} \quad \text{Eqn. 21}$$

Factoring out:

$$\Theta = \frac{\Delta \theta r_o^{5/3}}{\left(\frac{\theta_o}{c_p^2 \rho^2 g} \right)^{1/3} \dot{Q}^{2/3}} \quad \text{Eqn. 22}$$

Gives:

$$\left(\frac{\eta^{1/3}}{r_o} \right) L = 18.6 \left(\frac{c_p^2 \rho^2 g}{\pi^{1/3} h_c^{2/3} \theta_o} \right)^{1/3} \left(\frac{1}{\Theta} \right) \quad \text{Eqn. 23}$$

Which could be rewritten as:

$$\eta^{1/3} \left(\frac{L}{r_o} \right) = \frac{B}{\Theta} \quad \text{Eqn. 24}$$

Where:

$$B = 18.6 \left(\frac{c_p^2 \rho^2 g}{\pi^{1/3} h_c^{2/3} \theta_o} \right)^{1/3} \quad \text{Eqn. 25}$$

Eqn. 24 is in a similar form compared to the correlation from Yokoi's data except that the length scale L includes the height of the opening.

Using $\Delta\theta = 540^\circ\text{C}$, $\theta_0 = 290\text{ K}$, properties of air at standard pressure and 500°C and $h_c = 4000\text{ kcal/kg}$ for wood gave $B = 2.0$. Thomas and Law noted that $B = 2$ gave good results at lower values of L/r_o , but at higher values, $B = 1.3$ was more reasonable.

3.2.3 Law

The correlation from Webster's data was later modified by Law (1978) as:

$$z + H_o = 12.8 \left(\frac{R}{W_o} \right)^{2/3} \quad \text{Eqn. 26}$$

Where:

z = the flame length from the top of the opening, m

H_o = opening height, m

W_o = opening width, m

R = rate of mass loss of fuel, kg/s

This was deemed to provide a better fit to the existing data. This correlation is also used in EN 1991-1-2, with the burning rate converted to the heat release rate using a heat of combustion of 17.5 MJ/kg , as discussed in section 3.1.2:

$$z + H_o = 1.9 \left(\frac{\dot{Q}}{W_o} \right)^{2/3} \quad \text{Eqn. 27}$$

3.2.4 Quintiere and Cleary

Quintiere and Cleary (1994) applied dimensional analysis to examine heat flux levels and applied it to experimental external flames from National Research Council Canada (NRCC) full-scale façade tests (Oleszkiewicz, 1989) and Yokoi (1960). Quintiere and Cleary noted that they were not successful in producing a general correlation for heat flux above flames coming out of a window. The flame height in the NRCC façade experiments was reported by Quintiere and Cleary through a personal communication with Oleszkiewicz. A simplified flame height correlation was developed based on the previous work by Yokoi and Thomas and Law. Quintiere and Cleary started with Eqn. 24 and noting that, for the case where there was a wall above the window $\eta \approx 1$, Eqn. 24 can be simplified to:

$$\left(\frac{L}{r_o} \right) = \frac{B}{\theta} \quad \text{Eqn. 28}$$

B was selected as 2, as per Thomas and Law. For calculating θ from Eqn. 22, the parameters used were $\Delta\theta = 520^\circ\text{C}$, $\theta_0 = 290\text{ K}$, $c_p = 1.0\text{ kJ/(kg K)}$, $\rho = 0.45\text{ kg/m}^3$ (at 500°C) and $g = 9.81\text{ m/s}^2$. This gave:

$$L = z + H_o = 0.0321 \left(\frac{\dot{Q}}{D} \right)^{2/3} \quad \text{Eqn. 29}$$

Where:

z = flame height from the top of opening, m

H_o = opening height, m

\dot{Q} = heat release rate from burning taking place outside the opening, kW

$$D = 2r_o \text{ and } r_o = \sqrt{\frac{H_o W_o}{2\pi}}, \text{ m}$$

W_o = opening width, m

Quintiere and Cleary noted that this formulation gave estimates of flame height that were approximately double the flame heights measured in the NRCC façade tests and stated that a value of $B = 1$ would have been a better choice. This value was compared to the value from Thomas and Law of $B = 1.3$ for locations farther from the top of the window where heat loss may be a factor.

One aspect not considered by Quintiere and Cleary is that the value of $B = 2$ from Thomas and Law was based on a heat of combustion of 4000 kcal/kg (16.7 MJ/kg), but the NRCC façade tests used propane as the fuel source. Using the heat of combustion of 46.5 MJ/kg for propane gives $B \approx 1$. The revised correlation becomes:

$$L = z + H_o = 0.0161 \left(\frac{\dot{Q}}{D} \right)^{2/3} \quad \text{Eqn. 30}$$

3.2.5 Ohmiya et al.

Ohmiya et al. (2000) ran experiments that generated external combustion and derived a flame height correlation:

$$z = 0.65(\dot{Q}_{W_o}^*)^{2/3} W_o \quad \text{Eqn. 31}$$

Where:

z = flame height from the top of opening, m

$\dot{Q}_{W_o}^*$ = dimensionless heat release rate, $\dot{Q}_{W_o}^* = \frac{\dot{Q}_{ex}}{\rho_0 c_p T_0 \sqrt{g} W_o^{2/3}}$

W_o = the width of the opening, m

\dot{Q}_{ex} = heat release rate outside compartment, kW

T_0 = ambient temperature

The heat release rate outside of the compartment, \dot{Q}_{ex} , is calculated as follows:

$$\dot{Q}_{ex} = c_p R_{fo} \Delta T + \dot{Q} - \dot{Q}_{v,crit} \quad \text{Eqn. 32}$$

Where:

R_{fo} = the flow rate of the gases leaving the compartment, kg/s

ΔT = the temperature difference between the gases leaving the compartment and ambient, °C

\dot{Q} = the total heat release rate, kW

$\dot{Q}_{v,crit}$ = the maximum amount of heat release due to combustion in the compartment, kW

The flow rate of gases leaving the compartment is calculated as follows:

$$R_{fo} = 0.5A_o\sqrt{H_o} \quad \text{Eqn. 33}$$

And $\dot{Q}_{v,crit}$ is calculated as:

$$\dot{Q}_{v,crit} = 150A_o\sqrt{H_o} \left(\frac{A_T}{A_o\sqrt{H_o}} \right)^{2/5} \quad \text{Eqn. 34}$$

Where:

A_T = the total surface area in the compartment, m²

A correction term Δz is also employed:

$$\Delta z = 0.04\dot{Q}_{ex}^{*2}W_o \quad \text{Eqn. 35}$$

The correlation is from the best fitting curve, but as shown in Figure 6, there are points above the fitting curve that indicates that some of the actual flame heights are larger than the values calculated by the correlation.

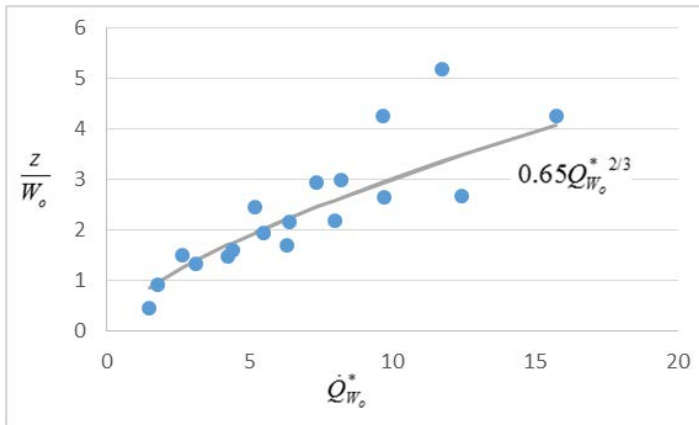


Figure 6. Data and correlation for flame height (Ohmiya et al., 2000, p. 382).

3.2.6 Delichatsios et al.

Delichatsios and his colleagues conducted experiments investigating various phenomena associated with flame extension out of an opening using mainly gas fuels (Delichatsios, 2014; Delichatsios et al., 2004; Delichatsios & Silcock, 2003; Lee et al., 2008). Flame height and heat flux on the façade wall and the opposite wall to an opening were measured, and correlations were developed.

In Figure 7 and Figure 8, data points were reproduced with the trendlines having the slopes recommended by the original authors of the paper (2/3 and 2/5 in a log-log plot). It should be noted that the exponential of 2/3 is typically derived from a line fire and 2/5 from an axisymmetric fire. However, this distinction is not clearly observed.

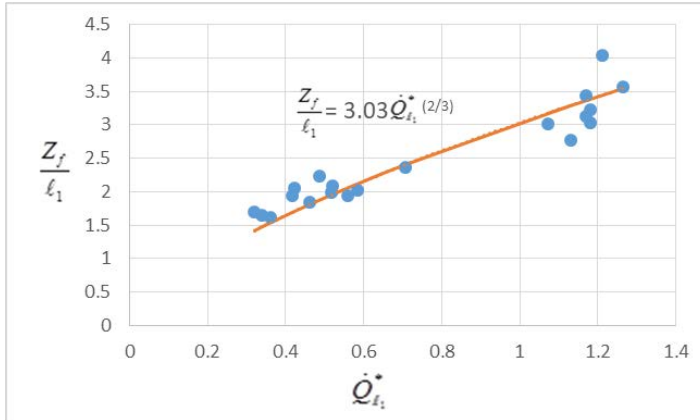


Figure 7. Flame height for dimensionless heat release rate < 1.3 (Lee et al., 2008).

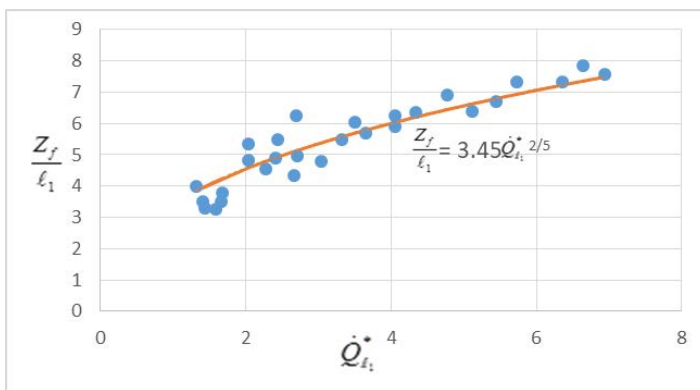


Figure 8. Flame height for dimensionless heat release rate ≥ 1.3 (Lee et al., 2008).

Where:

Z_f = flame height measured from the neutral plane, m

(The distance from the neutral plane height to the top of the opening was estimated to be $0.6 H_o$.)

$$l_1 = (A_o \sqrt{H_o})^{2/5}, \text{ m}$$

$$Q_{l_1}^* = \frac{\dot{Q}_{ex}}{\rho_\infty c_p T_\infty \sqrt{g} (l_1)^{5/2}}, \text{ dimensionless fire size}$$

Where:

\dot{Q}_{ex} = excess heat release rate generated out of an opening, kW

$$\begin{aligned} \dot{Q}_{ex} &= \dot{m}_f \Delta H_c - \dot{Q}_{comp} = (0.1 A_o \sqrt{H_o}) \Delta H_c - 3000(0.5) A_o \sqrt{H_o} \\ &= (0.1 \Delta H_c - 1500) A_o \sqrt{H_o} \end{aligned}$$

Eqn. 36

Where:

\dot{m}_f = fuel mass loss rate, kg/s

ΔH_c = heat of combustion, kJ/kg

Subsequently, Delichatsios et al. (2016) published similar correlations based on:

$$\frac{Z_f}{\ell_1} = 3.2\dot{Q}_{\ell_1}^{*2/3} \text{ for } \dot{Q}_{\ell_1}^* < 1.3$$

$$\frac{Z_f}{\ell_1} = 3.2\dot{Q}_{\ell_1}^{*2/5} \text{ for } \dot{Q}_{\ell_1}^* > 1.3$$

Eqn. 37

3.2.7 Summary of simple flame height correlations

Table 1 summarises the simple flame height correlations described earlier in this section that have been developed using different fuel types, fire sizes and compartment and opening configurations. Each correlation was derived based on a specific experimental data range, from which its valid application range is also defined. This limitation may be reduced or intended to be reduced by non-dimensionalising the correlation and variables to a certain degree. However, using such an approach may not be valid if the original correlation does not capture the entire parameters, and some of these parameters play a critical role at different scales. This intrinsic limitation is unfortunately often easily overlooked and the extent of errors is generally unknown. Before comparing the results, it should be also noted that all of the flame height correlations introduced above were derived from the best-fitting lines to the experimental data. This means that some data points are higher than the fitting lines i.e., flames can be taller than the predicted values from the correlations.

Table 1. Summary of flame height correlations.

| Authors | Key parameters and correlation | Experiment range |
|--|---|--|
| Thomas and Law (1972) | $z = 18.6 \left(\frac{R}{W_o} \right)^{2/3} - H_o$ $R = 0.09WH^{3/2} \text{ (ventilation limited)}$ | $9 < \eta < 45$ $0.5 < \frac{W}{D} < 2$ |
| Law (1978) | $z = 12.8 \left(\frac{R}{W_o} \right)^{2/3} - H_o$ $R = (0.18)A_o\sqrt{H_o} \left(\frac{W}{D} \right)^{1/2} (1 - e^{-0.036\eta})$ $\eta = \frac{A_T}{A_o\sqrt{H_o}}$ | $9 < \eta < 45$ $0.5 < \frac{W}{D} < 2$ |
| Quintiere and Cleary (1994) | $z = 0.0321 \left(\frac{\dot{Q}}{\sqrt{\frac{2A_o}{\pi}}}} \right)^{2/3} - H_o$ | Based on Yokoi's experiments ($\theta < 0.48$) |
| Ohmiya et al. (2000) Note that z is relative to the plume centreline, not the top of the opening. | $z = 0.65\dot{Q}_{W_o}^{*2/3} W_o + 0.04\dot{Q}_{ex}^2 W_o$ $\dot{Q}_{ex} = c_p R_{fo} \Delta T + \dot{Q} - \dot{Q}_{v,crit}$ $\dot{Q}_{v,crit} = 150A_o\sqrt{H_o} \left(\frac{A_T}{A_o\sqrt{H_o}} \right)^{2/5}$ $\dot{Q}_{W_o}^* = \frac{\dot{Q}_{ex}}{\rho_0 c_p T_0 \sqrt{g} W_o^{2/3}}$ | $1.5 < \dot{Q}_{W_o}^* < 11$ $0.25 < \frac{W_o}{H_o} < 2$ |

| Authors | Key parameters and correlation | Experiment range |
|---|--|--------------------------|
| Delichatsios et al. (Y. Lee et al., 2008) | For $\dot{Q}_{\ell_1}^* < 1.3, z = 3.03(\ell_1)\dot{Q}_{\ell_1}^{*2/3} - 0.6H_o$ For $\dot{Q}_{\ell_1}^* \geq 1.3, z_f = 3.45(\ell_1)\dot{Q}_{\ell_1}^{*2/5} - 0.6H_o$ $\dot{Q}_{\ell_1}^* = \frac{\dot{Q}_{ex}}{\rho_{\infty}c_pT_{\infty}\sqrt{g}(\ell_1)^{5/2}}$ $\ell_1 = (A_o\sqrt{H_o})^{2/5}$ | $0.3 < Q_{\ell_1}^* < 7$ |

3.2.8 Mizuno and Kawagoe

The projected unburned fuel air mixture out of an opening is turned upwards due to buoyancy and forms flames against or near a vertical wall. This may be similar to a wall fire where combustible wall surface materials burn or a pool fire of which the base is located next to a wall. One approach to estimate an external flame height is to characterise a virtual fire adjacent to the external wall and use a flame height calculation for a fire against a wall such as that developed by Mizuno and Kawagoe (1986). In the current study, the latter case is selected to be compared with the measured flame heights.

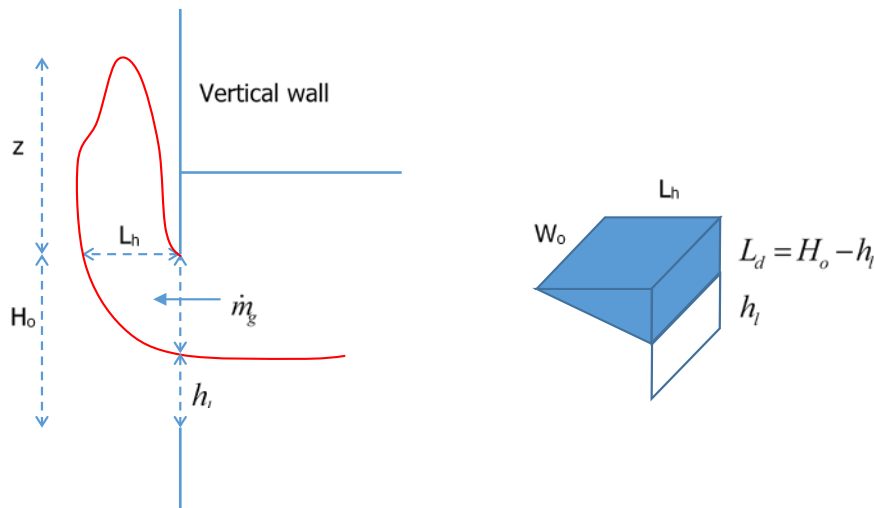


Figure 9. Section view of the projected flame and opening.

To estimate the fuel base area, which is commonly required to calculate the flame heights, the following assumptions were made:

- Projected flame height (z) can be modelled as a fire with the rectangular base area of L_h by W_o .
- Horizontal momentum change of the outflow is overcome by the vertical buoyancy force near the top of the opening.

$$\dot{m}_g u = (\rho_{\infty} - \rho_g)gV = (\rho_{\infty} - \rho_g)g \left(\frac{L_h W_o (H_o - h_l)}{2} \right) \quad \text{Eqn. 38}$$

Where:

\dot{m}_g = outflow mass, kg/s

u = averaged outflow velocity, m/s

ρ_∞ = ambient air density, kg/m³

ρ_g = outflow gas density, kg/m³

g = 9.81, m/s²

V = outflow volume, m³

L_h = estimated side length of imaginary burner, m

W_o = opening width, m

H_o = opening height, m

h_l = neutral plane height, m

Since:

$$\dot{m}_g = \rho_g \dot{V} = \rho_g A u = \rho_g W_o (H_o - h_l) (H_o - h_l) u \quad \text{Eqn. 39}$$

The average outgoing velocity (u) becomes:

$$u = \frac{\dot{m}_g}{\rho_g W_o (H_o - h_l)} \quad \text{Eqn. 40}$$

Inserting this velocity to the momentum and buoyancy correlation and rearranging it, L_h becomes:

$$L_h = \frac{2\dot{m}_g}{\rho_g (W_o (H_o - h_l))^2 (\rho_\infty - \rho_g) g} \quad \text{Eqn. 41}$$

From $\rho_g T_g = \rho_\infty T_\infty$, where the subscript g indicates the gas flow leaving the compartment, Eqn. 41 becomes:

$$L_h = \frac{2\dot{m}_g^2 T_g^2}{\rho_\infty^2 T_\infty (T_g - T_\infty) g (W_o (H_o - h_l))^2} \quad \text{Eqn. 42}$$

Assuming a circular fuel base, the equivalent diameter of the fuel base becomes:

$$D = \left(\frac{8W_o \dot{m}_g^2 T_g^2}{\pi \rho_\infty^2 T_\infty (T_g - T_\infty) g (W_o (H_o - h_l))^2} \right)^{0.5} \quad \text{Eqn. 43}$$

Then the fuel base diameter D , and $\dot{Q}_{ex} = \dot{m}_f \Delta H_c - 3000 \dot{m}_a$ can be used to calculate the flame heights using an existing correlation. The method to calculate \dot{m}_g , T_g and \dot{m}_a is explained in Appendix G.

In the current study, this existing correlation (Mizuno & Kawagoe, 1986) is used to compare the calculated flame heights with the experimentally measured flame heights:

$$z = 3.5 \dot{Q}_{ex}^*{}^n D \quad \text{Eqn. 44}$$

Where:

$$\dot{Q}_{ex}^* = \frac{\dot{Q}_{ex}}{\rho_{\infty} c_p T_{\infty} \sqrt{g} D^{5/2}}$$

$n = 2/5$ (for $\dot{Q}^* > 1$) - similar to a rectangular fire

$n = 2/3$ (for $\dot{Q}^* < 1$) - similar to a line fire

3.3 Heat flux from external flame

3.3.1 NRCC façade experiments

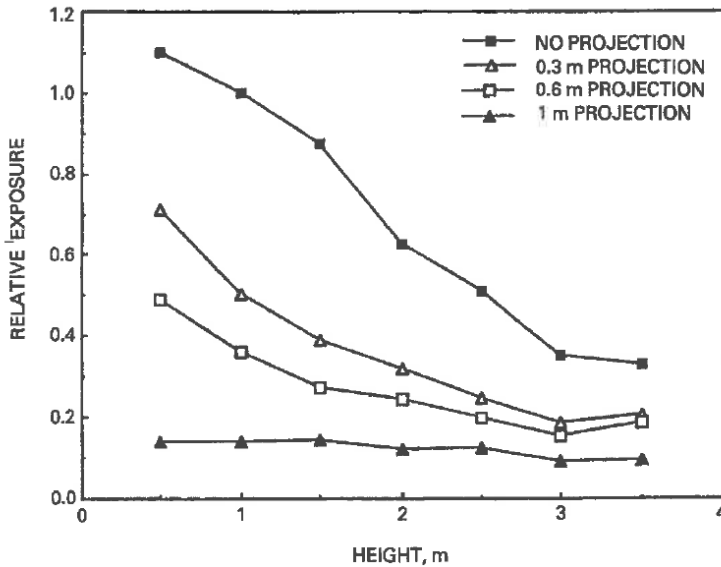
Oleszkiewicz (1989) conducted a full-scale experimental study investigating the heat flux on the façade wall above an opening using wood crib and propane gas fires. Heat release rates based on gas flow were available for the experiments using propane. Five different opening sizes in a 5.95 m (W) by 4.4 m (D) by 2.7 m (H) compartment were examined, and measured flame heights and heat fluxes are listed in Table 2.

Table 2. NRCC façade experiment summarised data (Oleszkiewicz, 1989) and experimental flame heights reported by Quintiere and Cleary (1994).

| Window | Window Dimensions | | $1.5A\sqrt{H_o}$ (MW) | Fuel flow energy rate (MW) | Flame height l_f (m) | Heat flux at x (m) above window (kW/m ²) | | | |
|----------|-------------------|-----------|--------------------------|-------------------------------|---------------------------|--|-------|-------|------|
| | W_0 (m) | H_0 (m) | | | | 0.5 | 1.5 | 2.5 | 3.5 |
| 1 | 0.94 | 2 | 4.0 | 5.5 | 5 | 43.9 | 12.4 | 7.7 | 3.9 |
| | 0.94 | 2 | 4.0 | 6.9 | 6 | 58.6 | 17.7 | 9.9 | 5.1 |
| | 0.94 | 2 | 4.0 | 8.6 | 7 | 75.5 | 25.9 | 15.9 | 8.1 |
| | 0.94 | 2 | 4.0 | 10.3 | | - | - | - | - |
| 2 | 0.94 | 2.7 | 6.3 | 5.5 | | 19.2 | 6.3 | 3.5 | 1.7 |
| | 0.94 | 2.7 | 6.3 | 6.9 | | 34.8 | 10.4 | 6 | 3 |
| | 0.94 | 2.7 | 6.3 | 8.6 | 6.2 | 53.2 | 15.9 | 9.8 | 4.8 |
| | 0.94 | 2.7 | 6.3 | 10.3 | | 68.3 | 23.2 | 13.7 | 6.7 |
| 3 | 2.6 | 1.4 | 6.5 | 5.5 | 3.9 | 24.5 | 22.9 | 13.2 | 11.5 |
| | 2.6 | 1.4 | 6.5 | 6.9 | 4.4 | 53.2 | 33.1 | 17.2 | 15.6 |
| | 2.6 | 1.4 | 6.5 | 8.6 | 5.1 | 104.3 | 58.6 | 51.2 | 28.3 |
| | 2.6 | 1.4 | 6.5 | 10.3 | 6.4 | 208.7 | 122.4 | 103.9 | 56.5 |
| 4 | 2.6 | 2 | 11.0 | 5.5 | | 10.5 | 5.2 | 4.5 | 2.9 |
| | 2.6 | 2 | 11.0 | 6.9 | 4.5 | 17.4 | 9.4 | 7.4 | 5.4 |
| | 2.6 | 2 | 11.0 | 8.6 | 5 | 29.5 | 14.8 | 12.6 | 8.2 |
| | 2.6 | 2 | 11.0 | 10.3 | 5.5 | 43.4 | 20.8 | 16.3 | 9.6 |
| 5 | 2.6 | 2.7 | 17.3 | 5.5 | | 6.5 | 2.9 | 2 | 1.4 |
| | 2.6 | 2.7 | 17.3 | 6.9 | 5.2 | 11.4 | 5.3 | 4.2 | 2.9 |
| | 2.6 | 2.7 | 17.3 | 8.6 | 5.9 | 17.4 | 8.1 | 5.7 | 3.6 |
| | 2.6 | 2.7 | 17.3 | 10.3 | 6.2 | 29.1 | 12.8 | 9.1 | 5.6 |

Subsequent experiments at NRCC (Oleszkiewicz, 1991) evaluated the effectiveness of horizontal projections (aprons) at reducing heat flux on a wall above flames projecting from an opening. Figure 10 shows a summary of his results. A 0.3 m apron decreased the heat flux by approximately 50% at 1 m above the window opening, while a 0.6 m

apron decreased the heat flux by approximately 60% at the same height. The heat flux above the window was nearly uniform with height using a 1 m apron and was approximately 15% of the value measured at 1 m without an apron.



© 1991 Springer Nature. Reprinted by permission from Springer Nature.

Figure 10. Heat flux data for various apron depths. Data is relative to readings at 1 m above opening with no projection (Oleszkiewicz, 1991).

3.3.2 Delichatsios et al.

Lee et al. (2008; 2009) conducted small scale fire tests measuring heat fluxes from the ejected flame on the front wall above and on a wall opposite to the opening. A propane gas burner was used as a fire source in a 0.5 m by 0.5 m by 0.5 m compartment. Three different opening sizes (0.1 m (W) by 0.25 m (H), 0.2 m (W) by 0.2 m (H) and 0.25 m (W) by 0.1 m (H)) with associated fire sizes (40, 50 and 20 kW, respectively) were explored. The distance between the two walls, which is denoted as D in Figure 11, also varied from 0.1 m to 0.5 m and ∞ .

Some of the heat flux data on the opposing wall is reproduced in Figure 11.

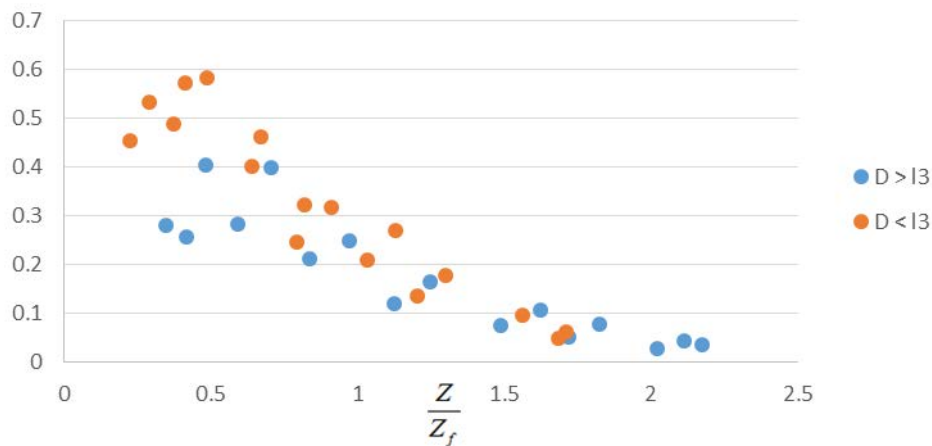


Figure 11. Heat flux on an opposing wall above an opening (Lee et al., 2009).

The y axis is either $\frac{\dot{q}_t'' Z_f}{\dot{Q}_{ext}/\ell_3} e^{0.6(\frac{\ell_3}{\ell_1})^{5.5}}$ for $D > \ell_3$ or $\frac{\dot{q}_t'' Z_f}{\dot{Q}_{ext}/D} e^{0.6(\frac{\ell_3}{\ell_1})^{5.5}}$ for $D < \ell_3$ in Figure 11.

Where:

$$\ell_1 = (A_o \sqrt{H_o})^{2/5}$$

$$\ell_3 = (A_o H_o^{4/3})^{3/10}$$

$$\dot{Q}_{ext} = \dot{m}_F \Delta H_c - 1500 A_o \sqrt{H_o}$$

Despite the slightly different term for the Y axis, it is found that heat flux is quickly decreasing once the measurement point is above the flame height where the X axis value equals to unity. Note that the peak heat flux is recorded somewhere around half of the flame height.

From this data set, Delichatsios et al. (2016) developed the following correlation for peak heat flux on a wall above a flame projecting from an opening:

$$\dot{q}_{t,max}'' = 0.35 \frac{\dot{Q}_{ext}}{Z_f e^{0.6(\frac{H_o}{\ell_1})} \ell_1} = 0.1 \frac{\dot{Q}_{\ell_1}^* \frac{1}{3} \rho_\infty c_p T_\infty \sqrt{g} \ell_1^{\frac{1}{2}}}{e^{0.6(\frac{H_o}{\ell_1})}} \quad \text{Eqn. 45}$$

With a heat flux distribution as a function of flame height:

$$\dot{q}_t'' = \dot{q}_{t,max}'' \text{ for } \frac{Z}{Z_f} < 0.8$$

Eqn. 46

$$\dot{q}_t'' = 0.64 \dot{q}_{t,max}'' \left(\frac{Z}{Z_f} \right)^{-2} \text{ for } \frac{Z}{Z_f} > 0.8$$

3.3.3 Yoshioka et al.

Full-scale fire tests were conducted in a compartment whose dimension was 3 m (W) by 4.3 m (D) by 1.7 m (H) to measure the incident heat flux on the façade wall (Yoshioka, Ohmiya, Noaki & Yoshida, 2011). An opening of 2 m (W) and 1.2 m (H) was located 0.5 m above the floor level on the wall of 3 m width. Four small vents of size 0.5 m (W) by 0.6 m (H) were placed on the opposite wall but closed for the tests shown in Table 3. Three fuels (propane gas, heptane and wood cribs) were used.

Table 3. Heat flux values (kW/m²) at various locations above the opening.

| Fire details | Test period | 0.9 m | | 1.2 m | | 1.5 m | | 2 m | |
|-----------------|-------------|--------------------------|--------------------------|-------------------------|--------------------------|-------------------------|--------------------------|-------------------------|--------------------------|
| | | Avg. | Max. | Avg. | Max. | Avg. | Max. | Avg. | Max. |
| 0.7 MW propane | 5 min | 7 kW/m ² | 15 kW/m ² | 7 kW/m ² | 16 kW/m ² | 6 kW/m ² | 11 kW/m ² | 7 kW/m ² | 14 kW/m ² |
| 1.4 MW propane | 5 min | 9 kW/m ² | 12 kW/m ² | 9 kW/m ² | 12 kW/m ² | 7 kW/m ² | 10 kW/m ² | 7 kW/m ² | 10 kW/m ² |
| 2.8 MW propane | 5 min | 24 kW/m ² | 28 kW/m ² | 15 kW/m ² | 17 kW/m ² | 20 kW/m ² | 25 kW/m ² | 19 kW/m ² | 23 kW/m ² |
| 2.6 MW heptane | 210 s | 115 kW/m ² | 167 kW/m ² | 83 kW/m ² | 116 kW/m ² | 74 kW/m ² | 107 kW/m ² | 86 kW/m ² | 137 kW/m ² |
| 2 MW wood cribs | 30 min | 13 kW/m ² | 16 kW/m ² | 11 kW/m ² | 13 kW/m ² | 11 kW/m ² | 14 kW/m ² | 10 kW/m ² | 11 kW/m ² |

The fire size in column 1 is the averaged value over the test period. A 0.8 m by 0.8 m by 0.1 m (H) metal tray containing 18 litres of heptane was used for the 2.6 MW heptane fire. One noticeable discrepancy exists between the 2.8 MW propane fire and 2.6 MW heptane fire. Since the fire sizes are averaged, the peak heat release rate is not known, which means the peak heat release rate for the heptane fire can be much higher than 2.6 MW for a short period of time. However, the average heat flux from the heptane fire is almost four times higher than that of propane gas fire.

For the 2.6 MW heptane fire, incident heat flux is reproduced in Figure 12 by digitising the original data. Heat flux increases until 120 s, and after that, it reaches almost the peak with some fluctuation until the heptane burns out. Considering the liquid fuel burning phenomena, it is assumed that the heptane was preheated for the first 120 s and a large amount of unburned gas was produced from 120 s by radiation from the hot upper gas layer and compartment walls. The unburned gas then created a large external flame resulting in extremely high heat fluxes. The radiation effects from the hot upper layer on the fuel generation rate cannot be captured with a gas burner fire.

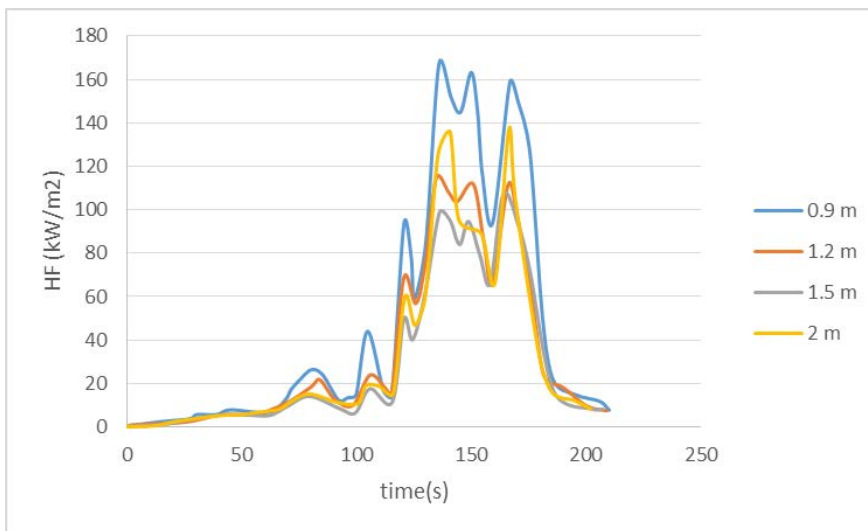


Figure 12. Incident heat flux profile for 2.6 MW heptane fire.

3.3.4 Back et al.

A joint Naval Research Laboratory/Hughes Associates (NRL/HAI) study by Back et al. (1994) investigated incident heat flux on a wall from square propane burner fires located against the wall. The burner edge lengths ranged from about 0.3 m to 0.7 m corresponding to 50–500 kW heat release rate. A total of nine tests were conducted, and their details are shown in Table 4 and Figure 13. The simple mean beam length approach was used to predict the peak heat flux:

$$\dot{q}_{peak}'' = E(1 - e^{-kL_m}) \quad \text{Eqn. 47}$$

Where:

\dot{q}_{peak}'' = peak incident heat flux, kW/m²

E = blackbody emissive power of the flame, kW/m²

k = extinction coefficient, 1/m

L_m = mean beam length, m

The mean beam length L_m was assumed to scale with the cube root of the flame volume, which gave:

$$\dot{q}_{peak}'' = E \left(1 - e^{-k_a \dot{Q}^{1/3}} \right) \quad \text{Eqn. 48}$$

Where:

\dot{Q} = heat release rate of burner, kW

k_a = fitting constant related to extinction coefficient, kW^{-1/3}

Back et al. determined E to be 200 kW/m² and k_a to be 0.09 kW^{-1/3} based on a curve fit of their experimental data. One outlier with a peak heat flux of approximately 120 kW/m² at a heat release rate of 500 kW was noted in the Back et al. data. The heat flux was found to be at a maximum from the burner up to 40% of the flame height on the wall adjacent to the centreline of the burner. From 40% to 100% of the flame height (the tip of the flame), the heat flux was found to linearly decrease to 20 kW/m². The heat flux further decreased above the tip of the flame. The correlations developed by the authors were as follows:

$$\dot{q}_{center-line}'' = \dot{q}_{peak}'' \frac{z}{FH} \leq 0.4 \quad \text{Eqn. 49}$$

$$\dot{q}_{center-line}'' = \dot{q}_{peak}'' - \frac{5}{3} \left(\frac{z}{FH} - \frac{2}{5} \right) (\dot{q}_{peak}'' - 20), 0.4 \leq \frac{z}{FH} \leq 1 \quad \text{Eqn. 50}$$

$$\dot{q}_{center-line}'' = 20 \left(\frac{z}{FH} \right)^{-5/3}, \frac{z}{FH} > 1 \quad \text{Eqn. 51}$$

Where:

$\dot{q}_{center-line}''$ = heat flux at height z on the centreline of the fire, kW/m²

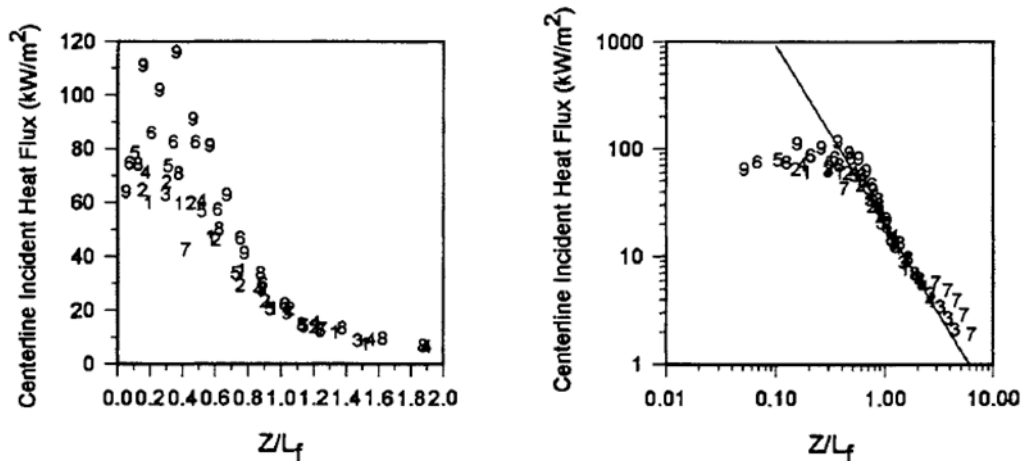
z = height above the burner, m

FH = flame height, m

Table 4. Test conditions and flame heights from Back et al. (1994).

| Test number | \dot{Q} (kW) | D (m) | Videotape FH | 500°C FH |
|-------------|----------------|---------|----------------|------------|
| 1 | 53 | 0.28 | 0.79 | 0.78 |
| 2 | 56 | 0.7 | 0.36 | 0.33 |
| 3 | 68 | 0.48 | 0.6 | 0.51 |
| 4 | 106 | 0.37 | 1.00 | 1.02 |
| 5 | 136 | 0.48 | 0.87 | 0.86 |
| 6 | 204 | 0.48 | 1.45 | 1.45 |
| 7 | 220 | 0.70 | 1.20 | 1.29 |
| 8 | 313 | 0.57 | 2.20 | 2.29 |
| 9 | 523 | 0.70 | - | 2.9 |

In Table 4, the parameter D is the burner edge length.



Used with permission from the International Association of Fire Safety Science (IAFSS).

Figure 13. Measured incident heat fluxes (Back et al., 1994).

3.3.5 Law

Law (1978) developed a methodology for calculating the temperature of external structural steel elements that can be used to calculate the heat flux on a wall from externally venting flames. This approach has been adopted in EN 1991-1-2. The methodology used for a fire venting from a single window opening (termed “no through draught” by Law) with an insulated flange spandrel beam engulfed in flames (i.e. only the face of the web is exposed to external heat transfer) is discussed here. In this case, Law estimated the steady-state temperature of a steel element based on the following equation:

$$\sigma\theta_s^4 + \alpha\theta_s = I_z + \alpha\theta_1 \quad \text{Eqn. 52}$$

Where:

θ_s = temperature of the steel, K

σ = Stefan-Boltzman constant, $5.67 \times 10^{-8} \text{ kW}/(\text{m}^2\text{K}^4)$

α = convective heat transfer coefficient, $\text{W}/(\text{m}^2\text{K})$

θ_1 = flame temperature adjacent to the bottom of the element, K

I_z = incident radiant heat flux, W/m^2

There are two options for calculating I_z , depending on whether the flame height is above the top of the element or not.

$$I_z = \epsilon_3\sigma \left(\frac{\theta_1^4 + \theta_2^4}{2} \right) \text{ if } FH > d_2$$

$$I_z = \epsilon\sigma \left(\frac{\theta_1^4 + \theta_x^4}{2} \right) \text{ if } FH < d_2 \quad \text{Eqn. 53}$$

Where:

θ_2 = flame temperature adjacent to the top of the element, K

θ_x = flame temperature at the tip of the flame, 520°C

d_2 = height of the element, m

ϵ = flame emissivity

The flame emissivity is calculated using the following equation:

$$\epsilon = 1 - e^{-0.30\lambda} \quad \text{Eqn. 54}$$

Where:

λ = flame thickness, m

The temperatures θ_1 and θ_2 are determined using the following equation for the temperature profile along the flame axis:

$$\theta_z = (\theta_w - \theta_o) * \left(1 - 0.4725 \left(\frac{L_x w_t}{\dot{Q}} \right) \right) + \theta_o \quad \text{Eqn. 55}$$

Where:

θ_w = temperature at the opening, K

L_x = length along the flame axis, m

w_t = flame width (equal to W_o)

The window temperature is found by solving this equation at the flame tip for θ_x , which is defined as 520°C. This equation is noted as being valid for $\frac{L_x w_t}{\dot{Q}} < 1$ in EN 1991-1-2. The flame geometry is as given in Figure 14. The convective heat transfer coefficient is calculated using the following equation:

$$\alpha = 4.67 \left(\frac{1}{d_{eq}} \right)^{0.4} \left(\frac{\dot{Q}}{A_v} \right)^{0.6} \quad \text{Eqn. 56}$$

Where:

d_{eq} = characteristic length of external structural element, m

In order to use this methodology to calculate the heat flux on the façade, Eqn. 52 was rearranged as follows:

$$\dot{q}'' = I_z - \sigma\theta_o^4 + \alpha * (\theta_1 - \theta_o) \quad \text{Eqn. 57}$$

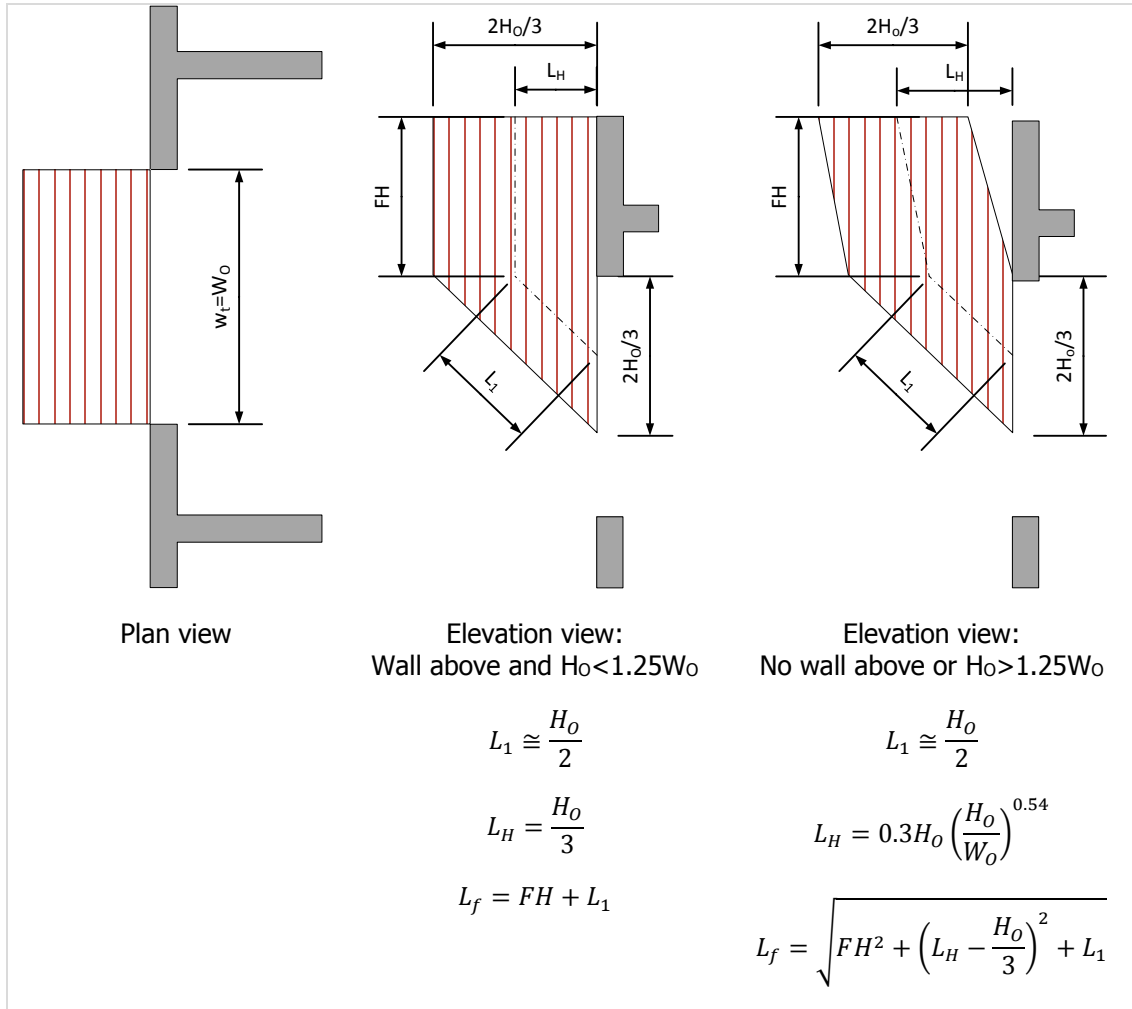


Figure 14. Flame geometry from Law (1978): no through draft, single opening.

3.3.6 Abecassis Empis

Abecassis Empis (2010) developed a simplified correlation for estimating the maximum heat flux \dot{q}'' in kW/m² on a wall above a flame projected from an opening at height Z in m above the top of the opening. For the condition of a single window opening from a compartment (no through draught), the correlation is as follows:

$$\dot{q}'' = 16 * (1 - \ln(Z)) \quad \text{Eqn. 58}$$

The maximum heat flux is given an uncertainty band of ± 10 kW/m², and the applicability is limited to a height range of $0.05 \text{ m} < Z < 2.7 \text{ m}$.

4. Modelling heat transfer from flames with FDS

Fire Dynamics Simulator (FDS) is a computational fluid dynamics (CFD) model and is one potential tool that can be used either to directly evaluate the effects of fire from external openings on building exteriors or as a virtual experimentation tool to develop simplified correlations for external opening flame characteristics.

FDS is widely used by fire engineers because it is provided free of charge from a reputable source and also because it has been extensively validated through comparison to existing experimental data (McGrattan et al., 2016). This validation includes flame height and heat flux from flames comparisons, including flames projecting from external openings.

The following section describes relevant comparisons of FDS output to experimental measurements from the FDS validation report. The validation report is continually being rerun through an automated system with the most current version of FDS. The version of FDS used for the validation report run described here is 6.5.2.

The ability of FDS to correctly model heat flux on an external surface from flames projected from an opening depends on several factors. The heat source must be correctly represented, with the correct amount of heat generated from combustion in the appropriate locations, represented by the overall heat release rate and the flame/plume geometry. Next, the heat transfer to the surface must be correctly modelled, including radiation (for which there is a submodel in FDS) as well as the convection, which depends on the ability of the fluid flow field to be correctly modelled.

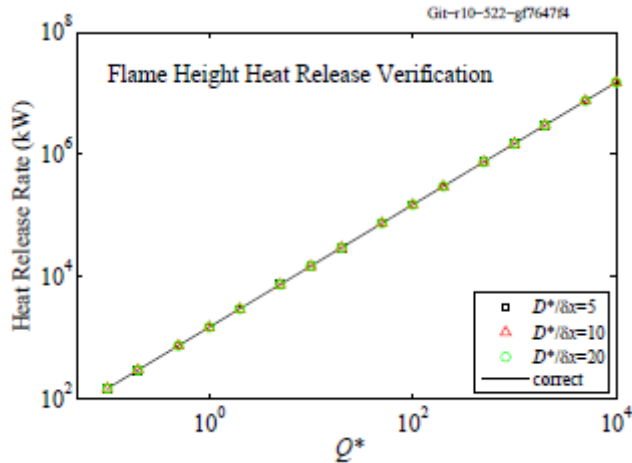
The validation information related to these aspects are covered here, starting from simple cases of the flame height and heat flux to an open target from free-burning flames in the open, progressing to heat flux from a free-burning flame to an adjacent wall to the final case of heat flux on an external wall from flame projecting from an opening. A subset of the validation results is included with best and worst-case agreements subjectively chosen for discussion. For full validation results, refer to the FDS validation report.

4.1 Heat release rate, flame height and flame profile

The ability of FDS to estimate flame height has been compared to a number of correlations and one set of experimental data for free-burning propane fires in 1 m by 1 m square pan burners. The experimental data comparison was limited to the heat release rate profile and not actual measured experimental flame heights.

The heat release rate was verified for each heat release level with three mesh resolutions. It should be noted that the fire was modelled as a surface producing a fixed fuel supply corresponding to the heat release rate per unit area (HRRPUA).

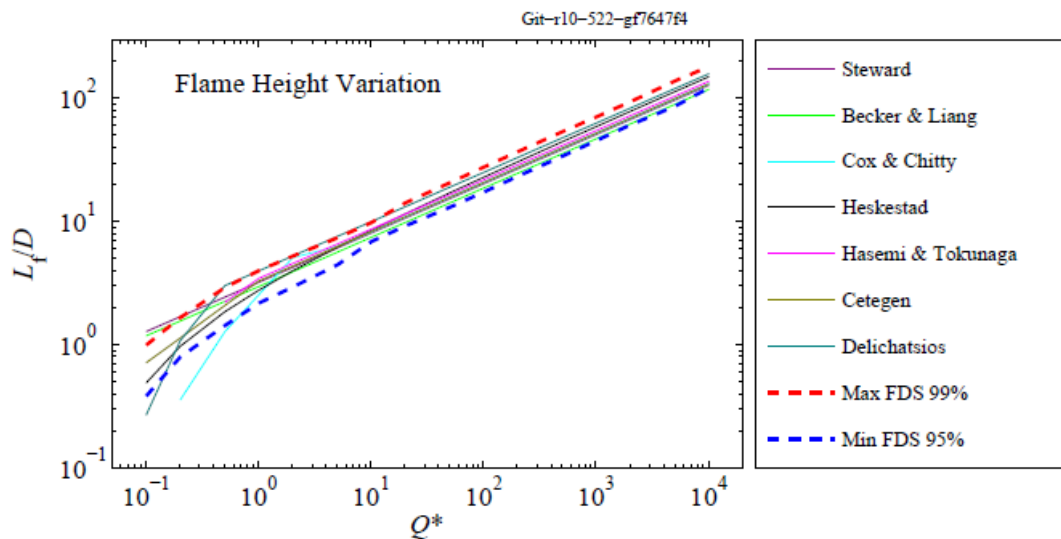
Figure 15 shows the heat release rate verification.



Reprinted courtesy of the National Institute of Standards and Technology, US Department of Commerce.

Figure 15. FDS heat release rate verification for 1 m x 1 m propane fires (McGrattan et al., 2016).

The top of the flame is estimated to coincide with the height where a set percentage of the heat release rate occurs below, obtained by numerically integrating the time-averaged heat release rate per unit area over the height of the domain. In the validation report, 95% and 99% of the total heat release rate are used as the threshold levels for comparison. FDS showed excellent agreement with the correlations considered, as shown in Figure 16.

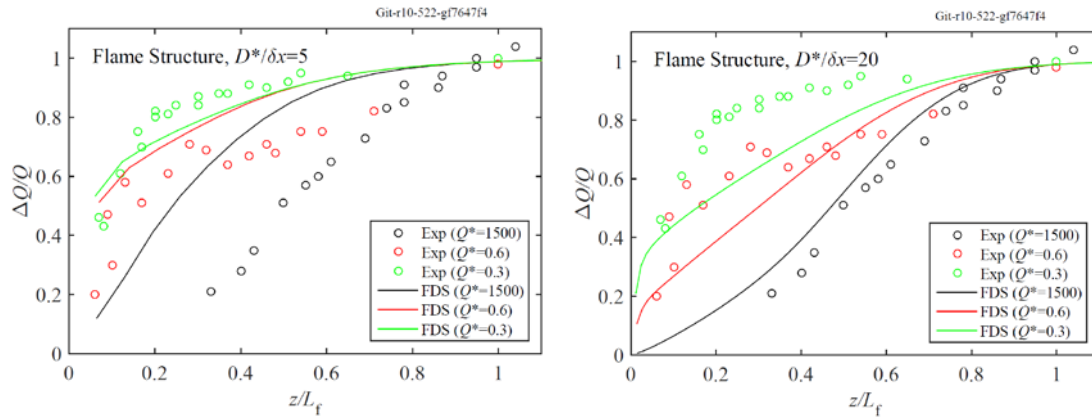


Reprinted courtesy of the National Institute of Standards and Technology, US Department of Commerce.

Figure 16. Comparison of flame heights from FDS to several correlations (McGrattan et al., 2016).

The flame heat release rate profile (heat release rate as a function of height) was compared to one set of experimental data for three mesh sizes. As the mesh was refined, the profile of the smaller fire improved, but the profile of the large fire deteriorated.

The two limits of the mesh refinement are shown in Figure 17.



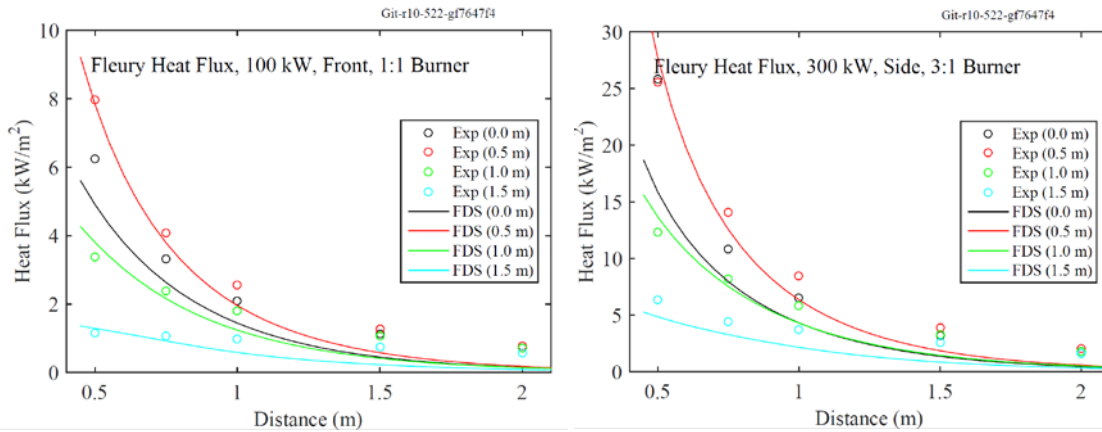
Reprinted courtesy of the National Institute of Standards and Technology, US Department of Commerce.

Figure 17. Comparison of FDS flame profile to experimental data (McGrattan et al., 2016).

4.2 Heat flux to targets

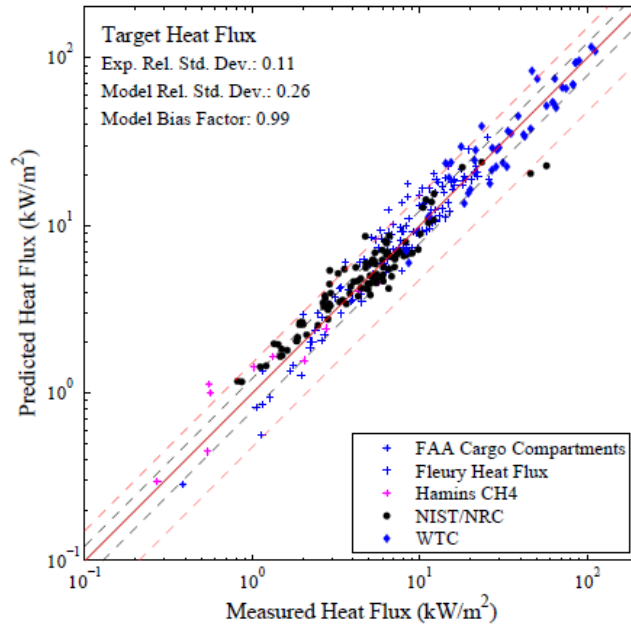
The basic ability of FDS to calculate the heat flux from a steady free-burning propane fire to a target was evaluated with comparison to an experimental study by Fleury (2010) among others.

Selected comparisons to Fleury’s experimental results are shown in Figure 18, and a log-log scatterplot comparing all of the experimental results to FDS results is shown in Figure 19.



Reprinted courtesy of the National Institute of Standards and Technology, US Department of Commerce.

Figure 18. Selected results from FDS heat flux comparisons to Fleury’s experimental data (McGrattan et al., 2016).

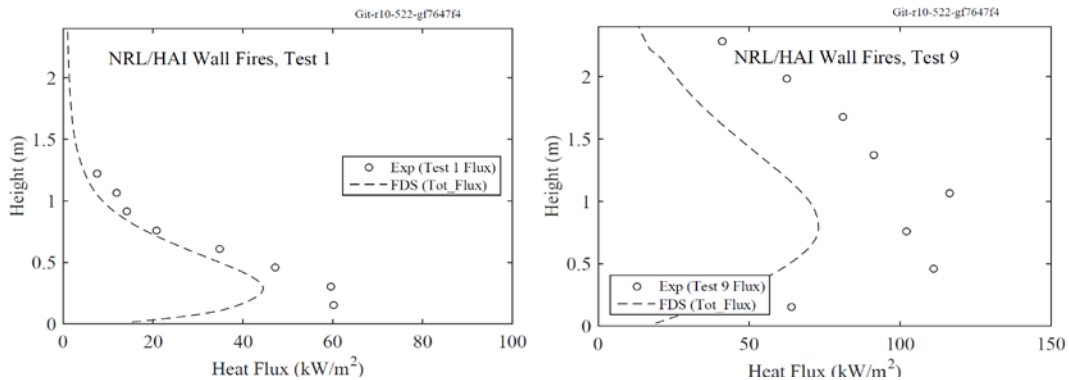


Reprinted courtesy of the National Institute of Standards and Technology, US Department of Commerce.

Figure 19. Scatterplot of FDS predicted heat flux values to targets compared to experimental measurements (McGrattan et al., 2016).

4.3 Heat flux on walls from adjacent flames

The NRL/HAI experiments by Back et al. described in section 3.3.4 were modelled in FDS. Selected results are shown in Figure 20, which represent the extremes of the best and worst fits. The heat flux estimated by FDS was a better fit for smaller fires than for larger fires.

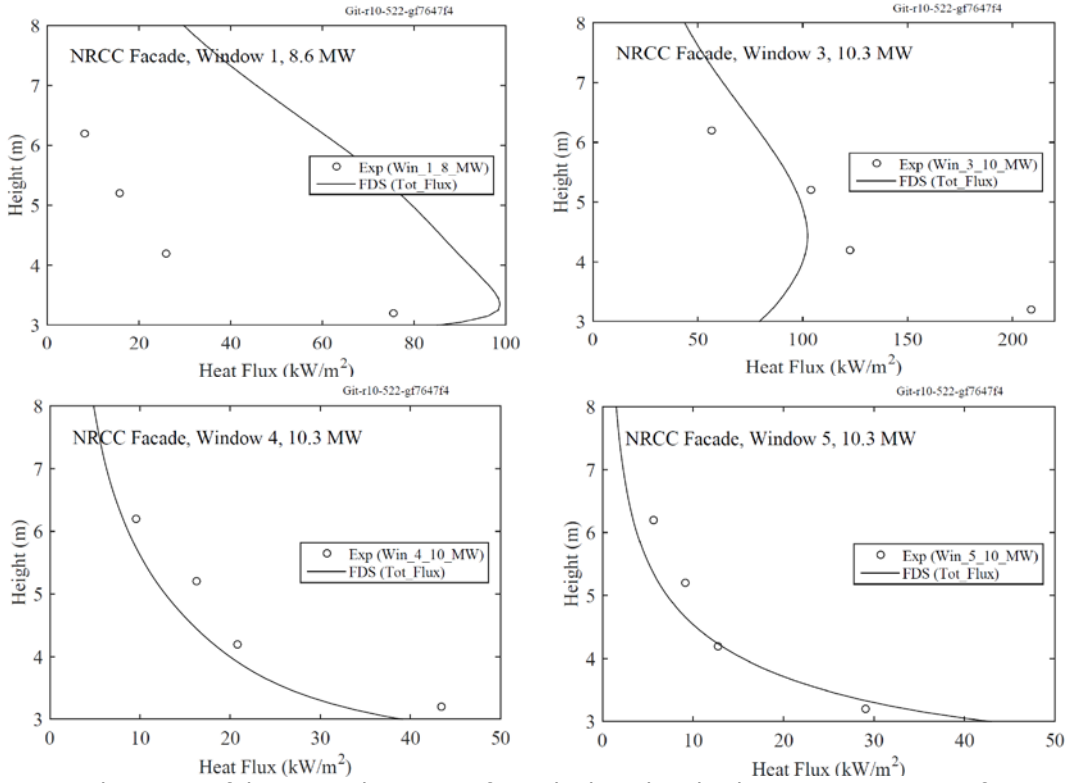


Reprinted courtesy of the National Institute of Standards and Technology, US Department of Commerce.

Figure 20. Selections from FDS heat flux comparisons to experimentally measured wall heat flux by NRL/HAI (Back et al.) (McGrattan et al., 2016).

4.4 Heat flux on external walls from flames projecting from openings

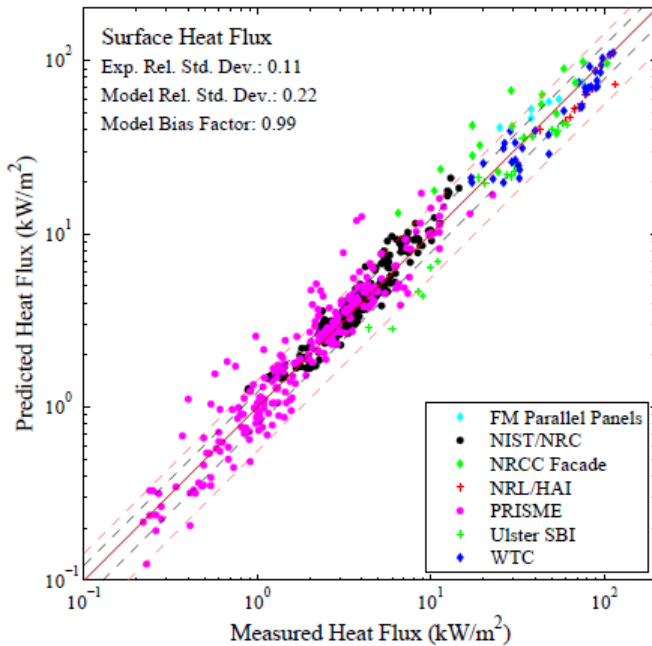
Heat flux from the NRCC façade experiments (Oleszkiewicz, 1989) was simulated in FDS. Heat release rates and flame heights calculated from FDS were not reported. Again, selected data shown in Figure 21 displays the range of fits to this experimental data set. FDS results matched experimental results better when the maximum heat flux was low.



Reprinted courtesy of the National Institute of Standards and Technology, US Department of Commerce.

Figure 21. Selected comparisons of FDS results to the NRCC façade experimental data (McGrattan et al., 2016).

A scatterplot of FDS validation results for heat flux to ceilings, walls and floors is shown in Figure 22.



Reprinted courtesy of the National Institute of Standards and Technology, US Department of Commerce.

Figure 22. Scatterplot of FDS predicted heat flux to walls, ceilings and floors compared to experimental measurements including NRL/HAI (Back et al.) and NRCC façade data (McGrattan et al., 2016).

4.5 Effects of aprons on heat flux on external walls from flames projecting from openings

Nilsson (2016) used FDS to investigate apron (horizontal projections) effects on the heat flux on a wall above a flame projecting from openings representing a window and a door. An additional lower rear opening that was 0.5 m high and 4.0 m wide was also included in the model, which is similar to the SP105 façade test compartment configuration. Relative and absolute exposures using adiabatic surface temperature and incident heat flux were used. A reduction in heat flux was demonstrated with horizontal projections, but the incident heat flux levels predicted were lower than 16 kW/m² in most instances, other than the reference window case with no apron, which exceeded 16 kW/m² up to approximately 0.8 m above the opening.

This was likely due to the heat release rates being considered (3.1 MW and 4 MW as a sensitivity check), which were lower than the ventilation limit for the two opening configurations (4.1 MW and 5.3 MW for the lower opening plus the window and door, respectively). These heat release rates were partially justified by noting that FDS simulations with underventilated fires had been shown to have large errors in previous research.

5. Experimental study

Multiple intermediate-scale fire tests were conducted with the following objectives:

- Understanding projected flame phenomena comprehensively using non-gas burner fuels.
- Comparing projected flame heights to the existing correlations for validation.
- Developing a method to estimate projected flame heights.
- Understanding heat flux levels on the wall above the opening.

A 1.3 m (D) × 1 m (W) × 0.8 m (H) compartment was located under an exhaust hood connected to an oxygen consumption calorimeter from which heat release rates were measured. The compartment was made of 15 mm thick calcium silicate boards, and a layer of 12 mm thick ceramic fibre board was added as an internal lining material. Their physical and thermal properties are included in Table 5.

Table 5. Physical and thermal properties of compartment materials.

| | Calcium silicate board ¹ | Ceramic fibre board ² |
|----------------------|-------------------------------------|----------------------------------|
| Thickness | 0.015 m | 0.012 m |
| Density | 975 kg/m ³ | 280 kg/m ³ |
| Thermal conductivity | 0.242 W/m-K | 0.0002×T(K)-0.05 W/m-K |
| Heat capacity | - | 1130 J/kg-K |

5.1 Compartment configuration and instrumentation

The main target measurements were projected flame heights out of an opening and heat flux values on the wall above the opening. Other measurements such as heat release rates based on fuel mass loss rates and compartment gas temperatures were also obtained to understand associated compartment and projected flame phenomena comprehensively. The compartment configuration is shown in Figure 23.

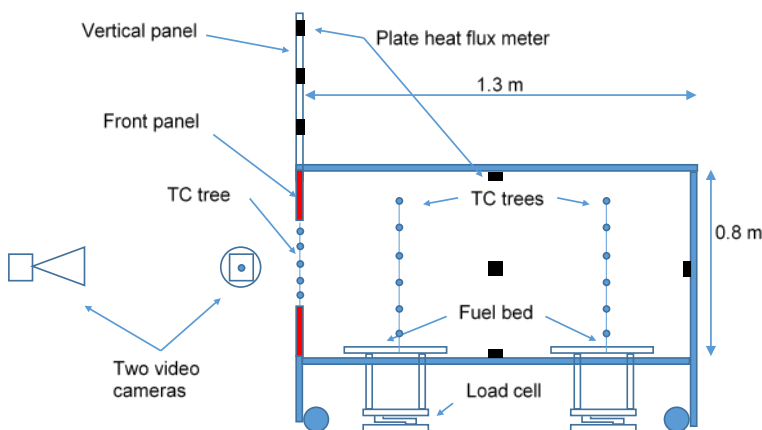


Figure 23. Compartment configuration and instrumentation.

¹ www.promat-ap.com/download/file/en/f4c8910657fd49ecb065a789008f381a?rev=9b977641-268d-4368-8f3b-48ee83df33dd

² www.forman.co.nz/media/emizen_banner/m/o/morgan_advanced_materials_superwool_plus_vacuuum_formed_board_datasheet.pdf

A total of six plate heat flux meters were located on the vertical panel above the opening as shown in Figure 24. In addition, five plate heat flux meters were located within the compartment: three on the side walls except the front panel, one on the ceiling and one on the floor.

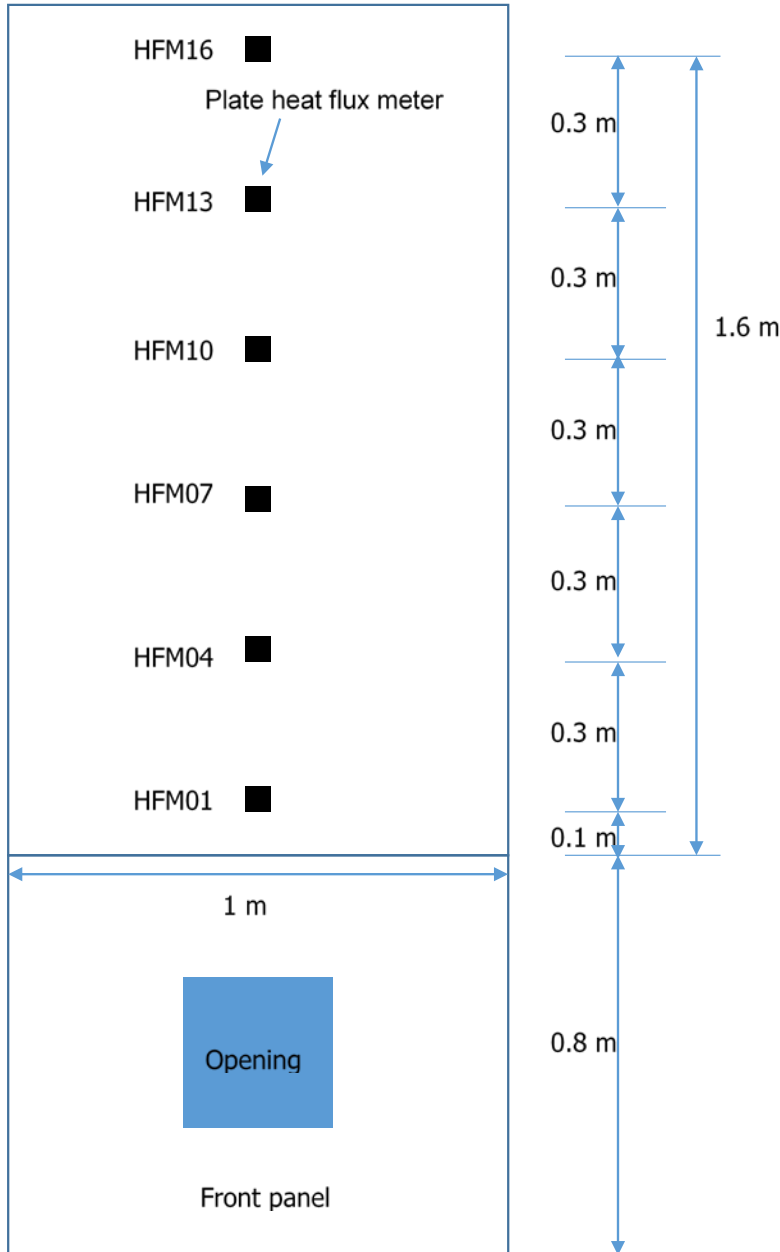


Figure 24. Heat flux meter locations (front elevation view).

Two fuel beds were located in the compartment to check the effect of the fuel location in the compartment on the heat release rate, projected flame heights and heat flux values. Each fuel bed was placed on a load cell (Avery Berkel T109 super-precision load cell, 30 kg) to measure fuel mass changes as shown in Figure 25.

Mass loss rate data was recorded to measure vaporisation or pyrolysis and was also used to estimate heat release rates based on the heat of combustion established from free-burning fires (outside of a compartment), assuming complete combustion.

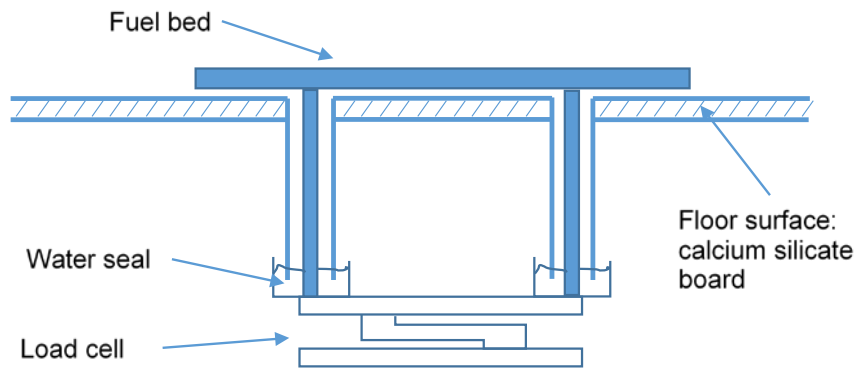


Figure 25. Section view of the fuel bed.

Two thermocouple trees were installed on the side walls at two different locations: one closer to the front panel and the other closer to the back panel. The detailed locations are included in Figure 26.

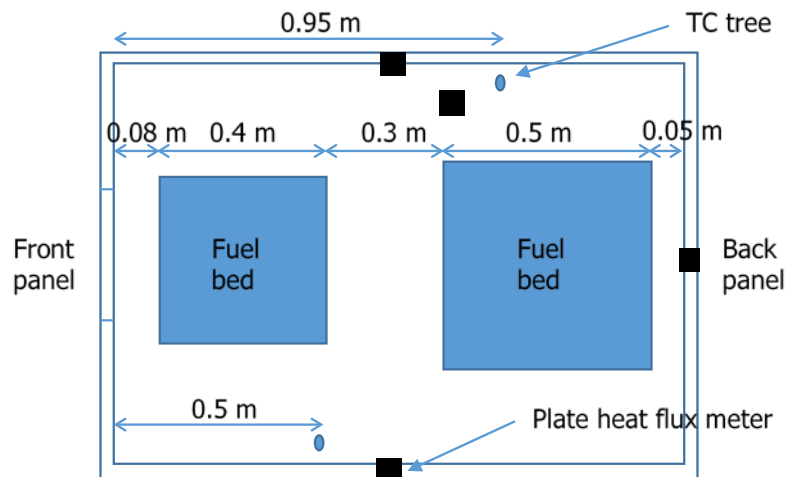


Figure 26. Plan view of the compartment.

Each tree consisted of seven Type K thermocouples located 0.05 m from the finished floor level with a 0.1 m separation distance. The thermocouple beads were positioned approximately 0.01 m off the wall surface. Additionally, five thermocouples were located at the opening with a 0.05 m separation distance to measure the incoming and exiting flow temperatures. The location of the thermocouples varied depending on the opening position in the front panel (details are provided in Appendix I).

The thermocouples and load cells were connected to the data acquisition system, which was a National Instruments cDAQ-9178 chassis with four NI9213 modules for thermocouples and one NI9237 module for load cells.

Two video cameras were used to record the front view and side view of projected flames. A scaled board was held on the centreline of the compartment opening at the start of each test in view of each camera to calibrate length to the number of pixels for flame height estimation from the video.

5.2 Experimental program

The majority of the tests used a 0.3 m square opening with the variations of opening locations in the front panel, fuel type, fuel location in the compartment and fuel surface area. Three additional tests examined variation of the opening size. Two were sized to use the same $A_o\sqrt{H_o}$ ventilation factor of $0.049 \text{ m}^{5/2}$ (ventilation-limited heat release rate = $1500A_o\sqrt{H_o} = 74 \text{ kW}$) but vary the aspect ratio from tall to wide (0.1 m wide by 0.625 m high and 0.5 m wide by 0.214 m high), and one doubled the ventilation factor by doubling the width (0.6 m high by 0.3 m wide).

5.2.1 Opening location in the front panel

An opening of 0.3 m (W) by 0.3 m (H) was made on the front panel (1 m (W) × 0.8 m (H)) being located at different heights: one in the middle and the other at the top of the panel as shown in Figure 27. For the other opening sizes, the opening was centred on the front panel.

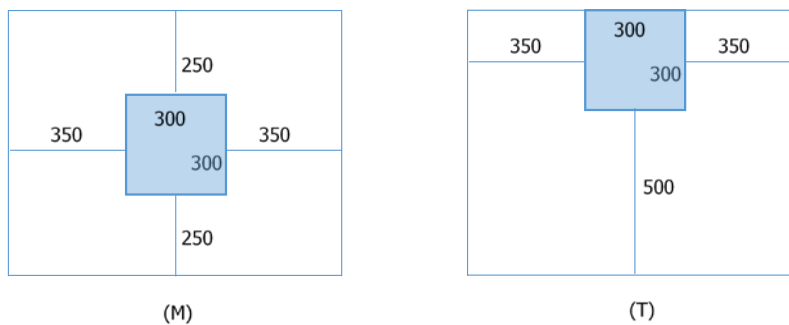


Figure 27. Location of opening in front wall.

5.2.2 Fuel

Two different fuels were used: heptane and wood cribs. Heptane has been widely used in fire tests due to its thermal stability at an ambient temperature and its chemical homogeneity. Wood cribs have been also frequently used due to their heat of combustion value and burning and fire spread behaviour similar to realistic fuels. Important thermal and fire properties of these fuels are summarised in Table 6.

Table 6. Thermal properties of heptane and wood cribs.

| Typical properties | Heptane | Wood cribs |
|---------------------------------------|-----------------------|--|
| Effective heat of combustion (kJ/g) | 41.2 | 18~12 (Babrauskas, 2008; Tewarson, 2008) |
| Stoichiometric air-to-fuel mass ratio | ~15 | ~5.7 (Babrauskas, 2008) |
| Heat of gasification (kJ/g) | 0.55 (Tewarson, 2008) | ~1–2.2 (Tewarson, 2008) |

The effective heat of combustion and stoichiometric mass-based air/fuel ratio are both approximately three times greater for heptane than for wood, which means that the amount of heat produced per mass of air is about the same for both fuels. The heat of gasification is between two and four times less for heptane compared to wood. The ratio of combustion energy to gasification energy is about 6–12 times higher for heptane when compared to wood. This means that heptane vaporisation should respond more to heat feedback than wood pyrolysis.

The heptane pan was located in a water bath to prevent warping while being heated by the flames as shown in Figure 28. The sides of this retention pan were insulated using a ceramic fibre blanket to minimise heat transfer to the pan.

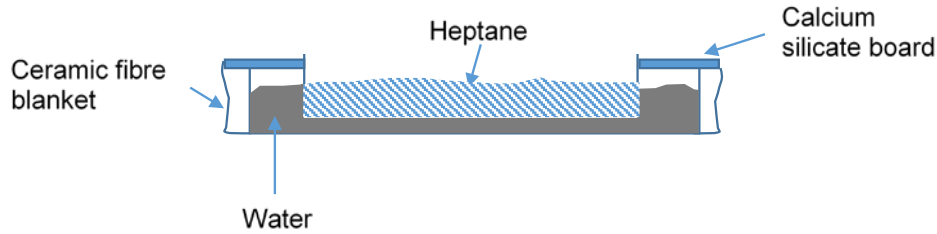


Figure 28. Section view of a heptane pan and a retention pan.

This configuration also promoted a relatively stable peak heat release rate and mass loss rate as shown in Figure 29. To exclude the evaporation of water in the fuel mass loss rate calculation, the gap between two pans was covered by a tightly fitted calcium silicate board.

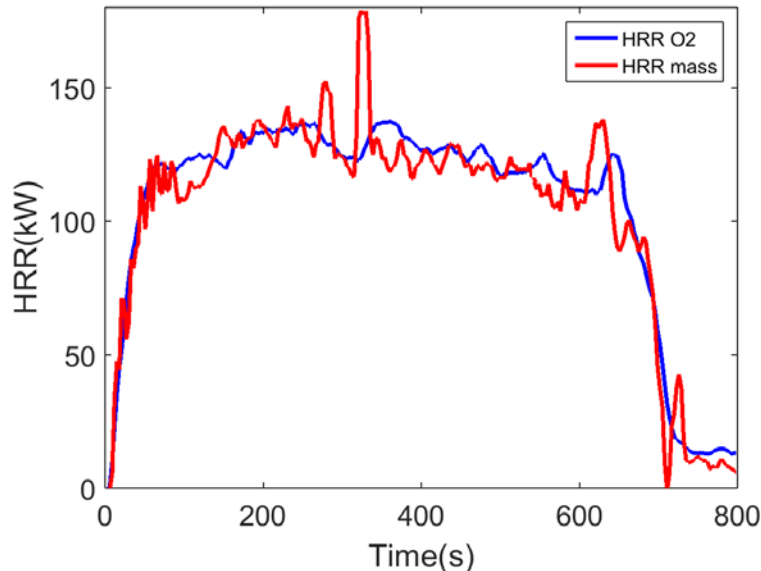


Figure 29. Free-burning heat release rate of a 2L heptane fire in a 300 mm by 300 mm pan.

The heat release rate measured with oxygen depletion calorimetry and the mass loss rate were compared for a free-burning fire consisting of 2 L of heptane in a 0.3 m by 0.3 m pan. Figure 29 compares the estimated heat release rate from the mass loss rate using an effective heat of combustion of 41.2 kJ/g with the heat release rate measured by oxygen depletion calorimetry.

Except for the short peak at about 300 s in the heat release rate estimated from mass loss, the two methods of determining heat release rates were in good agreement. Between 100 s and 600 s the heat release rate based on oxygen calorimetry had a mean of 126 kW and a standard deviation of 7 kW.

The mean heat release rate during this stable burning period represented 170% of the ventilation-limited heat release rate based on the ventilation factor of the standard 0.3 m square opening.

A wood crib was also used as a fuel type. Each wood crib was manufactured as shown in Figure 30 with 12 rows and eight cribs per row and was conditioned at 68°C and 50% RH for about 24 hours before each experiment. The material of wood was likely to be *Pinus radiata*, and its density after drying was approximately 476 kg/m³.

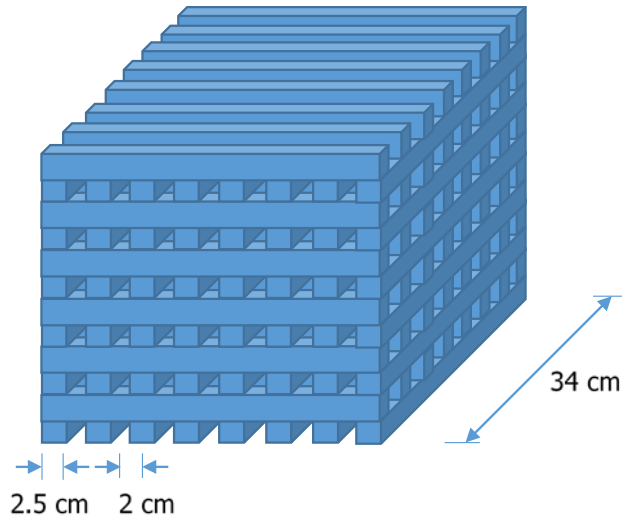


Figure 30. Wood crib configuration.

As for the heptane free-burning experiment, the heat release rate measured by oxygen depletion calorimetry was compared to the mass loss rate for a free-burning wood crib fire experiment. The oxygen depletion heat release rate and the estimated heat release rate based on the mass loss rate and an effective heat of combustion of 15.5 kJ/g for the free-burning wood crib fire are compared in Figure 31.

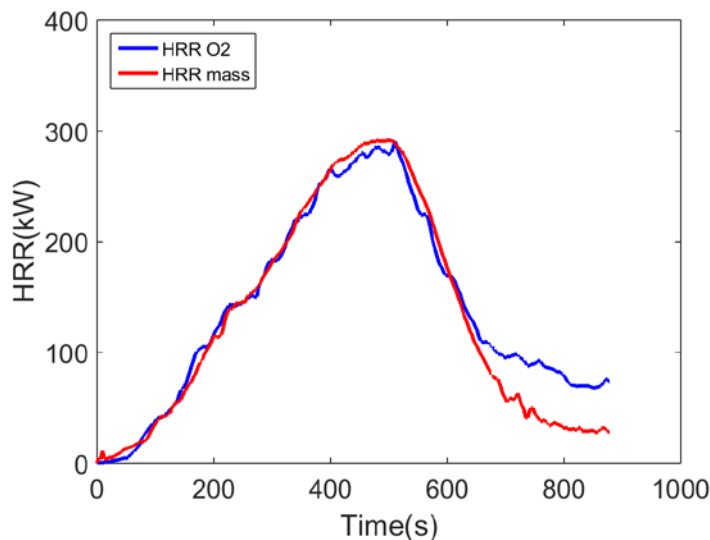


Figure 31. Free-burning heat release rate of the wood crib shown in Figure 30.

The deviation between the oxygen depletion heat release rate and the estimated heat release rate based on mass loss rate towards the end of the experiment can be explained by an increase in the effective heat of combustion as the gasified materials containing the majority of the hydrogen have mostly been driven off and the remaining material burning is mostly high carbon char, as observed by Babrauskas (2008). No stable burning period was observed with the wood crib – the heat release rate grew to a peak and then decayed. The peak heat release rate of 290 kW represented 390% of

the ventilation-limited heat release rate based on the ventilation factor of the standard 0.3 m square opening, and the heat release rate was above 150% of the ventilation-limited heat release rate from 200 s to 650 s.

The exposed surface area of wood in the crib was approximately 3.3 m², about 36 times greater than the surface area for the small heptane pool (0.09 m²). The heptane gasified at a much higher rate per fuel surface area (about 34 g/(m²s) at 126 kW) compared to the wood (about 6 g/(m²s) at 290 kW) and with the higher heat of combustion produced about 15 times more combustion energy per exposed surface area of fuel (1400 kW/m² for heptane compared to 90 kW/m² for wood).

Two alternative fuel beds were located in the compartment at the front and back. The front one was located close to the front panel and the opening, and the back one was close to the rear wall of the compartment. Both locations were centrally positioned between the side walls.

For the heptane fuel type, two different pan sizes were used: 0.3 m square and 0.4 m square resulting in fuel surface areas of 0.09 m² and 0.16 m², respectively. For the wood crib, only one wood crib size as shown in Figure 30 was used.

5.2.3 Test matrix

The experimental test matrix is shown in Table 7. The test IDs were named by taking the first letters of each variable (heptane or wood fuel type – middle or top opening location – front or back fuel location – 2L for 0.3 m pan or 3L for 0.4 m pan fuel surface area).

5.3 Flame height measurement

Projected flame heights were calculated at 50% intermittency after processing still frames extracted from the experimental video every 0.5 s. A flame region was extracted from each image as shown in Figure 32. The extracted images were overlapped over a 10-second period to identify the 50% intermittency region. Therefore, a single averaged flame height was obtained for every 10 seconds of experiment time.

The height from the neutral plane to the opening soffit is estimated to be 60% of the opening height and subtracted from the image analysis flame heights to obtain the flame height from the window soffit as shown in Figure 4.

5.4 Incident heat flux measurement

The plate heat flux meters were manufactured as shown in Figure 33 consisting of (from exposed side to unexposed side) a thin metal plate, two layers of ceramic fibre board and a calcium silicate board. The assembly was fastened together by two thin metal wires. The metal plate surface was sprayed with a black-coloured high-temperature paint such that the emissivity (or absorptivity) of the metal surface was assumed to be 0.9 (Veloo & Quintiere, 2013). To prevent abrasion of the calcium silicate board by the wire, a single layer of duct tape was applied to the back surface of the calcium silicate board. Details of the construction of the plate heat flux meters and the calibration and the heat flux measurement correlations are included in Appendix A and Appendix B, respectively.

Table 7. Test matrix.

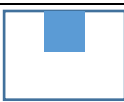
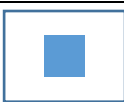
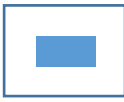
| Test ID | Symbolic ID (side view) | Opening location (front view) | Fuel type | Fuel location | Fuel surface area |
|----------------|---|---|------------|---------------|--|
| H-M-F-2L |  |  | Heptane | Front | 0.3m by 0.3m (2L) |
| H-M-B-2L |  |  | Heptane | Back | 0.3m by 0.3m (2L) |
| H-M-B-3L |  |  | Heptane | Back | 0.4m by 0.4m (3L) |
| H-T-F-2L |  |  | Heptane | front | 0.3m by 0.3m (2L) |
| H-T-B-2L |  |  | Heptane | Back | 0.3m by 0.3m (2L) |
| H-T-B-3L |  |  | Heptane | Back | 0.4m by 0.4m (3L) |
| W-M-F |  |  | Wood cribs | Front | Eight 0.025 m thick and 0.34 m long wood crib per row, 12 rows |
| W-M-B |  |  | Wood cribs | Back | Eight 0.025 m thick and 0.34 m long wood crib per row, 12 rows |
| W-T-F |  |  | Wood cribs | Front | Eight 0.025 m thick and 0.34 m long wood crib per row, 12 rows |
| W-T-B |  |  | Wood cribs | Back | Eight 0.025 m thick and 0.34 m long wood crib per row, 12 rows |
| H-100-625-B-3L |  |  | Heptane | Back | 0.4m by 0.4m (3L) |
| H-500-214-B-3L |  |  | Heptane | Back | 0.4m by 0.4m (3L) |
| H-600-300-B-3L |  |  | Heptane | Back | 0.4m by 0.4m (3L) |



Figure 32. Flame region identification.



Figure 33. A side view of the plate heat flux meter.

6. Experimental results

Experimental data from this study is included in graphical form in the appendices as listed below:

- Appendix D: Heat release rates and flame heights
- Appendix E: External wall heat flux
- Appendix F: Compartment temperatures
- Appendix G: Compartment heat flux
- Appendix H: Neutral plane heights
- Appendix I: Temperatures at the opening

6.1 Heat release and mass loss rates

The heat release rates measured by calorimetry (HRR-O₂) and estimated from the measured mass loss rate using the effective heat of combustion (HRR-Mass) are shown in Appendix D. The HRR-Mass represents the equivalent heat release of the fuel evaporating or pyrolysing from the fuel package and freely burning in the open. When comparing the two methods of determining the heat release rate, some common characteristics arose as shown in Figure 34.

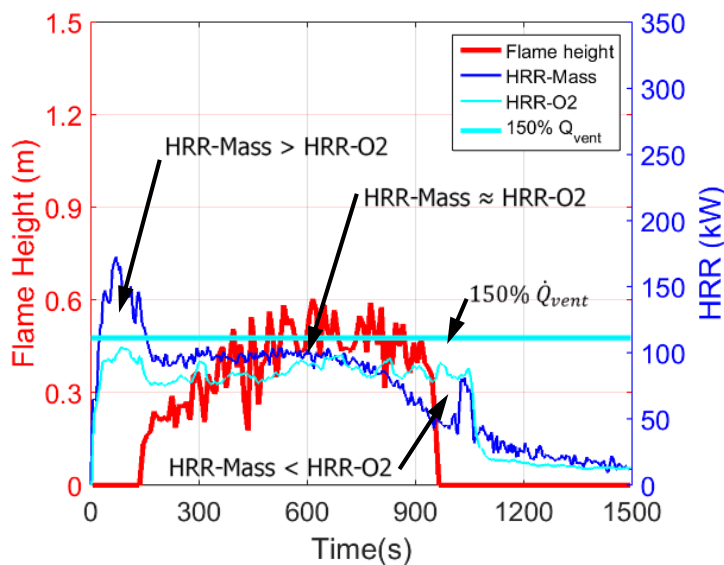


Figure 34. Flame height and heat release rate for experiment H-500-214-B-3L.

In the early stages, it was common for the heat release rate estimated from the measured mass loss rate to exceed the calorimetry heat release rate, particularly when no external flaming was observed. This indicates that excess fuel vapour was being produced that was either not burning or partially burning. If external flaming was established, the gap between the heat release rate determined via the two methods would decrease, which indicated that the fuel was burning near the same efficiency as in the free-burning experiments. In the decay phase, the heat release rate estimated from the measured mass loss rate would typically drop below the heat release rate determined by calorimetry. This was likely due to two factors: an accumulation of unburned fuel vapours or deposits burning once additional fuel vapour generation from the fuel package decreased (for both heptane and wood fires) and secondly, for the wood crib fires, an increase in the effective heat of combustion as observed in the wood free-burning experiment.

In the early stages of the fire, there was a large excess of fuel as noted by the excess HRR-Mass (mass loss based) compared to the HRR-O₂ (oxygen depletion calorimetry based). Once external flaming was observed, the gap decreased and then reversed as the fire entered the decay phase

6.1.1 Comparison to free-burning heat release rate

For the fires where a free-burning (no compartment) heat release rate comparison experiment was available (small heptane pool and wood crib fires), the compartment had a net effect of reducing the heat release rate in all experiments except one (H-M-F-2L), which had a peak heat release rate greater than measured in the free-burning experiment.

This was expected, as for both types of fires, the free-burning heat release rate was greater than the ventilation-limited heat release rate. The increase in heat release rate for experiment H-M-F-2L could have been due to the close proximity of the opening to the fuel surface, which would have allowed increased radiation feedback from the external flame to the fuel surface.

Despite the wood having a greater free-burning heat release rate than the small heptane pan, the maximum heat release rate was similar for both sources in all similar compartment ventilation scenarios except for the front-middle configuration. The maximum calorimetry-based heat release rate for the H-M-F-2L experiment was approximately 2.5 times greater than for the W-M-F case, as compared in Figure 35. The HRR-Mass and HRR-O₂ were in agreement for experiment H-M-F-2L once the external flame got established.

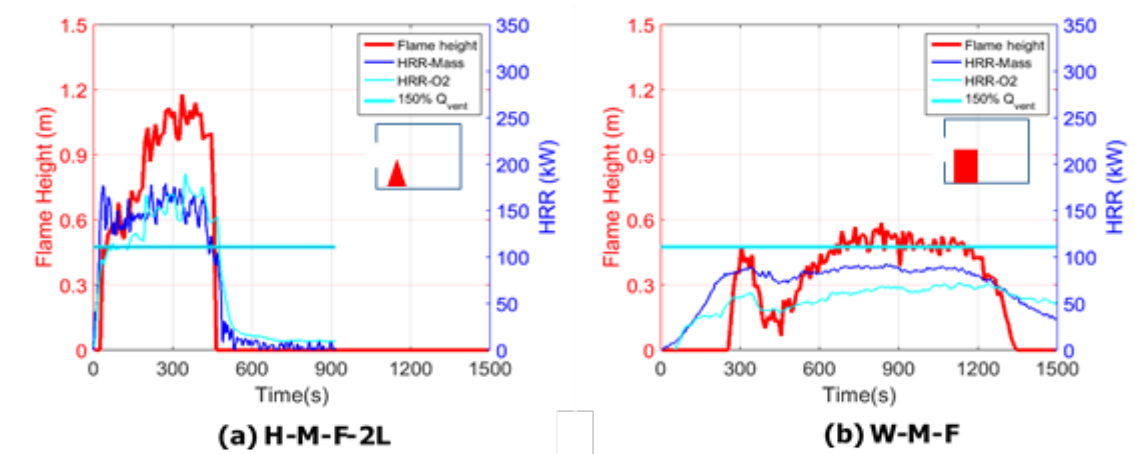


Figure 35. Flame height and heat release rate compared for experiments: (a) H-M-F-2L; (b) W-M-F.

6.1.2 Comparison to the theoretical ventilation-limited heat release rate

The ratio of the maximum heat release rate (calorimeter) to the theoretical ventilation-limited heat release rate in the compartment for each experiment is shown in Table 8. Four experiments had a maximum heat release rate that exceeded 150% of the theoretical ventilation-limited heat release rate (the C/VM2 design fire specification for flashover fires described in section 2.3) in the compartment. All had an opening centred at the mid-height of the compartment, three had the large heptane pool at the

back location and one had the small heptane pool at the front location. These experiments also had the greatest flame heights, shown in Figure 36.

Table 8. Ratio of maximum heat release rate (measured by calorimetry) to the ventilation-limited heat release rate for reduced-scale experiments.

| Fuel | Opening size (mm x mm) | Fuel location | $\dot{Q}_{max}/\dot{Q}_{vent\ limit}$ | |
|------------|------------------------|---------------|---------------------------------------|-------------|
| | | | Middle opening | Top opening |
| 2L heptane | 300 x 300 | Front | 257% | 133% |
| 2L heptane | 300 x 300 | Back | 128% | 119% |
| 3L heptane | 300 x 300 | Back | 236% | 142% |
| wood | 300 x 300 | Front | 97% | 135% |
| wood | 300 x 300 | Back | 122% | 115% |
| 3L heptane | 100 x 625 | Back | 255% | |
| 3L heptane | 500 x 214 | Back | 140% | |
| 3L heptane | 600 x 300 | Back | 231% | |

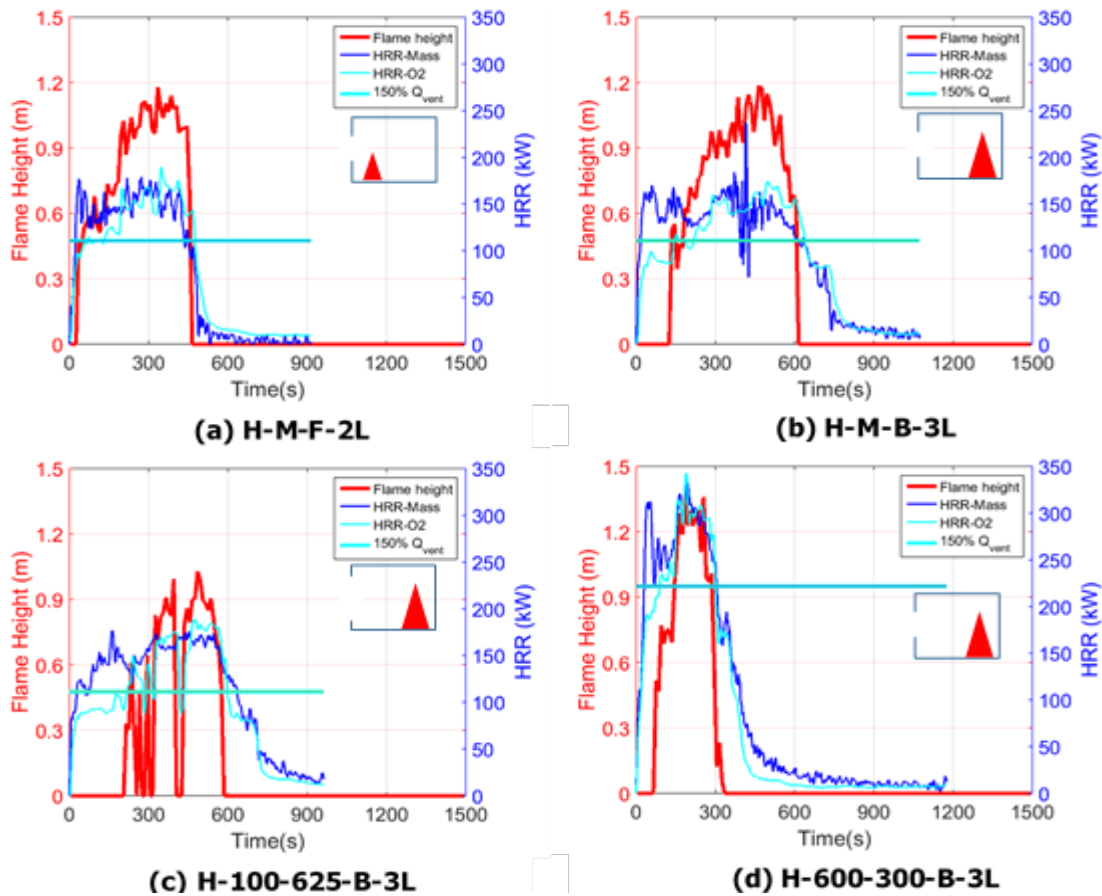


Figure 36. The flame height and heat release rate compared for experiments where the maximum HRR-O2 exceeded 150% of the ventilation-limited heat release rate.

The factors listed by Drysdale (section 3.1.3) of large fuel area and low heat of vaporisation responding to radiation feedback to create excess fuel vapour are a likely cause. The increased radiation feedback from burning near the adjacent opening could have compensated for the smaller fuel area in experiment H-M-F-2L. H-M-F-2L and H-M-B-3L had similar heat release rate characteristics except the longer duration of H-M-B-3L, which is expected due to the larger volume of fuel.

For the data in Table 8, the ventilation-limited heat release rate was 74 kW for all of the experiments except for the experiment with the 600 mm × 300 mm opening, which had a ventilation-limited heat release rate of 148 kW. For comparison, the Law correlation in Eqn. 7 predicts maximum heat release rate to ventilation-limited heat release rate ratios of 182% and 166% for wood-fuelled fires in the reduced-scale compartment with the 300 mm square and 600 mm x 300 mm openings, respectively.

The wood and small heptane pool fires had similar trends in maximum heat release rate for all configurations except for the front middle opening location. The heat release rate for the W-M-F fire may have been decreased due to the wood crib partially obstructing airflow through the vent. As previously discussed, the heat release rate for the H-M-F-2L fire may have been enhanced by the plume tilting out of the opening and additional radiation feedback from the external fire to the liquid heptane surface with the proximity of the opening to the pan. Of the five large heptane pool experiments, three had maximum HRR-O2 between 2.3 and 2.6 times the ventilation-limited heat release rate. This included experiment H-600-300-B-3L, which doubled the ventilation-limited heat release rate. Two of the large heptane pool experiments, H-T-B-3L and H-500-214-B-3L, had maximum HRR-O2 values between 1.4 and 1.5 times the ventilation-limited heat release rate. Maximum HRR-O2 values were 20% and 10% higher than the corresponding respective small heptane pool experiments (H-T-B-2L and H-M-B-2L) as shown in Figure 37.

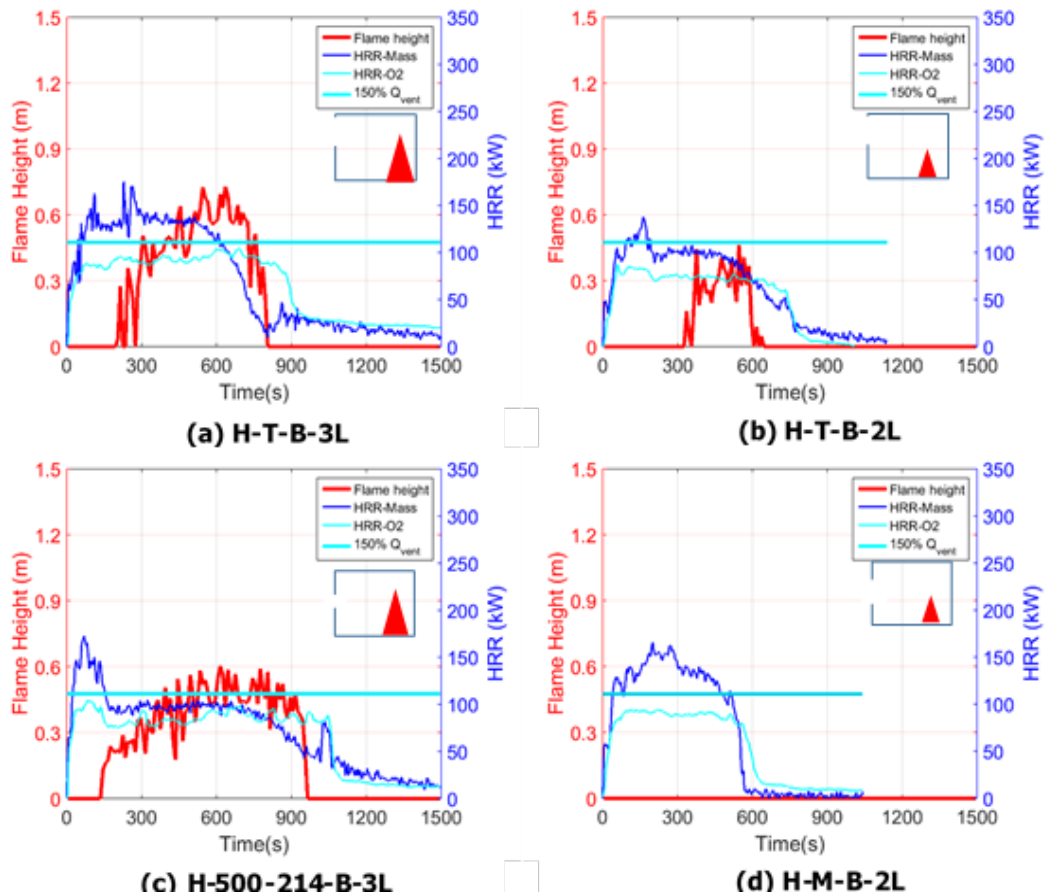


Figure 37. The flame height and heat release rate compared for heptane pool experiments where the maximum heat release rate did not exceed 150% of the ventilation-limited heat release rate and comparative small heptane pool experiments.

6.2 External flame heights

Measured external flame heights for each experiment are shown in Appendix D. There were three experiments where no or very little external flaming was observed: H-M-B-2L, W-M-B and W-T-B. These experiments had the lowest maximum HRR-O₂ other than the W-M-F experiment. As previously discussed, an explanation for the lower heat release rate in experiment W-M-F is that airflow into the opening was partially blocked by the proximity of the wood crib to the opening. The greatest external flame heights were observed for experiments H-M-F-2L, H-M-B-3L, H-100-625-B-3L and H-600-300-B-3L, as shown in Figure 35. As with the heat release rate characteristics, similar flame heights were observed with both H-M-F-2L and H-M-B-3L experiments, although there was a greater time delay before external flaming was observed and the flaming duration was longer (as expected due to the larger volume of fuel) with experiment H-M-B-3L.

6.2.1 Opening and fire location

No external flames were observed for the combination of the middle opening position and the back fire location for both wood crib and small heptane pool fires. Moving the opening to the top gave a slight increase in observed external flaming. This trend was not followed when the large heptane pool was used. Moving the fire to the front location increased the external flame height and duration for both the wood crib and small heptane fires (the large heptane pool fire was not used in the front position). At the front position, a greater external flame height was observed with the small heptane pool fire experiments when the opening was in the middle compared to the top position, while this trend was reversed with the wood crib fires. However, the duration of external flaming was approximately double for experiment W-M-F compared with experiment W-T-F.

6.2.2 Opening configuration and size

Comparing a tall (H-100-625-B-3L), square (H-M-B-3L) and wide (H-500-214-B-3L) opening in the middle position and with the same large heptane pool fire and fire location, the square opening configuration had the greatest external flame height, despite the fact that the maximum HRR-O₂ was measured with the tall opening. Some instability in the external flame was noted with the tall opening as the external flame tended to disappear occasionally. Both the flame height and the heat release rate were decreased in the wide opening experiment relative to the comparable tall and square experiments.

6.3 Heat flux on the external vertical wall above the opening

Heat flux levels on the vertical wall above the opening were strongly influenced by the presence of projected flames. Figure 38 demonstrates that, in H-M-B-2L and W-M-B where projected flames were not observed, the measured incident heat flux levels on the vertical wall above the opening were less than 10 kW/m². A maximum heat flux of approximately 17 kW/m² was seen during the brief period of observed external flame for experiment W-T-B as shown in Figure 39. With large projected flames, heat flux levels increased significantly almost up to a maximum of 50 kW/m² for experiments H-M-F-2L and H-M-B-3L as shown in Figure 40.

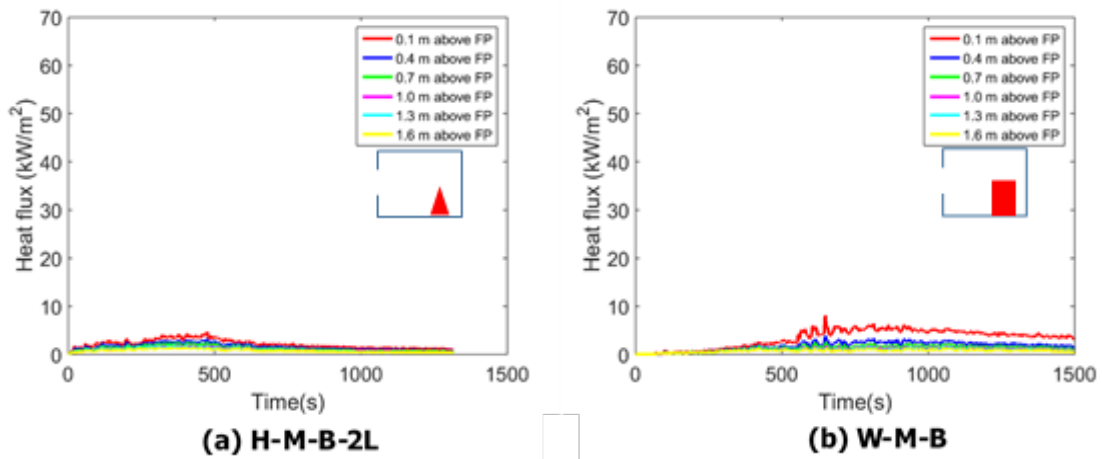


Figure 38. External wall heat flux levels for experiments without projected flames on the vertical panel.

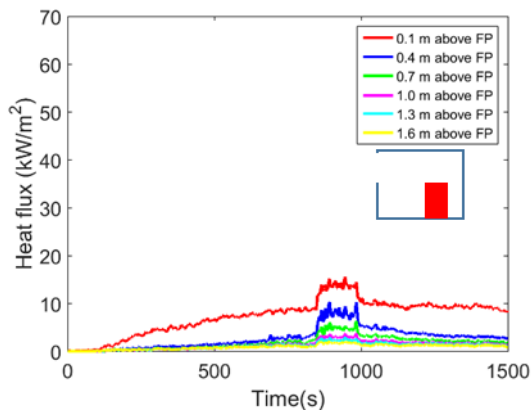


Figure 39. External wall heat flux levels for experiment W-T-B. A small external flame was observed for a short period of time just before 1000 s.

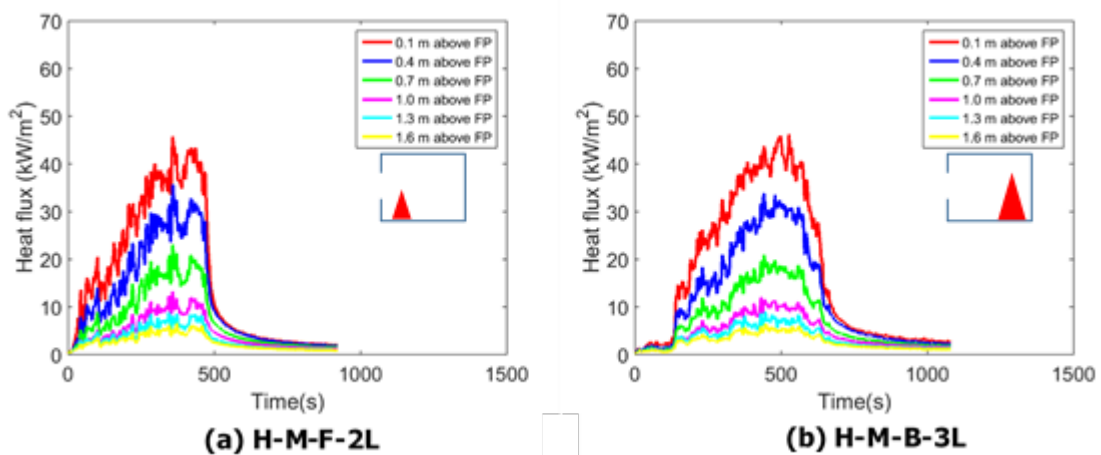


Figure 40. External wall heat flux levels for experiments using the 300 mm square opening with large projected flames on the vertical panel.

6.4 Apron experiments

The apron experiments were conducted using the H-M-B-3L configuration, chosen due to the large flame heights observed with the no-apron experiment. The flame heights and heat release rates are shown in Figure 41. Increasing the apron projection decreased the flame height. The peak HRR-O₂ values also reduced with increasing apron projection but remained above 150% of the ventilation-limited heat release rate, and burning duration increased.

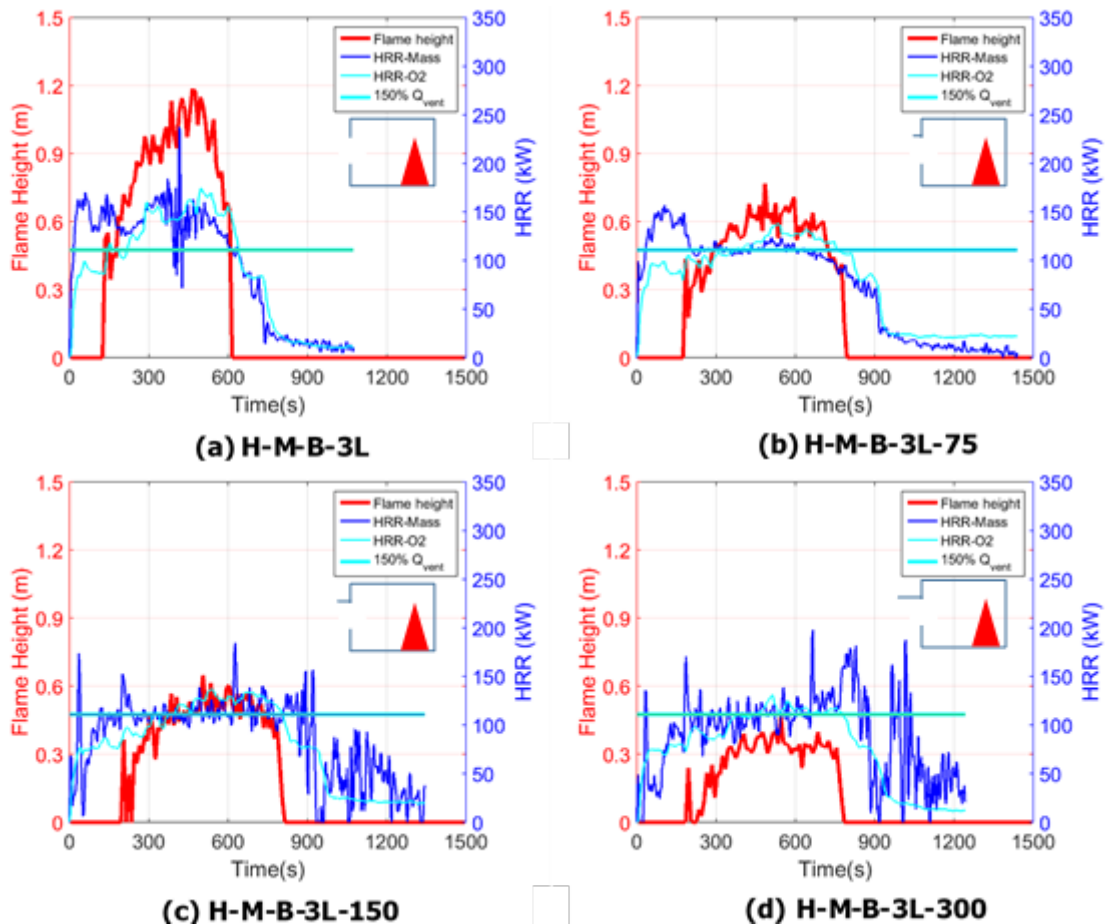


Figure 41. The flame height and heat release rate compared between the non-apron and apron experiments.

Images comparing the flame geometry near the maximum flame height for each experiment are shown in Figure 42. Larger apron projections tended to push the flame away from the upper wall, reducing flame contact height and duration.

The external wall heat flux measurements above the apron in Figure 43 demonstrate the effectiveness of the aprons in reducing the incident heat on the wall. A 75 mm apron projection decreased the peak heat flux measured at 0.1 m above the front panel approximately the same amount as a height increase to 0.4 m above the front panel for the no-apron case. Similarly, the 150 mm and 300 mm apron projections resulted in approximately the same peak heat flux as was recorded at 0.7 m and 1.3 m above the front panel for the no-apron case, respectively.

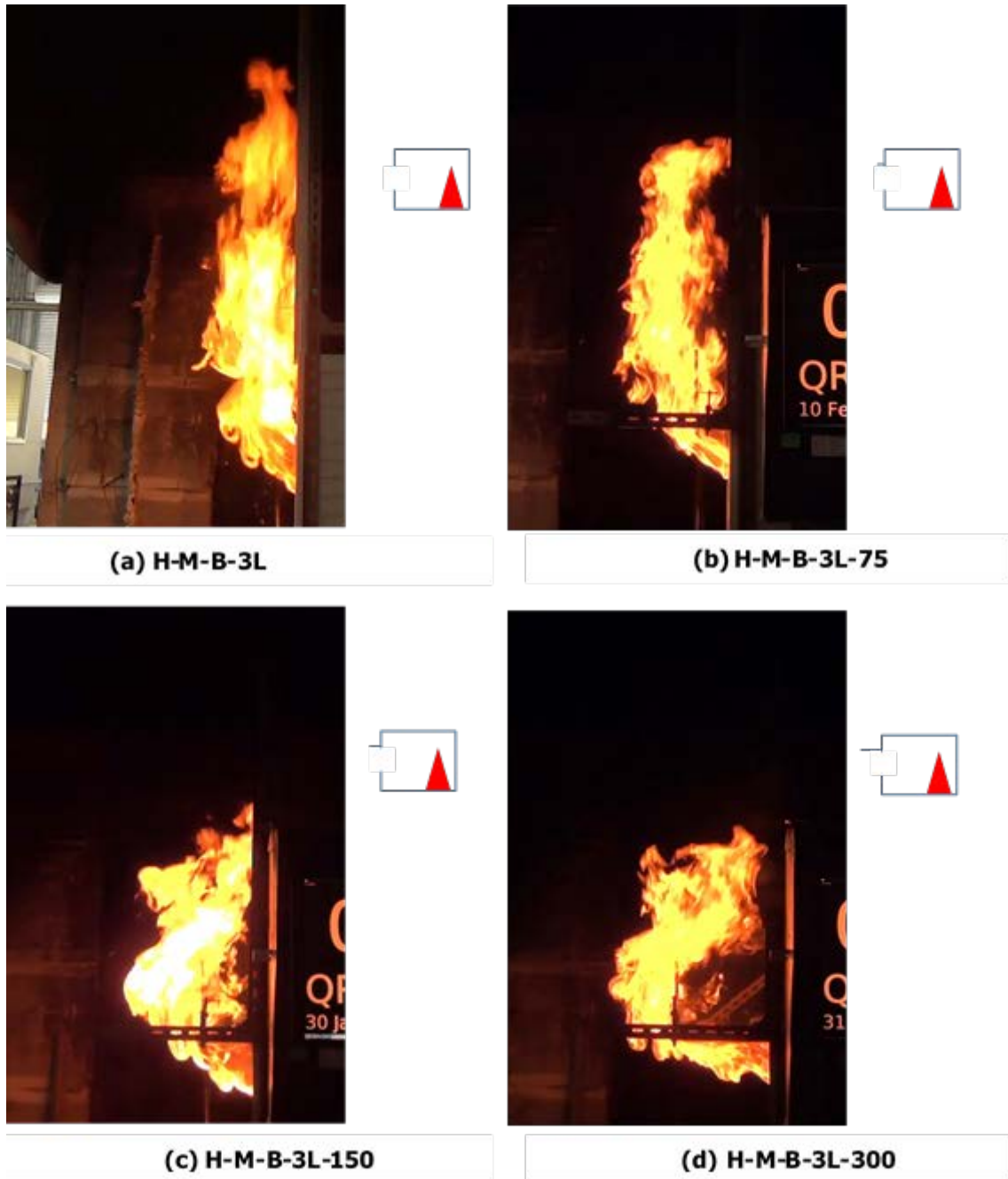


Figure 42. Representative flame images from maximum flame heights.

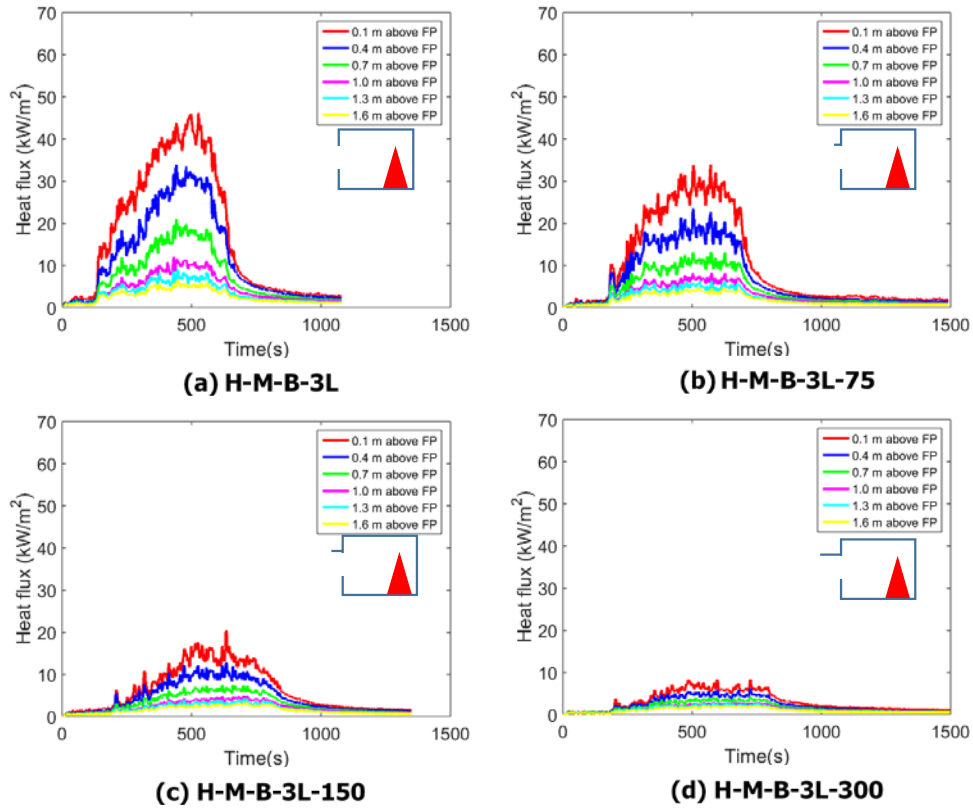


Figure 43. External wall heat fluxes measured in the apron and no-apron experiments.

7. Modelling radiation to external walls from experimental wall opening fire plumes using FDS

As discussed previously, FDS has the potential to be used to either directly model external wall opening fire plumes or as a virtual experimentation tool to develop simpler models. First, some further verification work was prudent to assess the ability of FDS to replicate the experiments in this study. FDS 6.5.1 and 6.5.2 were used for these simulations.

7.1 FDS modelling of reduced-scale experiments

Initially, the computational domain included the calorimeter hood itself and the flow induced by the calorimeter. The computational domain is shown in Figure 44.

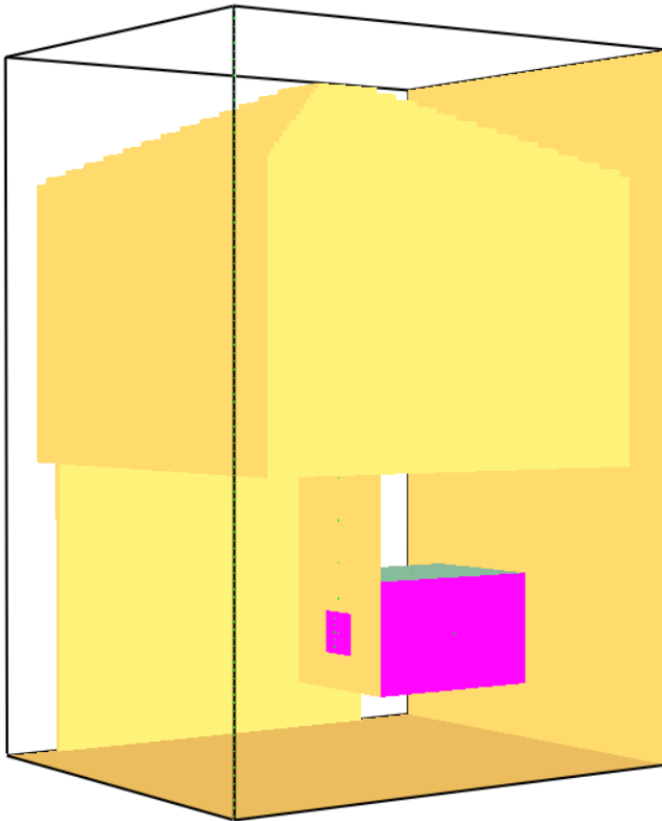


Figure 44. Initial FDS computational domain for simulating the experiments in this study.

The fire was represented in the initial model runs by a 300 mm by 300 mm pool of heptane, allowing FDS to estimate the fuel vaporisation and heat release rate. This approach was chosen as it represented the most realistic representation of the fire. The grid size was used 0.05 m. A comparison of the heat release rate for experiment H-M-F-2L is shown in Figure 45.

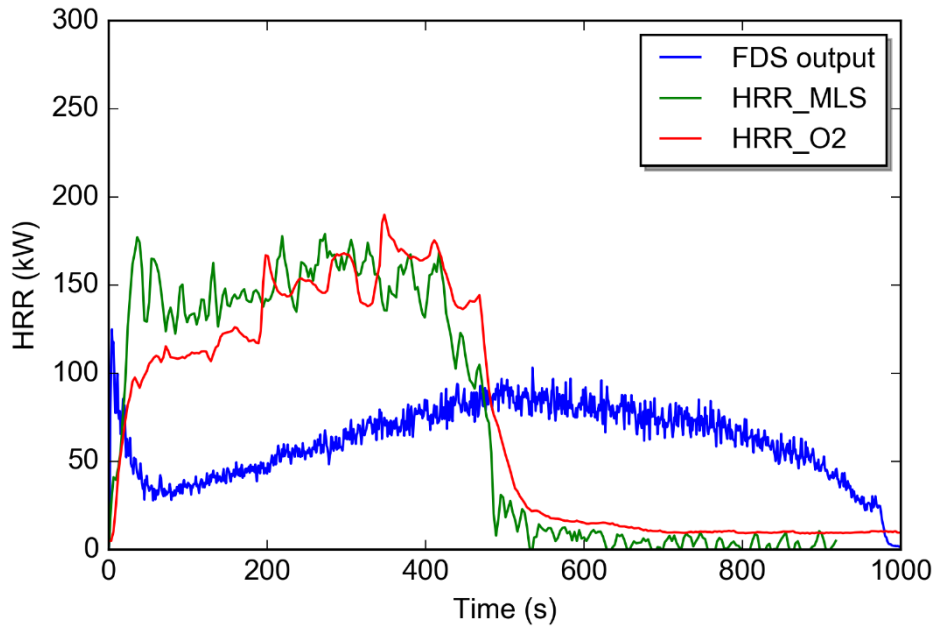


Figure 45. Comparison of the heat release rate from the H-M-F-2L experiment with the FDS simulation.

The heat release rate predicted by FDS showed a faster initial growth rate and initial peak followed by a decline that appeared to indicate ventilation was underpredicted by FDS. The next step was to systematically investigate why the heat release rate was not predicted well in FDS. First, the compartment was removed from the FDS simulation to compare the heat release rate for a free-burning 300 mm by 300 mm pool of heptane, eliminating the compartment radiation feedback and ventilation effects. The results are shown in Figure 46 and show that FDS was overpredicting the heat release rate and therefore vaporisation of the heptane by a factor of approximately two.

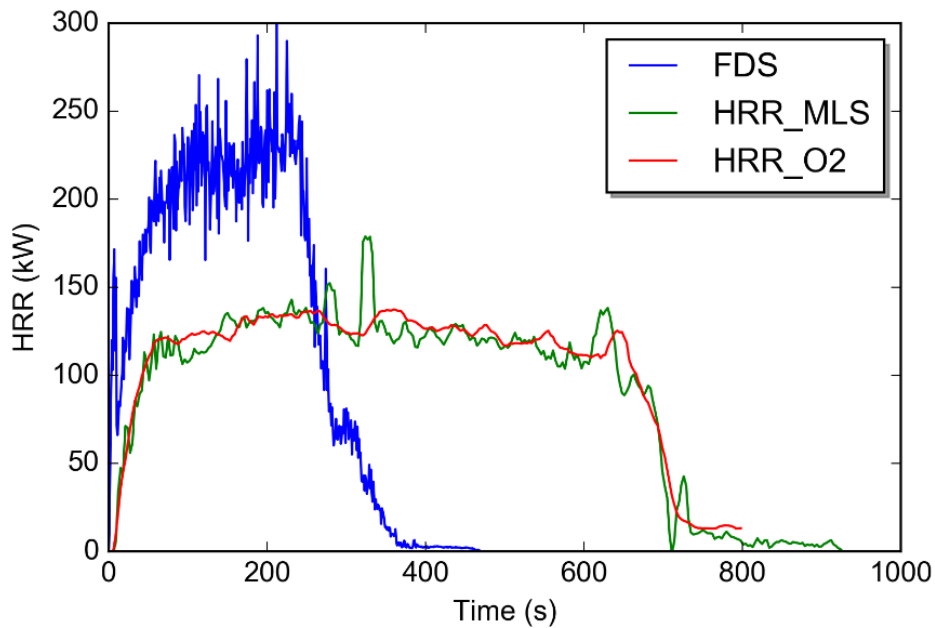


Figure 46. Comparison of the heat release rate from a free-burning 300 mm by 300 mm heptane pool experiment with the FDS simulation.

From this investigation, it appeared FDS was not doing an adequate job of simulating the heptane fire when defined as a pool. The goal of this research was not to investigate the ability of FDS to simulate fuel vaporisation or pyrolysis so the fire input was simplified to a specified heat release rate per unit area (HRRPUA) based on the fire area and experimentally measured fires. A ramp function for the HRRPUA was entered to approximately match the heat release rate measured by the calorimeter in the experiments. Figure 47 shows the comparison for an FDS run with no compartment.

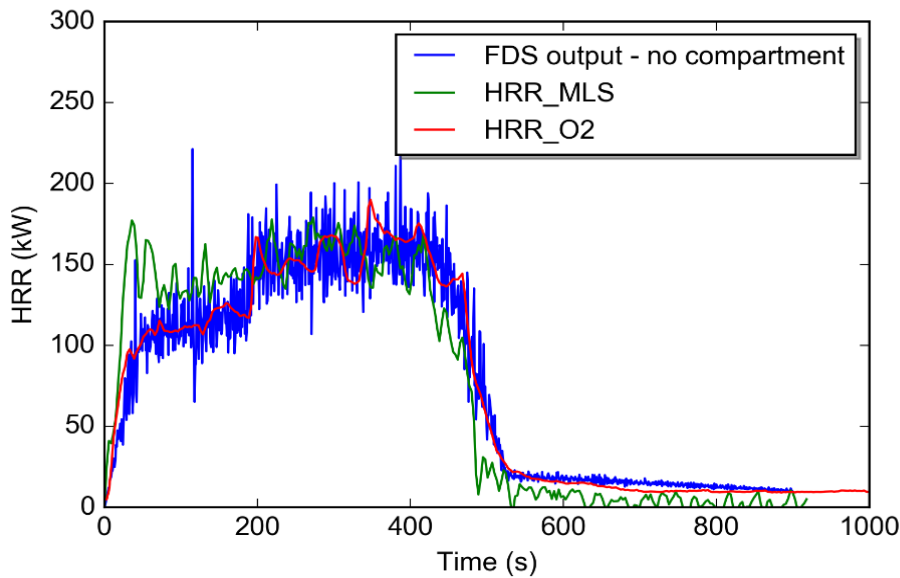


Figure 47. Comparison of heat release rate output from FDS with an input ramp HRRPUA based on the heat release rate measured experimentally by the calorimeter.

As this seemed to provide a satisfactory representation of the fire, the next step was to reintroduce the compartment and see what happened. The resulting heat release rate comparison is shown in Figure 48.

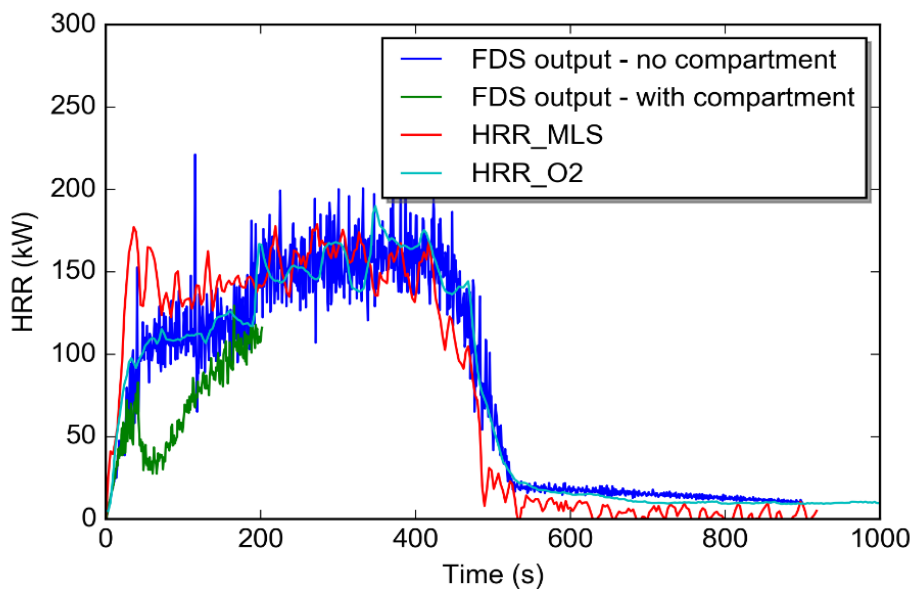


Figure 48. Comparison of FDS heat release rate output with a specified HRRPUA ramp with and without a compartment to experimental results.

With the prescribed heat release rate input, which is essentially a prescription of the amount of fuel vapour available to burn, the FDS prediction of what actually burned improved particularly in the initial growth of the fire, but the underprediction of ventilation again created a discrepancy up to approximately 200 s, at which time the simulation failed due to numerical instability. Based on these simulations and some other simulations comparing FDS 6.5 to FDS 5 results (Collier, 2015), it appeared that FDS was struggling to model the mixing of fresh air entering the compartment and/or the combustion occurring outside the compartment. One potential hypothesis was that the grid was not sufficiently refined to correctly model the movement of gases and mixing through the opening and outside the compartment. Therefore, the grid was refined and the computational domain reduced to maintain reasonable run times. The revised computational domain is shown in Figure 49.

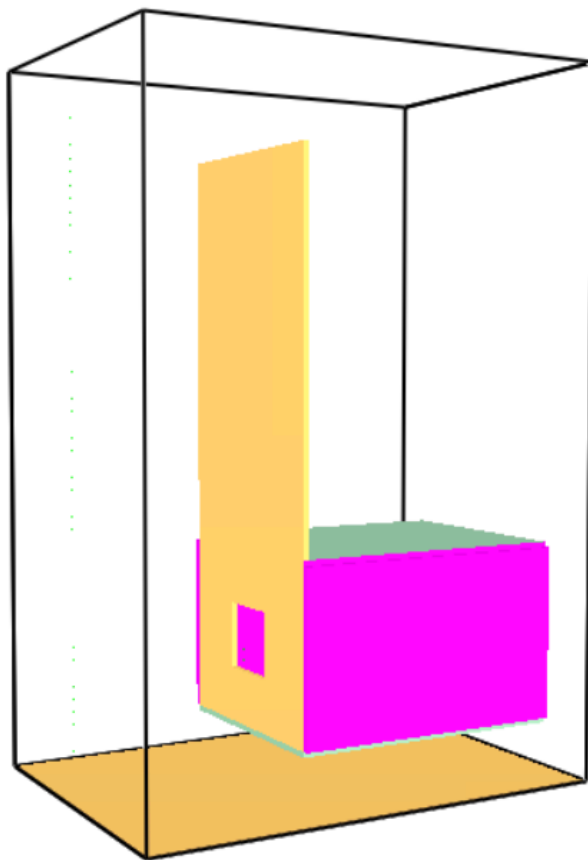


Figure 49. Reduced computational domain.

The grid size was reduced to 0.025 m and then 0.0125 m. At 0.0125 m, run times were excessive and problems with numerical stability were again encountered.

As a final attempt, the input fire was simplified. It was thought that, rather than following the calorimeter ramp, it might make more sense to follow the mass loss since that is more representative of the fuel leaving the pool and then the FDS heat release rate output (calculated as what is actually burning) should more closely represent the calorimeter heat release rate. Therefore, the input fire was simplified to a constant HRRPUA that would represent 150 kW based on the pool size. Preliminary results are shown in Figure 50. Again, what FDS predicted would burn was significantly less than what actually burned in the experiment, and numerical instabilities were still present. Based on these simulations, it was concluded that FDS could not adequately model the reduced-scale experiments.

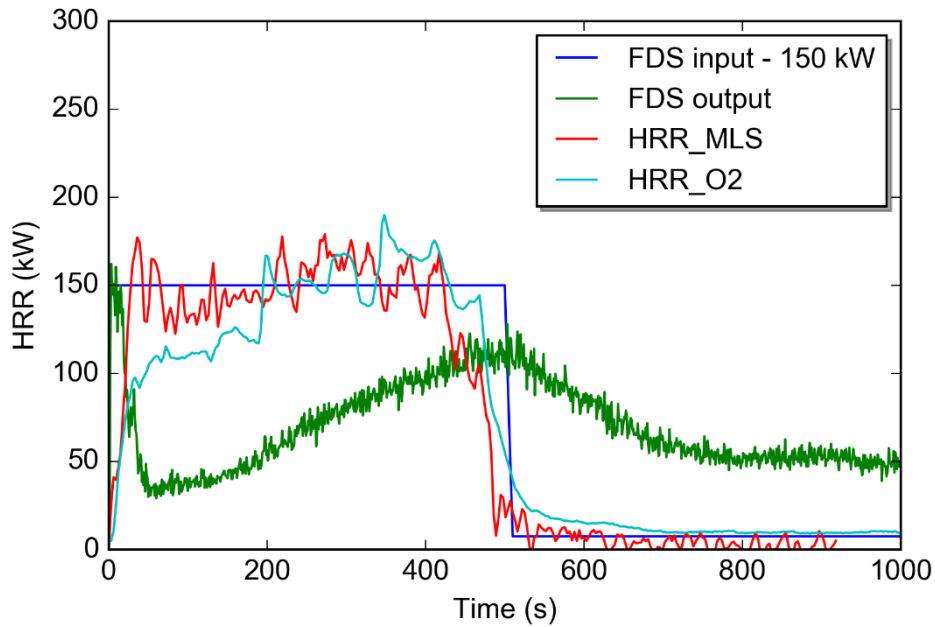


Figure 50. Comparison of FDS output for a constant 150 kW HRRPUA fire specification to the experimental heat release rate.

7.2 Additional FDS comparisons based on NRCC façade data

As discussed in section 4.4, the NRCC façade experiments have been simulated with FDS as part of the FDS validation suite of data sets. There were a number of limitations with the published comparisons between the FDS simulations and experiments. Only the data regarding heat flux on the façade was compared, the effect of refining the computational mesh was not considered and the apron experiments were not included. The NIST simulations were rerun to see how well FDS could simulate flame heights. For the mesh refinement study, the grid length dimensions were reduced from 0.1 m to 0.05 m. Otherwise, the input files were unchanged from the NIST validation suite.

7.2.1 Heat release rates

Heat release rates in the NRCC façade experiments were not measured by calorimetry but instead were reported based on propane flow, assuming complete combustion (Oleszkiewicz, 1989). The reduced-scale experiments completed in this study report indicate that complete combustion does not occur using solid or liquid phase fuels. Lee et al. (2008) compared fuel flow and calorimeter-based heat release rate measurements in reduced-scale experiments using methane and/or propane. When ramping the heat release rate past the ventilation limit, it was found that the heat release rate would plateau for a time at the ventilation limit and eventually catch up when external burning was well established. Therefore, there is some uncertainty as to whether the actual heat release rate produced in the NRCC façade experiments was actually equivalent to complete combustion. The following analysis assumes that there was complete combustion.

Figure 51 shows the FDS heat release rate output for four simulations of the NRCC façade experiment using the third window and a nominal heat release rate of 6.9 MW based on the propane fuel flow that is typical for all of the simulations. The heat release rate output from FDS typically would overshoot the constant heat release rate

input, then would undershoot for a period and then reach a stable phase at a mean of approximately the input heat release rate with periodic oscillations of up to ± 2 MW. Repeating the FDS simulations using the same input file and computer resulted in the output shown, where the initial heat release rate output was nearly identical until the oscillatory phase, at which point the oscillations diverged.

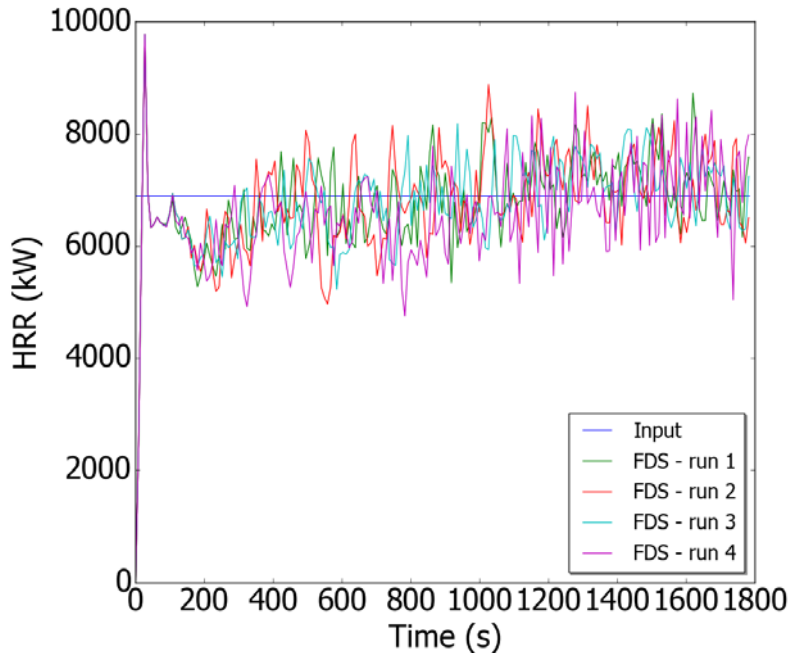


Figure 51. FDS heat release rate output for four coarse grid simulations of the NRCC façade experiment using the third window configuration and a nominal heat release rate of 6.9 MW.

7.2.2 Flame heights

Projected flame heights were estimated from the FDS heat release rate data similar to the method used in the NIST validation report as discussed in section 4.1. The HRRPUA device was used, which defaults to a time average over the final 50% of the simulation time. The heat release rate was checked to ensure it had reached the stable oscillating phase by the halfway point of the simulation. The height at which 99% of the heat had been released was used as the criteria for the tip of the flame. Comparisons to the experimentally measured flames are discussed in section 8.2.3.

7.2.3 Heat flux to the external wall

As per the NIST validation suite, heat flux was estimated using gauge heat flux devices that were time averaged over the final 50% of the simulation time. The gauge surface temperature of 50°C was retained as well.

7.2.4 NRCC façade experiments with aprons

The FDS validation suite did not include simulation of the NRCC façade experiments where aprons were used. The original FDS validation suite FDS input files were used with the addition of a 0.13 mm thick marinite apron as described in the NRCC apron experiments (Oleszkiewicz, 1991). The 5.5 MW no-apron case was compared with the simulated 5.7 MW apron as per the experiments. The results are compared in section 8.4.2.

8. Benchmarking existing tools with experimental data

The experimental data from this study was used to evaluate the C/VM2 heat release rate design fire criteria given in section 2, the models for flame height and heat flux given in section 3 and also the capabilities of FDS discussed in section 4.

8.1 Heat release rate

Experimental heat release rates were compared to the C/VM2 heat release rate design fire criteria and also the ability of FDS to model the heat released in a fire from an opening.

8.1.1 Comparison of the C/VM2 heat release rate design fire criteria to experimental results

Using a single design fire may not provide conservative results for all scenarios. When compared to the reduced-scale experimental results (Table 8), the 1.5 times ventilation-limited heat release rate C/VM2 design fire, which was targeted at tenability predictions in adjacent spaces, may be non-conservative for vertical external fire spread if the potential for a fuel package with a large exposed area and low heat of gasification (vaporisation or pyrolysis) exists. The higher heat release rate limit may also be considered for fuel packages located near an opening with a moderate area and low heat of gasification. To account for these fuel scenarios, increasing the heat release rate to 2.5 times (or 3 times to be conservative), the ventilation limit is likely prudent for vertical external fire spread. Other scenarios may require further modifications to the design fire. An example would be a structural design fire, as burn-out durations may be non-conservative with high heat release rate assumptions.

8.1.2 Ability of FDS to model heat release rate

Selected FDS data is presented in section 7. A review of the FDS simulations indicates that FDS can have problems representing the heat release rate accurately, particularly for reduced-scale compartments. FDS appeared to more successfully represent the heat release rate for the full-scale NRCC façade experiments. However, the comparison was made to the heat release rate estimation from propane flow rate assuming complete combustion, and it is unknown how accurate the complete combustion assumption was. Full-scale calorimetry experiments are required to check this assumption.

8.2 Flame height

Flame height comparisons were made for the correlations for the reduced-scale experiments completed for this study and the NRCC façade experiments where data was available. The maximum flame heights and a qualitative comparison of flame height and duration based on the time history were used for the reduced-scale experiments due to their transient nature. The average flame heights during stable burning were compared for the NRCC façade experiments using the correlations and FDS.

8.2.1 Correlation comparisons to reduced-scale experiments

Using the methods described in section 3.2, flame heights were calculated and compared with the experimentally obtained flame heights as shown in Appendix J.. A comparison of the experimental and measured maximum flame height for all experiments is shown in Figure 52 (linear scale) and Figure 53 (log-log scale). The linear scale plot is included for the data where flame heights were zero.

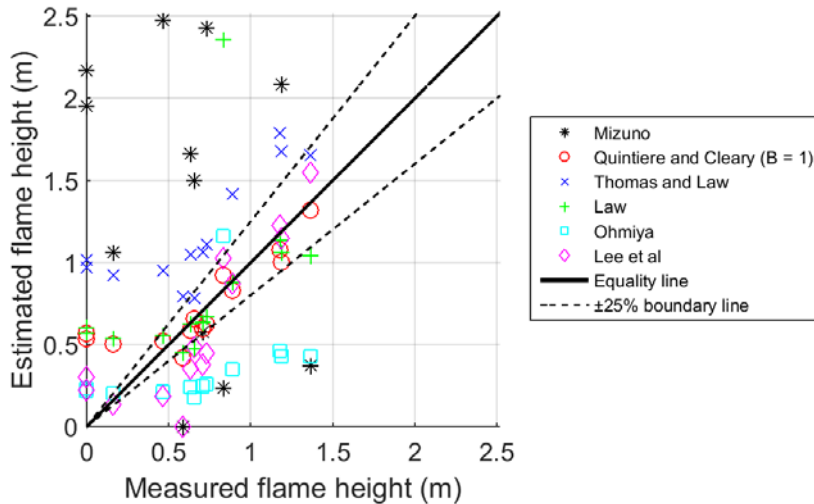


Figure 52. Comparison of estimated and measured maximum flame height for reduced-scale experiments (linear scale).

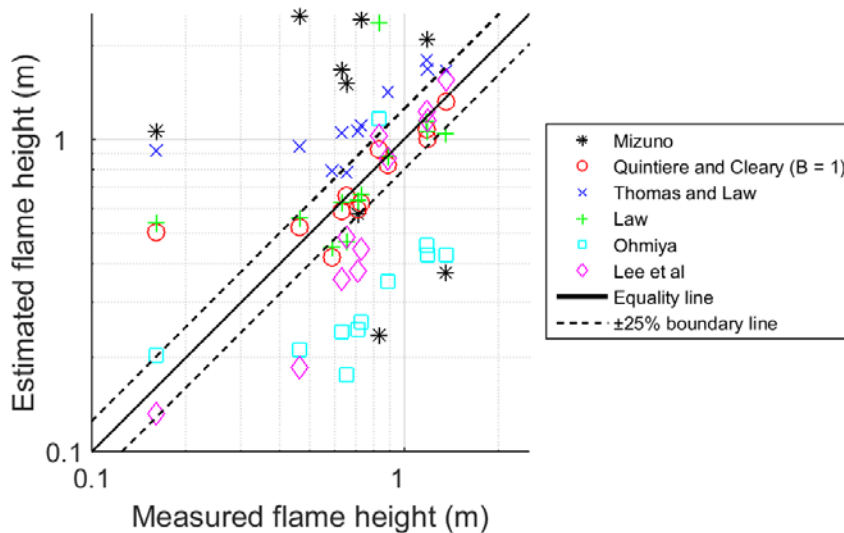


Figure 53. Comparison of estimated and measured maximum flame height for reduced-scale experiments (log-log scale). Equality and ±25% lines are shown.

A qualitative comparison of the flame height as a function of time is summarised in Table 9. Experimental observations in Table 9 are given for flame duration and flame height. The flame duration is relative to the period of each experiment when the heat release rate was approximately stable. The height criterion was short if the maximum flame height was less than 0.5 m, moderate if the flame height was between 0.5 m and 1.0 m and tall if the flame was greater than 1.0 m.

Table 9. Summary of qualitative comparisons between experimental flames and correlation estimates.

| Experiment | Flame | Experimental Observation | Mizuno | Quintiere and Cleary (B = 1) | Thomas and Law | Law | Ohmiya | Lee et al |
|----------------|----------|--------------------------|----------|------------------------------|----------------|-------|--------|-----------|
| H-M-F-2L | Duration | Long | Good | Good | Good | Good | Good | Good |
| | Height | Tall | Good | Good | Good | Under | Under | Good |
| H-T-F-2L | Duration | Moderate | Over | Over | Over | Over | Over | Over |
| | Height | Moderate | Over | Over | Over | Good | Under | Under |
| H-M-B-2L | Duration | No flame | Over | Over | Over | Over | Over | Over |
| | Height | No flame | Over | Over | Over | Over | Over | Over |
| H-T-B-2L | Duration | Short | Over | Over | Over | Over | Over | Under |
| | Height | Short | Over | Over | Over | Good | Under | Under |
| H-M-B-3L | Duration | Long | Over | Over | Over | Over | Over | Over |
| | Height | Tall | Over | Good | Good | Under | Under | Good |
| H-T-B-3L | Duration | Moderate | Over | Over | Over | Over | Over | Over |
| | Height | Moderate | Over | Over | Good | Under | Under | Under |
| W-M-F | Duration | Long | Under | Over | Over | Over | Good | Under |
| | Height | Moderate | Under | Over | Over | Over | Under | Under |
| W-T-F | Duration | Short | Good | Over | Over | Over | Over | Good |
| | Height | Moderate | Good | Over | Over | Over | Under | Under |
| W-M-B | Duration | No flame | Over | Over | Over | Over | Over | Good |
| | Height | No flame | Over | Over | Over | Over | Over | Good |
| W-T-B | Duration | Very short | Over | Over | Over | Over | Over | Good |
| | Height | Short | Over | Over | Over | Over | Good | Good |
| H-100-625-B-3L | Duration | Moderate | No flame | Over | Over | Over | Over | Good |
| | Height | Tall | No flame | Over | Over | Over | Good | Good |
| H-500-214-B-3L | Duration | Long | Under | Over | Over | Over | Over | Over |
| | Height | Moderate | Over | Over | Good | Under | Under | Good |
| H-600-300-B-3L | Duration | Moderate | No flame | Over | Over | Over | Good | Good |
| | Height | Tall | No flame | Good | Under | Under | Under | Good |

The Mizuno and Kawagoe method (section 3.2.8) did not provide a reasonable estimation of flame height in nearly all instances, with H-M-F-2L and W-T-F being exceptions as shown in Figure 54.

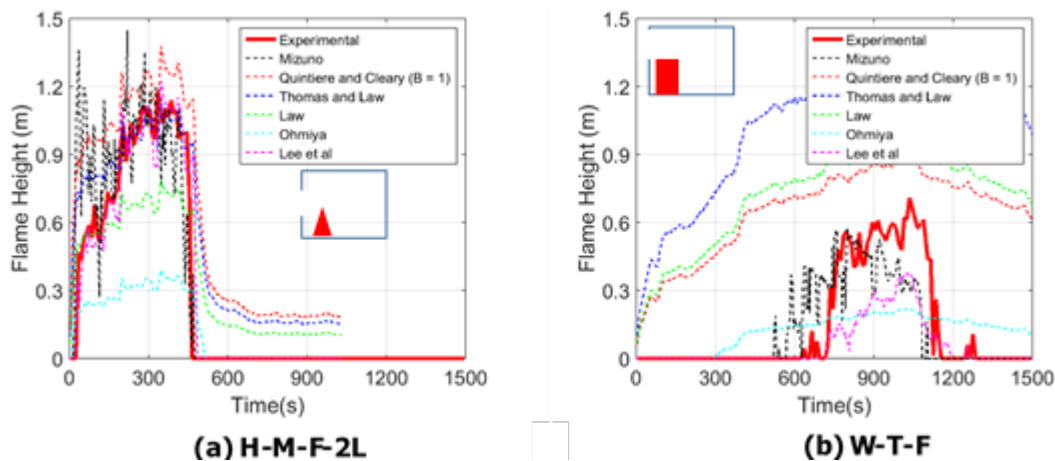


Figure 54. Comparison of flame heights for the H-M-F-2L and W-T-F experiment.

The Mizuno and Kawagoe method also predicted that no flame would occur in the H-100-625B-3L and H-600-300-B-3L experiments where there were relatively large flames present. The H-M-F-2L flame height was predicted well by all of the correlations except Law and Ohmiya et al., which underpredicted the flame height. The Quintiere and Cleary relation (section 3.2.4) with the B = 1 modification did not underpredict the flame duration or the flame height in any of the experiments. The Thomas and Law correlation (section 3.2.2) underpredicted the flame height in the H-600-300-B-3L

experiment. The Law correlation (section 3.2.3) underpredicted the flame height in five of the experiments but otherwise overpredicted the flame heights. The Ohmiya et al. method (section 3.2.5) predicted flames to occur when they did not in the H-M-B-2L and W-M-B experiments and overpredicted the small amount of flame that occurred in W-T-B. The Lee et al. correlation (section 3.2.6) provided the best match in the majority of cases but did underpredict the flame height for five experiments and the duration in two experiments.

8.2.2 Correlation comparisons to NRCC façade experimental data

Flame height correlations with the exception of the Mizuno and Kawagoe correlation (section 3.2.8) were compared to average flame heights reported for the NRCC façade experiments as shown in Figure 55 (linear scale) and Figure 56 (log scale).

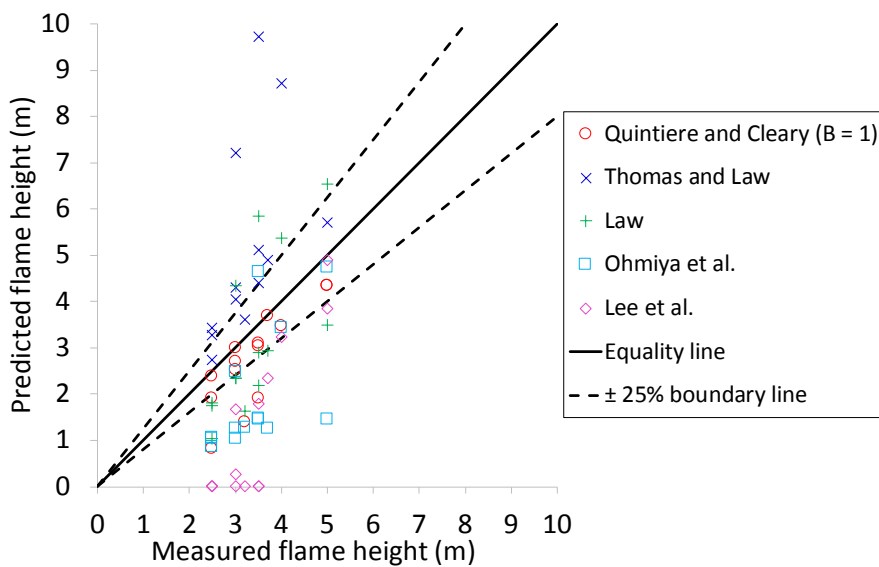


Figure 55. Linear scale comparison of estimated and measured average flame height for NRCC façade experiments using simple correlations. Equality and $\pm 25\%$ lines are shown.

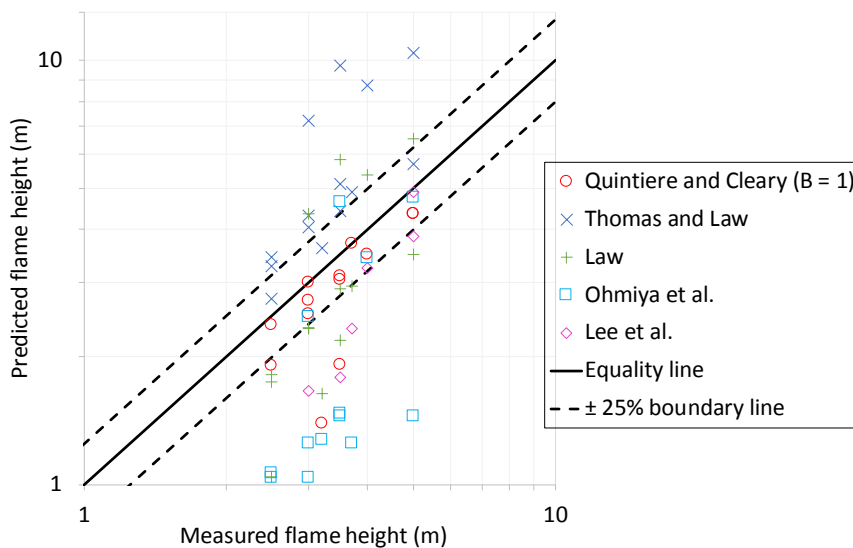


Figure 56. Log-log scale comparison of estimated and measured average flame height for NRCC façade experiments using simple correlations. Equality and $\pm 25\%$ lines are shown.

The general trend of predictions for most correlations was similar to the reduced-scale experiments. The Thomas and Law correlation (section 3.2.2) had a trend of overpredicting flame heights, and Law (section 3.2.3), Ohmiya et al. (section 3.2.5) and Lee et al. (section 3.2.6) had a trend of underpredicting flame heights, as also seen in the reduced-scale comparison. The most notable changes were that the Quintiere and Cleary correlation (section 3.2.4) with $B = 1$ tended to underpredict flame heights, and Lee et al. severely underpredicted flame heights, predicting a flame height of zero for seven experiments. This was due to the total heat release rate being less than the ventilation-limited heat release rate for these instances.

8.2.3 FDS comparisons to NRCC façade experimental data

Time-averaged flame heights calculated from FDS as described in section 7.2.2 were compared to the NRCC façade experimental results as shown in Figure 57. The Quintiere and Cleary correlation with $B = 1$ is included for comparison and both coarse and fine FDS computational grids. The fine computational grid simulations did produce less scatter than the coarse grid simulations but tended to underpredict the flame height to a greater extent and in more instances. The Quintiere and Cleary correlation with $B = 1$ outperformed both the FDS coarse and fine simulations in nearly all cases.

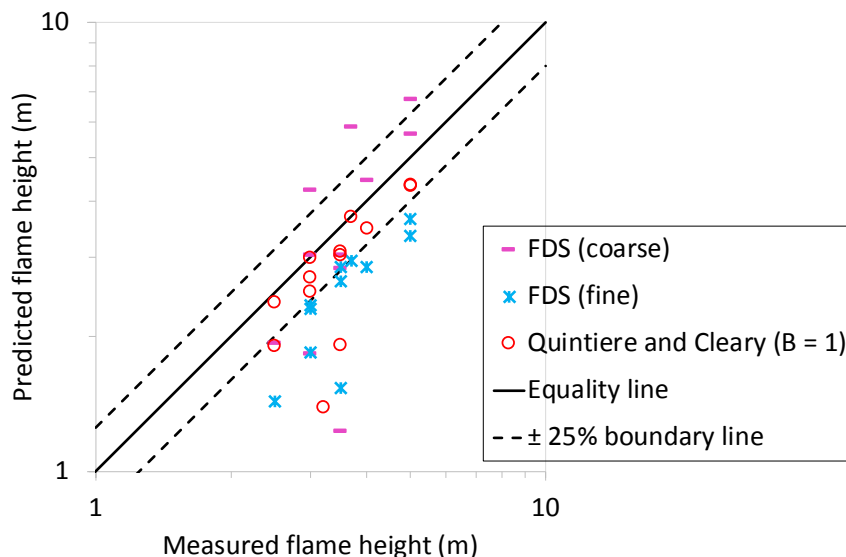


Figure 57. Comparison of estimated and measured average flame height for NRCC façade experiments using FDS. Equality and $\pm 25\%$ lines are shown.

8.3 Estimation of incident heat flux on the vertical wall

The incident heat flux on the vertical wall was compared using the Back et al. (section 3.3.4), Delichatsios et al. (section 3.3.2), Law (section 3.3.5) and Abecassis Empis correlations (section 3.3.6) for the reduced-scale experiments and NRCC façade experiments.

8.3.1 Back et al. and Delichatsios et al. correlations comparison to reduced-scale experiments (no apron)

The Back et al. and Delichatsios et al. correlations for maximum heat flux were compared to all of the reduced-scale experimental data where substantial flames (W-T-B is excluded) were projected and no aprons were used as shown in Figure 58. Note that the base of the flame was taken to be at 40% of the opening height as per

Delichatsios et al. Arbitrary \dot{q}_{peak}'' values of 25 kW/m² and 50 kW/m² were used for comparison, since the heat release rate varied continuously through the experiments. Both correlations matched the reduced-scale data fairly well with these defined \dot{q}_{peak}'' values. There was a large amount of scatter in the data, but this may be explained by differences in the response time of the flame height measurement and the heat flux measurements and random variations in flame tilt.

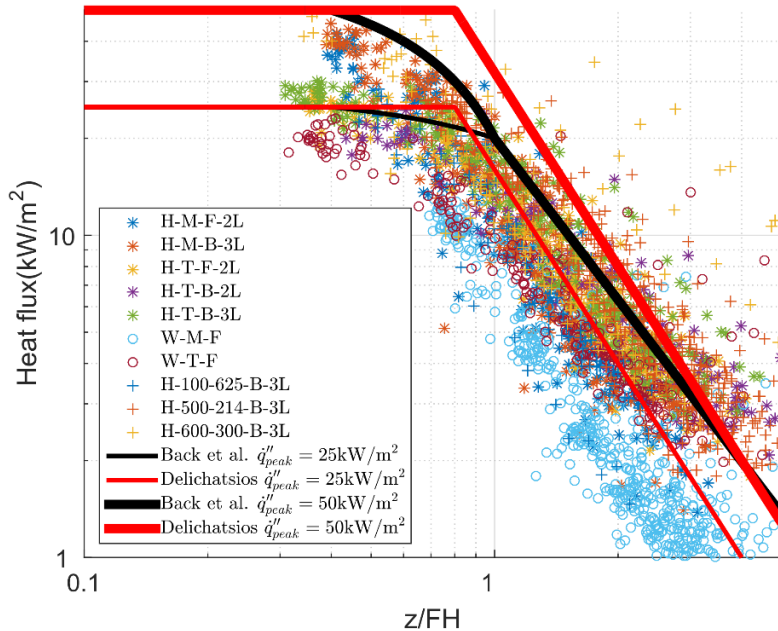


Figure 58. Comparison of Back et al. and Delichatsios et al. correlations to reduced-scale experiments with significant flaming and no aprons.

In general, the top opening experiments were observed to follow the slope of the Back et al. correlation above the tip of the flame ($z/FH = 1$), while the middle opening experiments followed the slope of the Delichatsios et al. correlation as shown in Figure 59, with the notable exception of experiment H-500-214-B-3L. It appears from this observation that openings with the soffit at the ceiling level or wide aspect ratio openings may produce heat fluxes that are more similar to the characteristics of a burner adjacent to a wall.

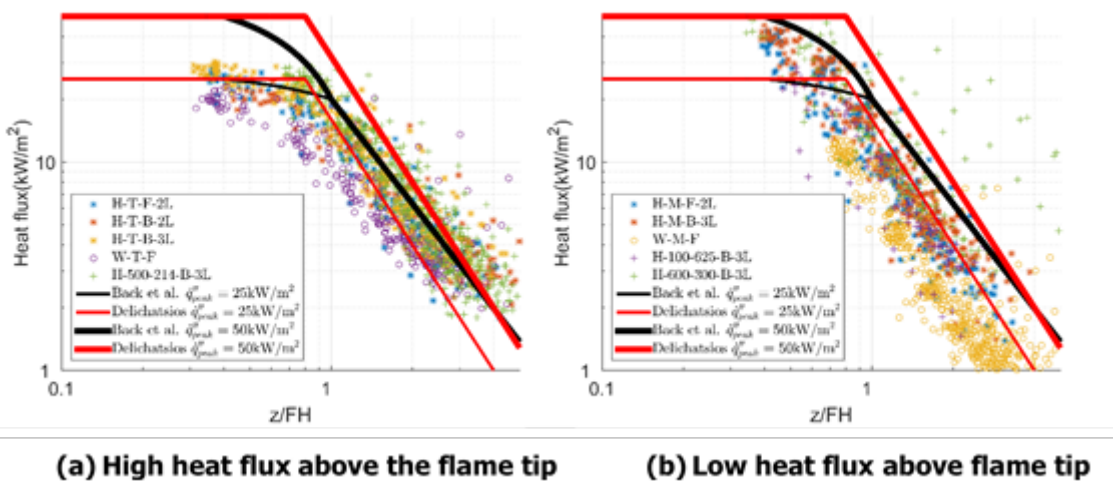


Figure 59. Reduced-scale experimental comparisons to Back et al. and Delichatsios et al. for experiments, split by heat flux slope above flame tip.

8.3.2 Back et al., Delichatsios et al. and Law peak heat flux predictions

Another aspect where the Back et al. correlation did not provide a good prediction of the heat flux was the \dot{q}_{peak}'' value predicted from the total heat release rate. This is not unexpected because the Back et al. correlation for \dot{q}_{peak}'' was developed from data for a burner next to a wall. The \dot{q}_{peak}'' value for the flames projected from openings was less than that predicted for a burner of the same total heat release rate next to a wall, which is likely a reflection of the heat lost in the compartment and the horizontal momentum of the flames leaving the opening. A new correlation for \dot{q}_{peak}'' was developed based on the reduced-scale experimental data, the NRCC façade data and the data from Lee et al. and Yoshioka et al. This correlation replaces the total heat release rate cube root term that was used as a volume scale in the Back et al. mean beam length correlation (Eqn. 48) with the opening width W_o multiplied by the relative total heat release rate to the ventilation-limited heat release rate squared as follows:

$$\dot{q}_{peak}'' = E_v * \left(1 - e^{-k_v \left(\left(\frac{\dot{Q}}{\dot{Q}_{vent\ lim}} \right)^2 W_o \right)} \right) \quad \text{Eqn. 59}$$

Where:

$$E_v = 75 \text{ kW/m}^2$$

$$k_v = 0.7 \text{ 1/m}$$

This correlation acknowledges that the external flame width will be limited by the opening width and scales the mean beam length by the fraction of heat release rate expected to occur outside of the compartment squared. The lower blackbody emission E_v reflects the physical situation with a portion of the heat released inside the compartment and also the horizontal flame momentum tending to push the flame farther from the exterior surface. A comparison of the above correlation and the experimental peak heat flux values is shown in Figure 60.

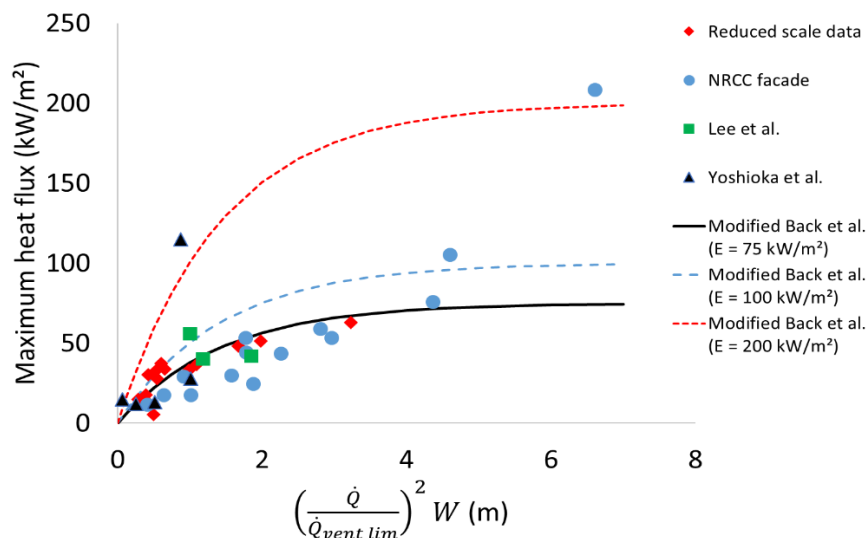


Figure 60. Peak heat flux experimental data and modified Back et al. correlation.

There are three outliers that are substantially above the correlation, which were the Yoshioka et al. 2.6 MW heptane fire (with a 2.0 m wide by 1.2 m tall opening) and the NRCC façade experiment 8.6 MW and 10.3 MW fire through the 2.6 m wide by 1.4 m

tall opening. Again, this indicates that large fires projecting through wide aspect ratio openings may provide higher heat fluxes than anticipated. It appears that using an E_v value of 100 kW/m² may be more conservative for most external flaming scenarios, while in some cases where extremely high heat fluxes may be encountered, an E_v value of 200 kW/m² may be warranted. This value is equivalent to the value used by Back et al. for propane burners next to a wall.

A comparison of the predictions of the modified Back et al. and Delichatsios et al. peak heat flux correlations to the measured peak heat fluxes in the reduced-scale experiments and NRCC façade experiments is shown in Figure 61 (Figure 62 log-log scale). The Law method described in section 3.3.5 was also included, using the height of the lowest heat flux meter in the experiments from the window soffit to calculate the convective heat transfer coefficient and flame temperatures. Flame heights were not identified for the Lee et al. and Yoshioka et al. experiments so could not be used for the Delichatsios et al. peak heat flux correlation.

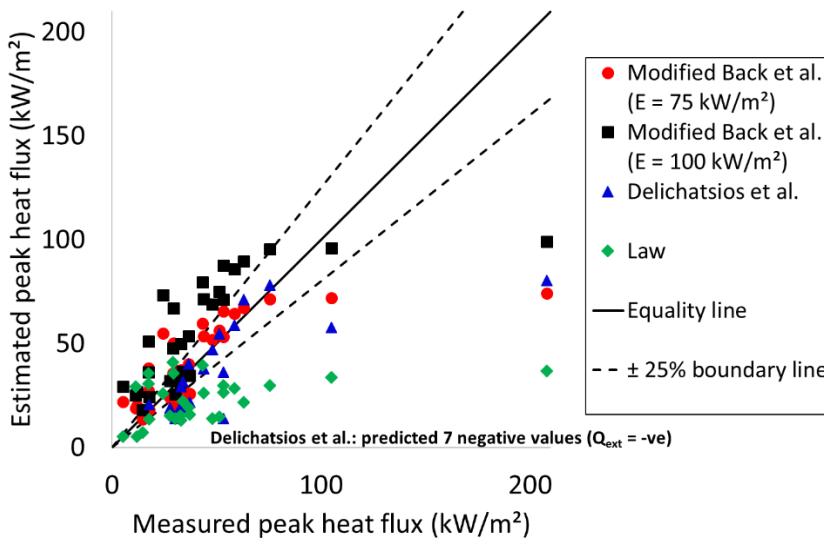


Figure 61. Comparison of modified Back et al., Delichatsios et al. and Law peak heat flux correlation predictions for the reduced-scale and NRCC façade experimental data (no aprons).

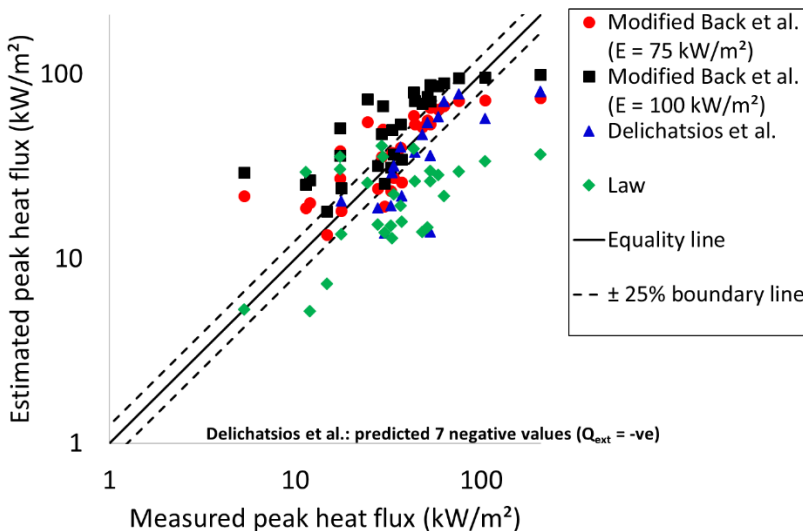


Figure 62. Comparison of modified Back et al., Delichatsios et al. and Law peak heat flux correlation predictions for the reduced-scale and NRCC façade experimental data (no aprons, log-log scale).

All three methods of calculating peak heat flux underpredicted the two experimental outliers above 100 kW/m². Also, the Delichatsios et al. correlation predicted negative values for the peak heat flux for one reduced-scale experiment and six NRCC façade experiments when the actual heat release rate was less than the ventilation-limited heat release rate. The factor $\frac{L_x W_t}{\dot{Q}}$ in the Law window flame temperature correlation (Eqn. 55) was greater than one for 75% of the reduced-scale and NRCC façade data points. In these cases, a value of 1 was used, which resulted in a window flame temperature of approximately 1000°C. Greater values of the factor caused unrealistic window flame temperature predictions. The Law method had greater scatter and tended to underpredict the peak heat flux in more instances.

The Back et al. and Delichatsios et al. correlations were then used to estimate the heat flux measured by each heat flux meter in the reduced-scale experiment using the heat release rate and flame height at 10-second intervals. The modified Back et al. peak heat flux correlation was used for the Back et al. heat flux profile, and the Delichatsios et al. peak heat flux correlation was initially used for the Delichatsios et al. heat flux profile. Linear density scatter plots of all of the reduced-scale experimental data (excluding apron experiments) are shown in Figure 63.

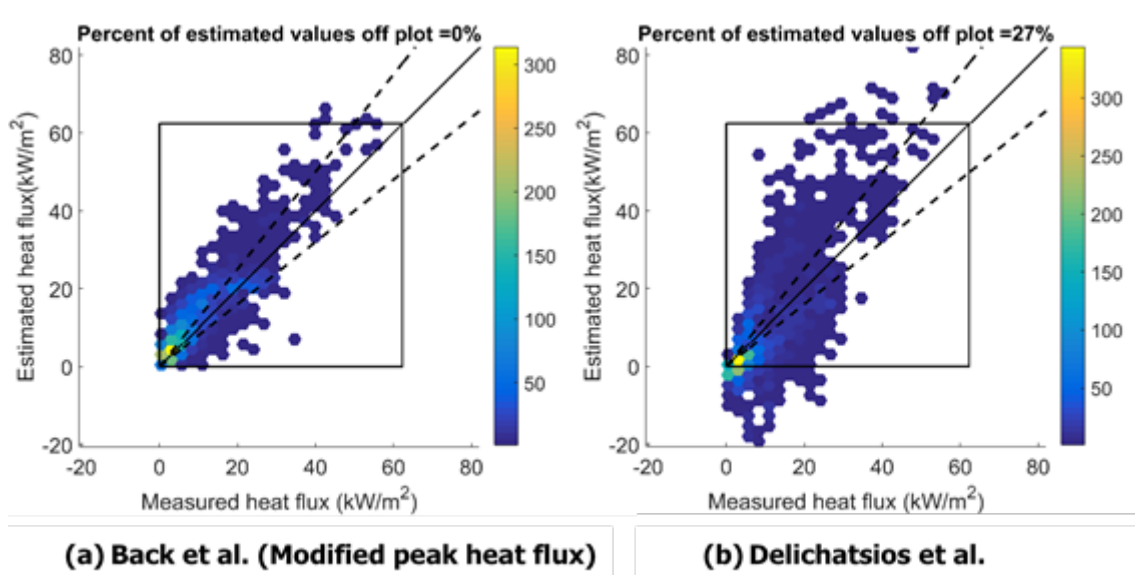


Figure 63. Back et al. and Delichatsios et al. correlation comparisons to reduced-scale data (no aprons) using 10-second interval measured heat release rates and flame heights.

The colour scale represents the number of data points in each hexagon. The box on the plots represents the range from 0 to 110% of the maximum measured heat flux, with the percent of values outside of the box reported at the top of the figure (rounded to the nearest whole number, so small numbers of points outside the box may be reported as 0%). Note that the axes have been scaled to retain a one-to-one aspect ratio while including the full range of the estimated heat flux values for both correlations.

The Delichatsios et al. peak heat flux correlation struggled with the time-varying experimental data. Low flame height fluctuations resulted in estimations of overly high peak heat flux, while heat release rate fluctuations dropping below the ventilation-limited heat release rate caused negative peak heat fluxes to be predicted.

To see the effect of the peak heat flux correlation, the data was reanalysed using the modified Back et al. peak heat flux correlation for the Delichatsios et al. heat flux profile, shown in Figure 64. Note that the Back et al. correlation plot values have not changed, but the scale has changed due to the smaller range of heat flux predicted by the Delichatsios et al. correlation. The Delichatsios et al. heat flux profile correlation provided improved estimation of the heat flux using the modified Back et al. peak heat flux correlation.

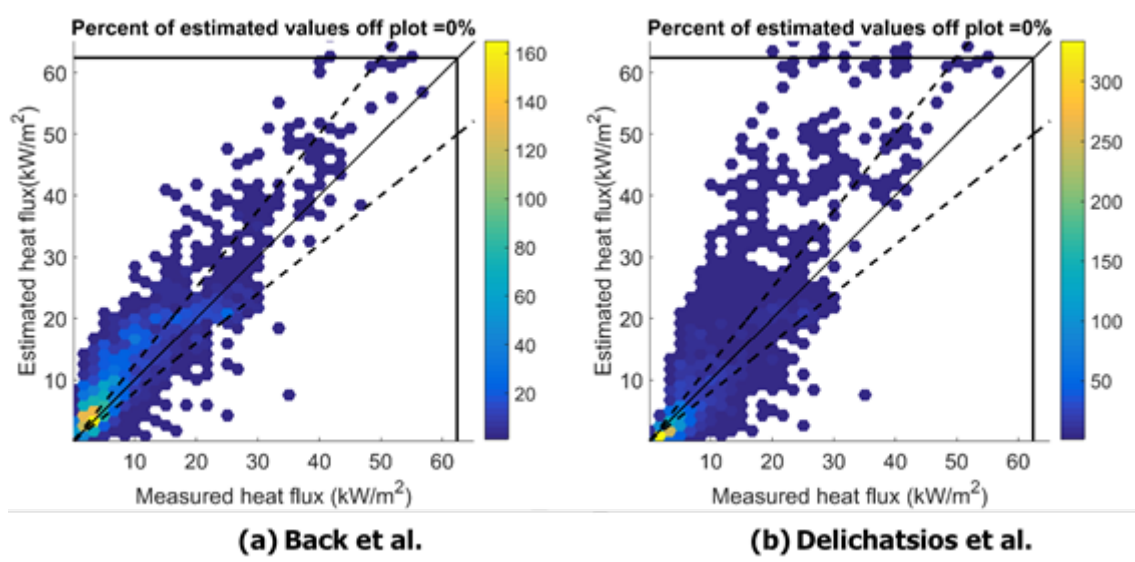


Figure 64. Back et al. and Delichatsios et al. heat flux profile comparisons to reduced-scale data (no aprons) using the modified Back et al. peak heat flux correlation.

8.3.3 Abecassis Empis correlation comparison to reduced-scale experiments

The Abecassis Empis correlation was compared to the average and maximum heat fluxes at the measured heights for the reduced-scale experiments as shown in Figure 65 and Figure 66. Figure 65 and Figure 66 both show the ± 10 kW/m² uncertainty band that was nominated by Abecassis Empis as red lines.

The Abecassis Empis correlation generally tended to overpredict the average heat flux but underpredicted the maximum heat flux in some instances for lower heights. Notably, the experiments that the Back et al. correlation underpredicted the heat flux for with the opening soffit at the ceiling level (H-T-F-2L, H-T-B-2L and H-T-B-3L) were overpredicted by the Abecassis Empis correlation.

The Abecassis Empis correlation was also compared to the reduced-scale experimental data (excluding apron experiments) on 10-second intervals, shown in Figure 67. The Abecassis Empis correlation is only a function of the height above the window soffit, which creates the discrete levels of estimated heat flux (with slight variation due to window geometry and position). The overpredictions occurred during periods of lower external flaming and heat release, since the correlation does not take these factors into account.

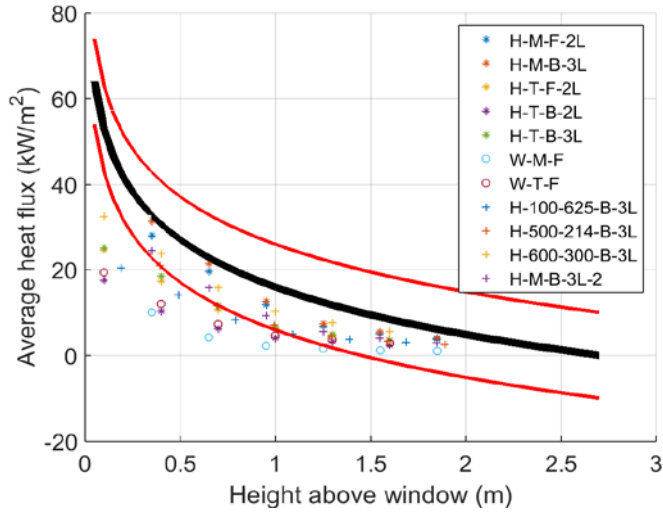


Figure 65. Comparison of Abecassis Empis correlation to average heat flux from reduced-scale experiments (no aprons).

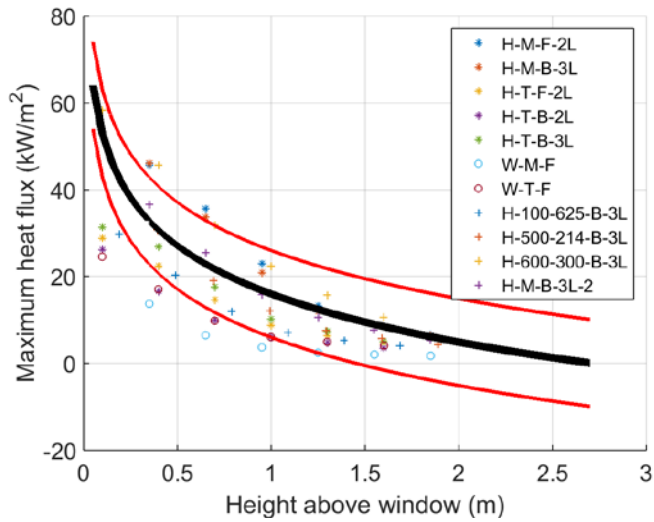


Figure 66. Comparison of Abecassis Empis correlation to maximum heat flux from reduced-scale experiments (no aprons).

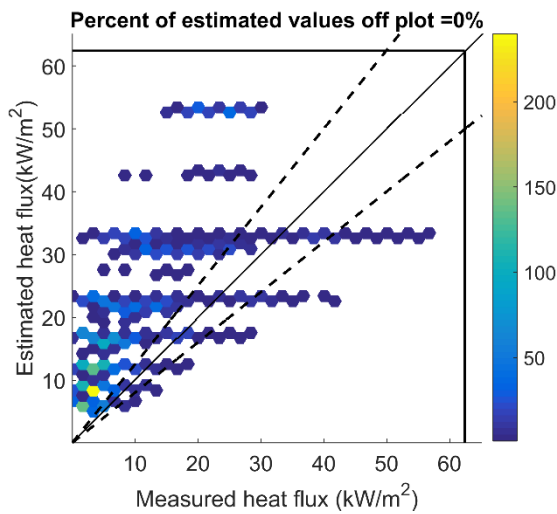


Figure 67. Abecassis Empis heat flux profile correlation compared to reduced-scale experimental data (no aprons).

8.3.4 Back et al. and Delichatsios et al. correlations comparison to NRCC façade experiments

A comparison of the Back et al. and Delichatsios et al. correlations using peak heat fluxes of 75 kW/m² and 100 kW/m² to the NRCC façade experimental heat flux data is shown in Figure 68. Most of the NRCC façade data fell below the Back et al. correlation and was quite scattered, and there were two experiments where the peak heat flux was greater than 75 kW/m². However, it does provide a reasonably conservative estimate for z/FH values greater than approximately 0.5 (greater than half of the flame height). The Delichatsios et al. correlation is substantially more conservative at z/FH values greater than 0.5 for high peak heat fluxes such as were seen in the large-scale NRCC façade experiments when compared to the reduced-scale experiments.

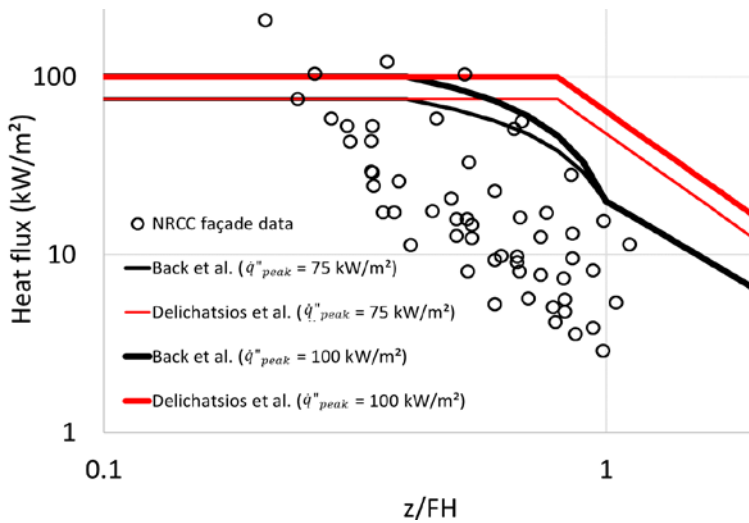


Figure 68. Comparison of Back et al. correlation to NRCC façade experiments.

8.3.5 Abecassis Empis correlation comparison to NRCC façade experiments

The Abecassis Empis correlation was compared to the NRCC façade experimental heat flux data for experiments where the flame height was reported as shown in Figure 69.

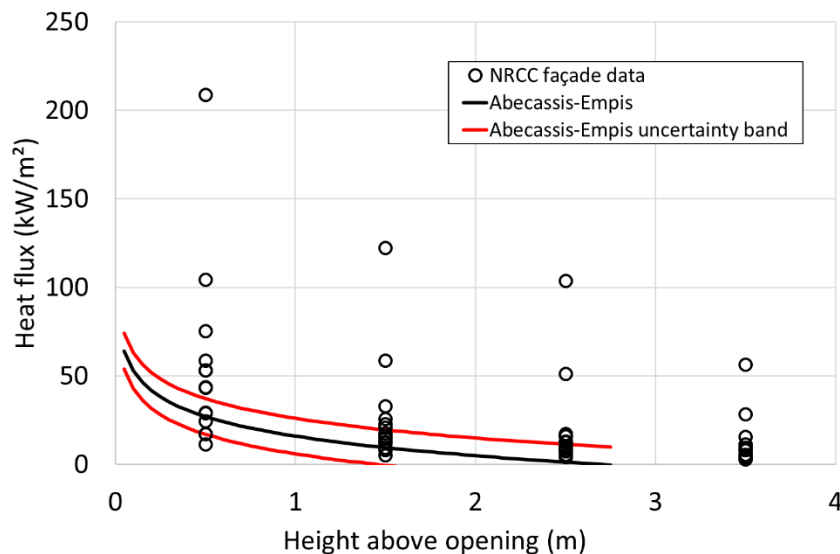


Figure 69. Comparison of Abecassis Empis correlation to NRCC façade experiments.

The Abecassis Empis correlation underpredicted the heat flux when the peak heat flux measured was above 40 kW/m², which corresponded to flame heights greater than 3 m.

8.4 Apron heat flux comparison

8.4.1 Heat flux correlation comparison to reduced-scale apron experiments

The Back et al., Delichatsios et al. and Abecassis Empis heat flux correlations were compared to the reduced-scale apron experimental heat flux data. The Back et al. and Delichatsios et al. correlations could factor in the addition of the apron to some extent because they are a partial function of the flame height, which is reduced as the apron projection increases. The Abecassis Empis correlation estimation is a function of height above the window opening only and does not change with the addition of an apron. A comparison of the Back et al. and Delichatsios et al. correlations using the arbitrary peak heat fluxes of 25 kW/m² and 50 kW/m² is shown in Figure 70. The slope of the experimental heat flux above the flame tip ($z/FH > 1$) tended to match the Back et al. correlation slope.

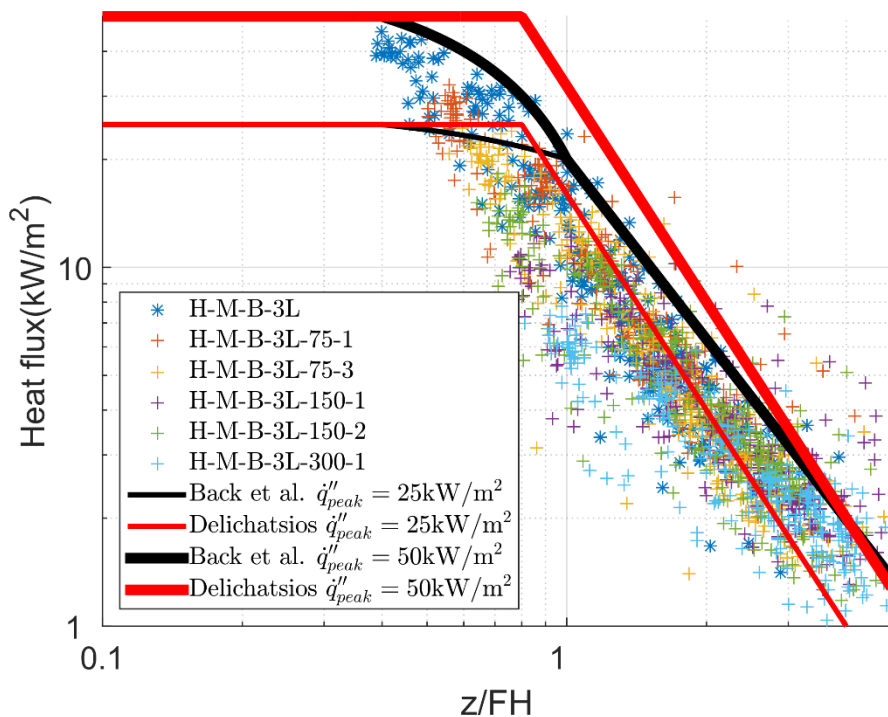


Figure 70. Back et al. and Delichatsios et al. comparison to reduced-scale experimental data where aprons were used.

8.4.2 NRCC façade apron experiments FDS heat flux comparison

Flame heights were not reported for the NRCC façade apron experiments, so the Back et al. and Delichatsios et al. correlations could not be compared. However, FDS simulations were possible because the heat release rate could be reasonably represented. Comparisons of the predicted heat flux on the wall for 0.3 m, 0.6 m and 1.0 m aprons with the simulated and measured heat flux for the no-apron case are shown in Figure 71.

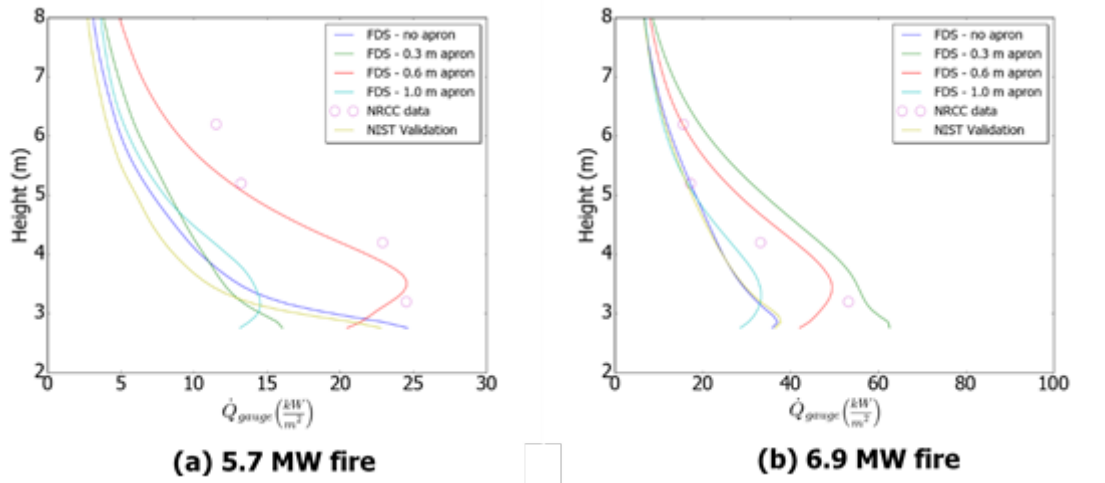


Figure 71. FDS heat flux results comparisons to NRCC façade experiments with aprons.

Contrary to the NRCC experiments, the FDS simulations did not show a consistent decrease in heat flux with the use of an apron. The simulated heat fluxes for the 0.6 m apron provided the best match to the no-apron experimental measurements. The reason for this is unknown, but one possible explanation is that the horizontal momentum of the flame coming out of the opening is underpredicted in FDS, so the horizontal flame projection in the FDS simulation with a 0.6 m apron is similar to the experimental flame projection with no apron.

9. External flame projection design guidelines

Based on the information provided in the previous sections, guidelines are provided here for modelling heat flux from flames projected from openings to the external surface immediately above the opening.

9.1 Design fire heat release rate input

One of the major factors that influences the amount of radiation on an external wall is the heat that is being released in the compartment and adjacent to the wall outside. As mentioned in section 8.1, the C/VM2 guidance of 150% of the ventilation-limited heat release rate seems reasonable for most instances, with the exceptions of large fuel surface areas with low fuel heat of gasification or fuel packages located very close to the opening. In these instances, 250% of the ventilation-limited heat release rate is more representative. However, further justification of the design fire for specific circumstances may be necessary because no data has been identified that indicates whether this trend will continue to greater excess heat release rate or not.

Care should be taken to ensure the heat release rate is reasonable when using FDS to model flames projecting from openings. Factors that can be used to evaluate the heat release rate in an FDS model include comparing the output heat release rate to the theoretical ventilation-limited heat release rate and the free-burning heat release rate for the fuel package or FDS fire definition (heat release rate per unit area).

9.2 Openings

The heat flux from wide aspect ratio openings and openings with the soffit at or close to ceiling level should be carefully evaluated. Adding a factor of safety to the predicted heat flux may be prudent where these compartment geometries are present.

9.3 Estimating projected flame height

Based on the data provided, the recommended methods for evaluating projected flame heights from openings are the Quintiere and Cleary correlation (using $B = 1$), FDS or the Lee et al. correlation. The Thomas and Law correlation can be used as well but may provide an excessive level of conservatism. Sensitivity analysis should be conducted when using FDS or the Lee et al. correlation in particular because there have been shown to be instances where both methods underpredict the flame height.

9.4 Estimating maximum heat flux incident on a wall above a projected flame

The Back et al. correlation is recommended for estimating the maximum heat flux incident on a wall. The peak heat flux correlation developed in this report should be used with caution if it predicts a heat flux near the maximum of 75 kW/m^2 or if a very large fire with a wide aspect ratio opening is expected. The Back et al. heat flux profile correlation becomes independent of peak heat flux above the flame tip. The Abecassis Empis correlation appears appropriate for short flames such as those seen in the reduced-scale experiments, but caution should be used if flame heights exceed 3 m or estimated peak heat flux levels exceed 40 kW/m^2 . The upper uncertainty bound is recommended to provide a level of conservatism for design.

The Delichatsios et al. heat flux profile correlation works well for moderate peak heat fluxes but starts to become overly conservative if high heat fluxes are expected. The Delichatsios et al. peak heat flux correlation should be used with caution for fires that are not underventilated and low flame heights.

9.5 Evaluation of Acceptable Solution spandrel and apron requirements

The spandrel and apron requirements in the New Zealand Acceptable Solutions, as described in section 2.2, are evaluated here using the recommended correlations discussed earlier in this section. Three heat flux levels are used as the criteria: 20 kW/m², 16 kW/m² (the Building Code clause 3.6 1 m radiation criterion) and 12.5 kW/m². Several sources including NFPA 80A *Recommended practice for protection of buildings from exterior fire exposures* and Collier (1996) have used 12.5 kW/m² as the typical minimum critical heat flux for ordinary combustible material piloted ignition. It is possible for some materials to ignite at heat fluxes below 12.5 kW/m², but the duration of heat exposure is likely to be long. Delichatsios et al. (2016) proposed using 20 kW/m² and 70 kW/m² as the critical heat flux for normal and tempered glazing failure, respectively.

In relation to the effectiveness of spandrels and aprons, the Fire Engineering Design Guide (Spearpoint, 2008, p. 113) makes the important observation that the objective with spandrels and aprons is only to reduce the incident radiation and hence the likelihood of vertical external fire spread, rather than preventing it from occurring.

The spandrel-only requirement of 1.5 m can be evaluated directly using the recommended correlations discussed earlier in this section. Table 10 shows the heights above an opening where the described heat flux levels are predicted using the Abecassis Empis correlation as a first approximation. The heat flux at the top of a spandrel that is 1.5 m high is predicted to be 9.5 kW/m² using the nominal correlation and 19.5 kW/m² using the upper uncertainty bound. Reductions of height to 1.24 m and 1.0 m increase the heat flux predicted by the nominal correlation to 12.5 kW/m² and 16 kW/m², respectively. Using the upper bound of the Abecassis Empis correlation, increasing the height to 1.87 m and 2.33 m reduces the heat flux to 16 kW/m² and 12.5 kW/m², respectively. However, as previously noted, these results may not be conservative for large flames.

Table 10. Evaluation of New Zealand Acceptable Solution spandrel criteria using the Abecassis Empis correlation.

| Z (m) | Abecassis-Empis maximum heat flux (kW/m ²) | |
|-------|--|-------------|
| | nominal | upper bound |
| 0.78 | 20.0 | 30.0 |
| 1.00 | 16.0 | 26.0 |
| 1.24 | 12.5 | 22.5 |
| 1.50 | 9.5 | 19.5 |
| 1.87 | 6.0 | 16.0 |
| 2.33 | 2.5 | 12.5 |

A comparison can also be made using the 150% ventilation-limited heat release rate criteria, the Quintiere and Cleary (B = 1) correlation and the Back et al. correlation for some typical openings. Results are shown in Table 11.

Table 11. Evaluation of New Zealand Acceptable Solution spandrel criteria using the 150% ventilation-limited heat release rate criteria and recommended flame height and heat flux correlations.

| Opening Type | Width (m) | Height (m) | $\dot{Q}_{vent\ lim}$ (MW) | Flame height for | | \dot{q}''_{max} (kW/m ²) | Z@ \dot{q}''_{max} (m) |
|-----------------------------|-----------|------------|----------------------------|---|--|--|--------------------------|
| | | | | $\dot{Q} = 150\% \dot{Q}_{vent\ lim}$ (m) | | | |
| Door | 0.8 | 2 | 3.4 | 2.7 | | 20.0 | 2.7 |
| | | | | | | 16.0 | 3.1 |
| | | | | | | 12.5 | 3.6 |
| Small window | 1 | 1 | 1.5 | 2.2 | | 20.0 | 2.2 |
| | | | | | | 16.0 | 2.5 |
| | | | | | | 12.5 | 2.9 |
| Medium window | 2 | 1.5 | 5.5 | 3.8 | | 20.0 | 3.8 |
| | | | | | | 16.0 | 4.3 |
| | | | | | | 12.5 | 5.0 |
| Ranchslider or large window | 2.5 | 2 | 10.6 | 4.9 | | 20.0 | 4.9 |
| | | | | | | 16.0 | 5.6 |
| | | | | | | 12.5 | 6.5 |

The heights above the window where the heat flux criteria of 20 kW/m², 16 kW/m² and 12.5 kW/m² are located are given in the last column of the table. The flame height calculated for the door opening is consistent with the flame heights observed in the experiments listed by Collier (2015) that have been completed at BRANZ in the past using a similar opening size. The required heights range from 50% greater to 333% greater than the 1.5 m soffit requirement in the Acceptable Solutions.

Alternatively, the heat release rate that would be expected to result in the heat flux criteria at 1.5 m can be calculated for these openings as shown in Table 12.

Table 12. Fire sizes predicted to cause heat flux criteria to be reached at the New Zealand Acceptable Solution spandrel criteria (1.5 m) using recommended flame height and heat flux correlations.

| Opening Type | Width (m) | Height (m) | \dot{q}''_{max} (kW/m ²) | Flame height (m) | \dot{Q} (MW) | $\dot{q} / \dot{q}_{vent\ lim}$ |
|-----------------------------|-----------|------------|--|------------------|----------------|---------------------------------|
| Door | 0.8 | 2 | 20.0 | 1.50 | 3.2 | 0.95 |
| | | | 16.0 | 1.31 | 3.0 | 0.88 |
| | | | 12.5 | 1.13 | 2.7 | 0.81 |
| Small window | 1 | 1 | 20.0 | 1.50 | 1.5 | 1.03 |
| | | | 16.0 | 1.31 | 1.4 | 0.92 |
| | | | 12.5 | 1.13 | 1.2 | 0.81 |
| Medium window | 2 | 1.5 | 20.0 | 1.50 | 3.5 | 0.64 |
| | | | 16.0 | 1.31 | 3.2 | 0.58 |
| | | | 12.5 | 1.13 | 2.9 | 0.52 |
| Ranchslider or large window | 2.5 | 2 | 20.0 | 1.50 | 5.7 | 0.54 |
| | | | 16.0 | 1.31 | 5.3 | 0.50 |
| | | | 12.5 | 1.13 | 4.8 | 0.46 |

All of the heat release rates are at or below the ventilation-limited heat release rate. The door and ranchslider openings can be compared to the NRCC façade window 1 and 4 experiments. The calculated heat release rates are somewhat conservative when compared to the NRCC façade data, but this is to be expected due to the previously discussed conservative nature of the correlations.

These two comparisons show that the Acceptable Solution spandrel requirement is in general significantly less onerous (also potentially non-conservative) than calculations based on the C/VM2 design fire. For most practical openings, fires do not have to become underventilated before typical heat flux criteria is exceeded at 1.5 m above the opening. The experimental data has shown that the C/VM2 design fire is possible for typical fuel packages although further full-scale testing with typical solid and liquid fuels would be useful to further develop the design fire.

There is not much information available to compare the apron requirements in the Acceptable Solution to other than the NRCC façade data since FDS modelling was not able to reproduce the results from the NRCC façade tests. However, based on the relative exposure estimates from the NRCC façade data, a rough estimate can be made as summarised in Table 13. The Building Code heat flux criterion of 16 kW/m² is used in this figure along with the peak heat flux calculated using the C/VM2 design fire. At an apron projection of 0.3 m, the heat flux criterion is reached at 2.3 m or 2.8 m above the window. The Acceptable Solutions allow a spandrel height of 1.0 m. At an apron projection of 0.6 m, the heat flux criterion is reached between 1.3 m and 2.3 m, while the Acceptable Solutions allow a spandrel height of 0.0 m. At an apron projection of 1.0 m, the heat flux criterion is not reached so no spandrel would be required.

Table 13. Evaluation of New Zealand Acceptable Solution apron criteria using the 150% ventilation-limited heat release rate criteria and recommended flame height and heat flux correlations.

| Opening Type | Width (m) | Height (m) | Apron (m) | $Z@q''_{max}=16 \text{ kW/m}^2$ (m) |
|-----------------------------|-----------|------------|-----------|-------------------------------------|
| Door | 0.8 | 2 | 0.0 | 3.1 |
| | | | 0.3 | 2.3 |
| | | | 0.6 | 1.3 |
| | | | 1.0 | 0.0 |
| Small window | 1 | 1 | 0.0 | 2.5 |
| | | | 0.3 | 2.3 |
| | | | 0.6 | 1.4 |
| | | | 1.0 | 0.0 |
| Medium window | 2 | 1.5 | 0.0 | 4.3 |
| | | | 0.3 | 2.8 |
| | | | 0.6 | 2.3 |
| | | | 1.0 | 0.0 |
| Ranchslider or large window | 2.5 | 2 | 0.0 | 5.6 |
| | | | 0.3 | 2.8 |
| | | | 0.6 | 2.3 |
| | | | 1.0 | 0.0 |

The notable international example of the Bouwkunde fire discussed in section 3 appears to corroborate the findings in this report. While the Acceptable Solution requirements appear to be non-conservative when compared with the experimental data and predictions using the correlations as described above, the occurrence of vertical fire spread from flames projecting from openings in New Zealand buildings is unknown. Further research may be useful to examine fire spread from flames projected from openings in a risk-informed basis since the probability of large flames from openings occurring may be quite low.

10. Conclusions

The objective of this study was to provide knowledge and guidance for considering the hazard of flames projected from openings in building fire safety design. Regulatory requirements in New Zealand were presented as well as an overview of existing fire science literature and tools for evaluating flames projected from openings. A reduced-scale experimental programme was undertaken to provide additional data for benchmarking and better understanding of projected flame behaviour. Design fire and tool recommendations were made based on comparisons to observations in the experimental programme and literature data. These recommendations are summarised as follows:

- Based on the reduced-scale experiments, the C/VM2 guideline for post-flashover design fire heat release rate of 150% of the ventilation-limited heat release rate is reasonable for most scenarios, with the exceptions of fuels with large surface areas and low heat of gasification (high volatility) or fuels located directly adjacent to an opening. In that case, the heat release rate should be increased to 250% of the ventilation-limited heat release rate, although further research is required to determine if further increases are necessary in extreme circumstances. It should be noted that these recommendations only apply when designing for vertical external fire spread and do not apply for other design scenarios.
- FDS can accurately model the flame height and heat flux from freely burning fires but does not always represent fuel burning in an accurate manner for ventilation-limited fires in compartments. Care should be taken to review the FDS output heat release rate to ensure it is as expected.
- The Lee et al. flame height correlation provided the most accurate representation of flame height when compared to the reduced-scale experiments and the NRCC façade experimental data. However, it was unconservative at times. The Quintiere and Cleary method using $B = 1$ provided a good representation but was more conservative, so is recommended for design purposes based on the information in this report.
- The Abecassis Empis heat flux correlation is reasonable when flame heights in the order of 1 m are expected. It will underpredict heat flux if higher flame heights are expected.
- The Back et al. heat flux correlation provided a good match to external wall heat flux using a new correlation for peak heat flux for flames projected from openings. However, some experimental outliers had a peak heat flux above 75 kW/m^2 , which was not well predicted by the new correlation, so this correlation should be used with caution if high heat fluxes are expected or if the peak heat flux is critical. The peak heat flux does not influence the Back et al. heat flux correlation at heights above the flame height. Also, reduced-scale fires with a wide opening aspect ratio or opening soffit at ceiling level produced heat fluxes at higher wall locations that were underpredicted by the Back et al. model.
- The Delichatsios et al. heat flux profile correlation provides comparable results to Back et al. for moderate peak heat fluxes. The Delichatsios et al. peak heat flux correlation should be used with caution for fires that are not underventilated and for short flame heights.
- FDS worked reasonably well for predicting flame heights for large-scale external fires from openings but did not predict external wall heat fluxes well. Extra care with FDS is recommended for this scenario to ensure that the heat release rate output by FDS is what is expected. It is recommended that the external wall heat flux be checked with a correlation if FDS is used.



The Acceptable Solution requirements for spandrels and aprons were found to be non-conservative when compared to experimental data, the Building Code external heat flux requirements and the C/VM2 design fire heat release rate for typical opening sizes. However, further analysis may be beneficial to determine the overall risk of fire spread from flames projecting from openings based on the probability of large flames occurring.

11. Future work

The experiments completed for this study focused on one opening ventilation factor, with only one experiment looking at a doubled ventilation factor. More experiments looking at additional opening geometries would be useful. Experiments with larger fuel surface areas and more highly volatile fuels would provide information on cases where greater heat release rates relative to the ventilation limit may occur. Additional data from full-scale experiments (particularly with calorimetry heat release rate measurements) would provide greater confidence in the ability of the tools to predict heat flux for real building fires. There is limited data available on the effects of aprons on the heat flux on walls from projected flames, so more experiments in this area are recommended.

Additional FDS modelling to investigate fuel burning outside of openings and in underventilated compartments as well as the estimated heat flux on surfaces would provide more understanding of why there are discrepancies between FDS and experimental results. Further work could be undertaken to include a projected flame module in B-RISK for fire safety practitioners to use. A risk-informed study of the potential for fire spread from flames projected from openings is recommended to further evaluate the Acceptable Solution criteria for spandrels and aprons and the C/VM2 guidance for modelling fires projecting from openings.

References

- Abecassis Empis, C. (2010). *Analysis of the compartment fire parameters influencing the heat flux incident on the structural façade*. (PhD thesis). University of Edinburgh, Scotland. Retrieved from <https://www.era.lib.ed.ac.uk/handle/1842/4188>
- Babrauskas, V. (2008). Heat release rate, Sect. 3, Ch. 1. In P. J. DiNenno, D. Drysdale, C. L. Beyler, W. D. Walton, R. L. P. Custer, J. R. Hall, Jr. & J. M. Watts, Jr. (Eds.), *The SFPE Handbook of Fire Protection Engineering* (4th ed., pp. 3-1-3–59). Quincy, MA, USA: National Fire Protection Association.
- Back, G., Beyler, C., DiNenno, P. & Tatem, P. (1994). Wall incident heat flux distributions resulting from an adjacent fire. *Fire Safety Science*, 4, 241–252. <https://doi.org/10.3801/IAFSS.FSS.4-241>
- Bullen, M. L. & Thomas, P. H. (1979). Compartment fires with non-cellulosic fuels. *Symposium (International) on Combustion*, 17(1), 1139–1148. [https://doi.org/10.1016/S0082-0784\(79\)80108-3](https://doi.org/10.1016/S0082-0784(79)80108-3)
- Collier, P. (1996). *Method for determining safe separation distances between buildings in the event of fire*. Technical Recommendation No. 13. Judgeford, New Zealand: BRANZ Ltd.
- Collier, P. (2015). *Characterising fire plumes from openings in external walls*. BRANZ Study Report SR320. Judgeford, New Zealand: BRANZ Ltd.
- de Ris, J. L. & Khan, M. M. (2000). A sample holder for determining material properties. *Fire and Materials*, 24(5), 219–226. [https://doi.org/10.1002/1099-1018\(200009/10\)24:5<219::AID-FAM741>3.0.CO;2-7](https://doi.org/10.1002/1099-1018(200009/10)24:5<219::AID-FAM741>3.0.CO;2-7)
- Delichatsios, M. (2014). Enclosure and facade fires: Physics and applications. *Fire Safety Science*, 11, 3–27. <https://doi.org/10.3801/IAFSS.FSS.11-3>
- Delichatsios, M. A., Ryan, J., Tian, N. & Zhang, J. (2016). *Vertical safe separation distance between openings in multi-storey buildings having a fire resistant spandrel*. Presented at the 2nd International Seminar for Fire Safety of Facades, Lund, Sweden. <https://doi.org/10.1051/mateconf/20164604003>
- Delichatsios, M. A., Silcock, G. W. H., Liu, X., Delichatsios, M. & Lee, Y.-P. (2004). Mass pyrolysis rates and excess pyrolysate in fully developed enclosure fires. *Fire Safety Journal*, 39(1), 1–21. <https://doi.org/10.1016/j.firesaf.2003.07.006>
- Delichatsios, M. & Silcock, G. (2003). Fully involved enclosure fires: Effects of fuel type, fuel area and geometry. *Fire Safety Science*, 7, 59–73. <https://doi.org/10.3801/IAFSS.FSS.7-59>
- Drysdale, D. (1998). *An introduction to fire dynamics*. Edinburgh, Scotland: John Wiley & Sons.
- Fleury, R. (2010). *Evaluation of thermal radiation models for fire spread between objects* (Master's thesis). University of Canterbury, New Zealand. Retrieved from <http://ir.canterbury.ac.nz:80/handle/10092/4959>

- He, Y., Fernando, A. & Luo, M. (1998). Determination of interface height from measured parameter profile in enclosure fire experiment. *Fire Safety Journal*, (31), 19-38. [https://doi.org/10.1016/S0379-7112\(97\)00064-7](https://doi.org/10.1016/S0379-7112(97)00064-7)
- Ingason, H. & Wickstrom, U. (2007) Measuring incident radiant heat flux using the plate thermometer. *Fire Safety Journal*, 42, 161-166. <http://dx.doi.org/10.1016/j.firesaf.2006.08.008>
- Karlsson, B., & Quintiere, J. G. (2000). Pressure profiles and vent flows for well-ventilated enclosures. In *Enclosure Fire Dynamics*. Boca Raton, FL, USA: CRC Press.
- Kawagoe, K. (1958). *Fire behaviour in rooms*. Tokyo, Japan: Building Research Institute, Ministry of Construction.
- Law, M. (1978). Fire safety of external building elements. The design approach. *Engineering Journal*, 15(2), 59-74.
- Lee, Y., Delichatsios, M. & Silcock, G. (2008). Heat flux distribution and flame shapes on the inert facade. *Fire Safety Science*, 9, 193-204. <https://doi.org/10.3801/IAFSS.FSS.9-193>
- Lee, Y.-P., Delichatsios, M. A., Ohmiya, Y., Wakatsuki, K., Yanagisawa, A. & Goto, D. (2009). Heat fluxes on opposite building wall by flames emerging from an enclosure. *Proceedings of the Combustion Institute*, 32(2), 2551-2558. <https://doi.org/10.1016/j.proci.2008.06.130>
- McGrattan, K., Hostikka, S., McDermott, R., Floyd, J., Weinschenk, C. & Overholt, K. (2016). *Fire Dynamics Simulator technical reference guide. Volume 3: Validation*. NIST Special Publication 1018-3. Gaithersberg, MD, USA: National Institute of Standards and Technology.
- Mizuno, T. & Kawagoe, K. (1986). Burning behaviour of upholstered chairs: Part 3, Flame and plume characteristics in fire test. *Fire Science and Technology*, 6(1+2), 29-37. <https://doi.org/10.3210/fst.6.29>
- Nilsson, M. (2016). *The impact of horizontal projections on external fire spread – a numerical comparative study.*, Lund, Sweden: Lund University.
- Ohmiya, Y., Hori, Y., Safimori, K. & Wakamatsu, T. (2000). Predictive method for properties of flame ejected from an opening incorporating excess fuel. *Fire Safety Science*, 4, 375-386.
- Oleszkiewicz, I. (1989). Heat transfer from a window fire plume to a building facade. *ASME HTD – Collected Papers in Heat Transfer*, 123, 163-170.
- Oleszkiewicz, I. (1991). Vertical separation of windows using spandrel walls and horizontal projections. *Fire Technology*, 27(4), 334-340. <https://doi.org/10.1007/BF01039884>
- Park, H., Meacham, B. J., Dembsey, N. A. & Goulthorpe, M. (2014). Enhancing building fire safety performance by reducing miscommunication and misconceptions. *Fire Technology*, 50(2), 183-203. <https://doi.org/10.1007/s10694-013-0365-2>
- Quintiere, J. G. & Cleary, T. G. (1994). Heat flux from flames to vertical surfaces. *Fire Technology*, 30(2), 209-231. <https://doi.org/10.1007/BF01040003>

- Seigel, L. G. (1969). The projection of flames from burning buildings. *Fire Technology*, 5(1), 43–51. <https://doi.org/10.1007/BF02591612>
- Spearpoint, M. (Ed.). (2008). *Fire engineering design guide* (3rd ed.). Christchurch, New Zealand: Centre for Advanced Engineering.
- Tewarson, A. (2008). Generation of heat and gaseous, liquid and solid products in fires, Sect. 3, Ch. 4. In P. J. DiNenno, D. Drysdale, C. L. Beyler, W. D. Walton, R. L. P. Custer, J. R. Hall, Jr. & J. M. Watts, Jr. (Eds.), *The SFPE Handbook of Fire Protection Engineering* (4th ed., pp. 3-109-3–194). Quincy, MA, USA: National Fire Protection Association.
- Thomas, P. H. (1960). Buoyant diffusion flames. *Combustion and Flame*, 4(4), 381–382.
- Thomas, P. H. (1961). *On the heights of buoyant flames*. Fire Research Note 489. Borehamwood, UK: Fire Research Station.
- Thomas, P. H. & Law, M. (1972). *The projection of flames from burning buildings*. Fire Research Note 921. Borehamwood, UK: Fire Research Station.
- Thornton, W. M. (1917). XV. The relation of oxygen to the heat of combustion of organic compounds. *Philosophical Magazine Series 6*, 33(194), 196–203. <https://doi.org/10.1080/14786440208635627>
- Veloo, P. S. & Quintiere, J. G. (2013) Convective heat transfer coefficient in compartment fires. *Journal of Fire Sciences*, 31(5), 410-423. <https://doi.org/10.1177/0734904113479001>
- Webster, C. T. & Raftery, M. M. (1959). *The burning of fires in rooms, part II. Tests with cribs and high ventilation on various scales*. Fire Research Note 401. Borehamwood, UK: Fire Research Station.
- Wong, W. C.-K. (2012). *CFD flame spread model validation: Multi-component data set framework* (Master's thesis).: Worcester Polytechnic Institute, Worcester, MA, USA.
- Yokoi, S. (1960). *Study on the prevention of fire-spread caused by hot upward current*. Tokyo, Japan: Building Research Institute, Ministry of Construction.
- Yoshioka, H., Ohmiya, Y., Noaki, M. & Yoshida, M. (2011). Large-scale facade fire tests conducted based on ISO 13785-2 with noncombustible facade specimens. *Fire Science and Technology*, 31(1), 1–22. <https://doi.org/10.3210/fst.31.1>

Appendix A: Heat flux meter calibration

The plate thermometer heat flux meters were calibrated being subjected to varying incident heat fluxes from a cone calorimeter heater. The cone radiator was rotated by 90° such that the heat flux meter was facing the radiator horizontally as shown in Figure 72.



Figure 72. Cone and heat flux meter configuration.

The calculated incident heat fluxes were then compared to the heat flux values measured by a Schmidt-Boelter heat flux gauge. The heat flux measurements with the Schmidt-Boelter gauge and the plate thermometer gauges were not taken simultaneously since the heat flux profile across the cone heater is not uniform. Instead, the heat flux measured by the Schmidt-Boelter gauge at the centre of the cone heater was correlated with the temperature of the cone heater. The Schmidt-Boelter gauge was then replaced by the plate thermometer heat flux gauge, which was positioned at the centre of the cone heater and the same distance as the Schmidt-Boelter gauge was placed. Repeatability of the heat flux relationship with cone heater temperature was then checked with the Schmidt-Boelter gauge after the plate thermometer measurements were taken.

While the Schmidt-Boelter heat flux gauge responds to net absorbed heat flux (with an absorptance of 0.95), it is calibrated to incident irradiation. Thus, the following energy balance shown in Figure 73 was used to estimate the incident radiation heat flux on the plate thermometer heat flux meters.

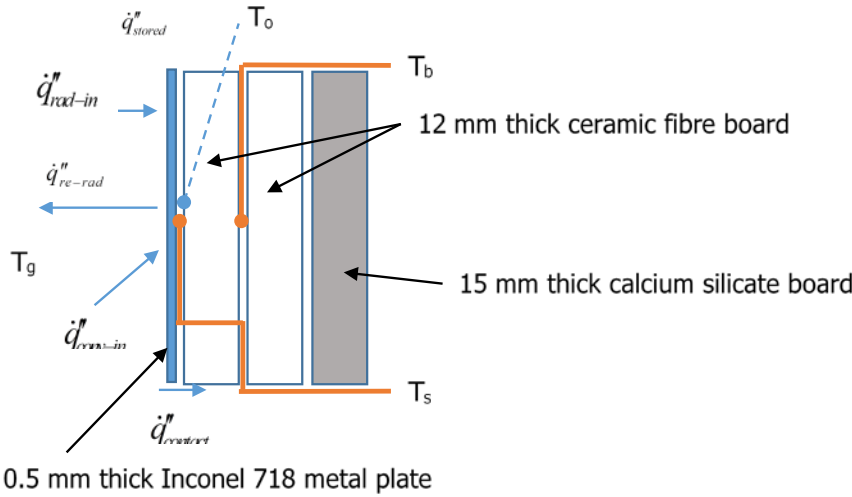


Figure 73. Section view of plate thermometer heat flux meter.

Considering the metal plate to be the control volume:

$$\dot{q}''_{stored} = \dot{q}''_{in} - \dot{q}''_{out} \quad \text{Eqn. 60}$$

Therefore:

$$\dot{q}''_{stored} = \dot{q}''_{rad-in} + \dot{q}''_{conv-in} - \dot{q}''_{re-rad} - \dot{q}''_{contact} \quad \text{Eqn. 61}$$

Often, $\dot{q}''_{contact}$ was treated as conductive heat loss in the form of $h_{cont}(T_s - T_o)$ (Ingason & Wickström, 2007; Veloo & Quintiere, 2013). This approach showed a good agreement when the plate temperature (T_s) became stable at a given constant incident heat flux. However, in varying heat fluxes and during the initial heating period, the approach of de Ris and Khan (2000) showed a better agreement. In the current study, the latter method was used.

Therefore, substituting various terms into Eqn. 61 gives:

$$\rho c_p \delta \frac{dT_s}{dt} = \varepsilon_s \dot{q}''_{inc-rad} + h_c(T_g - T_s) - \varepsilon_s \sigma T_s^4 - [\varepsilon_{bs} \sigma (T_s^4 - T_o^4) + h_{cont}(T_s - T_o)] \quad \text{Eqn. 62}$$

Then the incident radiative heat flux becomes:

$$\dot{q}''_{inc-rad} = \frac{1}{\varepsilon_s} \left(\rho c_p \delta \frac{dT_s}{dt} + h_c(T_s - T_\infty) + \varepsilon_s \sigma T_s^4 + [\varepsilon_{bs} \sigma (T_s^4 - T_o^4) + h_{cont}(T_s - T_o)] \right) \quad \text{Eqn. 63}$$

Where:

$\dot{q}''_{inc-rad}$ = incident radiative heat flux

ε_s = surface emissivity of the blackened metal plate (=0.9)

ρ = density of the metal plate (=8020 kg/m³, measured)

- c_p = specific heat of the metal plate (=435 J/kgK)³
- δ = thickness of the metal plate (=0.00051 m, measured)
- T_s = surface temperature of the metal plate
- h_c = convective heat transfer coefficient
- ε_{bs} = emissivity of the back surface of the metal plate facing the insulation
- σ = Stefan-Boltzman constant (=5.67×10⁻⁸ W/m²K⁴)
- T_o = first node temperature of the insulation facing the metal plate
- h_{cont} = conduction correction factor accounting for conductive heat loss

In this correlation, T_s is directly measured and four unknown parameters – h_c , ε_{bs} , T_o and h_{cont} – are included.

The convective heat transfer coefficient, h_c , was calculated from an empirical correlation for a vertically oriented plate for natural convection (Ingason & Wickström, 2007):

$$h_c = 4.0 \left(\frac{T_s - T_{amb}}{L} \right)^{1/4} (T_s + T_{amb})^{-0.16} \quad \text{Eqn. 64}$$

The back-surface emissivity, ε_{bs} , was assumed to be 0.5. The surface emissivity of a shiny metal plate is typically approximately 0.3, but the plate became slightly dull after tests by oxidation. Regardless, it was found that the heat flux was not sensitive to the back-surface emissivity.

The surface node temperature of the ceramic fibre board, T_o , was calculated using a numerical method for a transient heat conduction analysis as shown in Figure 74.

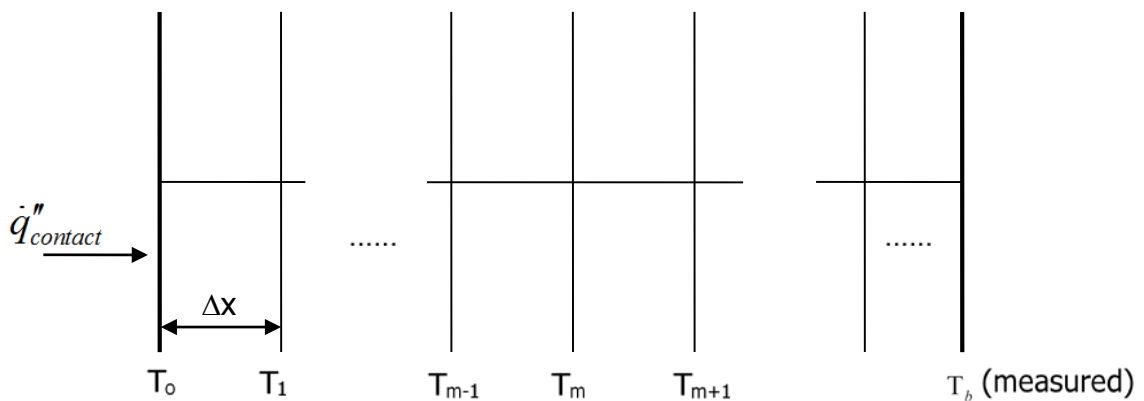


Figure 74. Conceptual discretisation of the ceramic fibre board.

The following governing equation (GE) can be used to describe heat transfer in the ceramic fibre board, assuming it is one-dimensional conduction:

³ www.espi Metals.com/index.php/78-technical-data/inconel-718/91-inconel-718

$$\frac{dT}{dt} = \alpha \frac{d^2T}{dx^2} \quad \text{Eqn. 65}$$

Where:

$$\alpha = \frac{k}{\rho c_p}, \text{ thermal diffusivity, m}^2/\text{s}$$

k = thermal conductivity, W/(m K)

Discretising the thickness of the board into nodes, the GE Eqn. 65 can be rewritten for node m at timestep i as:

$$\frac{T_m^{i+1} - T_m^i}{dt} = \alpha \frac{T_{m-1}^i - 2T_m^i + T_{m+1}^i}{dx^2} \quad \text{Eqn. 66}$$

Where:

m is an index representing the nodal position

i is an index representing the timestep

Which can in turn be rewritten as:

$$T_m^{i+1} = \left(\frac{k_{ins}}{\rho_{ins} c_{p,ins}} \right) \frac{dt}{dx^2} (T_{m-1}^i - 2T_m^i + T_{m+1}^i) + T_m^i \quad \text{Eqn. 67}$$

Where the *ins* subscript refers to ceramic fibre properties.

Eqn. 67 can be applied to solve for the temperature at any interior nodes within the ceramic fibre board at increasing timesteps. The initial condition at t = 0 s was assumed to be uniform temperature of T_b throughout the ceramic fibre board. The surface node temperature, T_b , was directly measured. An energy balance was used to determine the remaining boundary condition for T_o as shown in Figure 75.

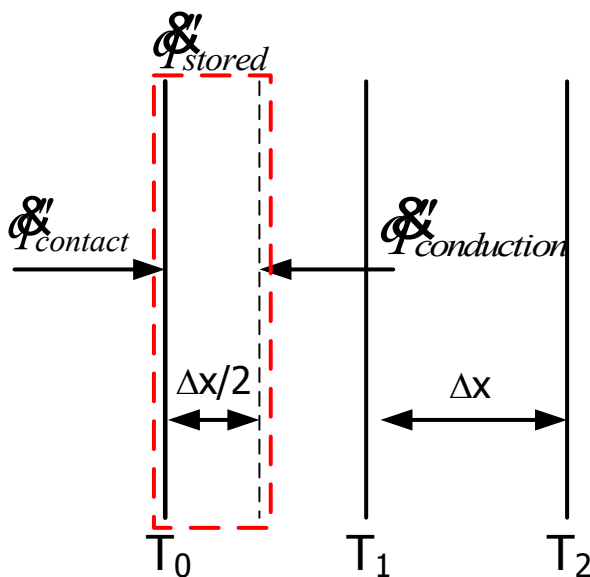


Figure 75. Energy balance of insulation surface node in contact with the Inconel plate.

The interior surface boundary condition becomes:

$$\Delta E = E_{in} - E_{out}$$

Eqn. 68

$$\dot{q}_{stored}'' = \dot{q}_{contact}'' + \dot{q}_{conduction}''$$

Eqn. 68 can be rewritten in terms of two adjacent node temperatures as:

$$\rho_{ins} c_{p,ins} \frac{\Delta x}{2} \frac{T_0^{i+1} - T_0^i}{\Delta t} = \varepsilon_{bs} \sigma (T_s^{i4} - T_0^{i4}) + h_{cont} (T_s^i - T_0^i) + k_{ins} \frac{T_1^i - T_0^i}{\Delta x}$$

Eqn. 69

And therefore:

$$T_0^{i+1} = \frac{2\Delta t}{\rho_{ins} c_{p,ins} \Delta x} \left[\varepsilon_{bs} \sigma (T_s^{i4} - T_0^{i4}) + h_{cont} (T_s^i - T_0^i) + \frac{k_{ins}}{\Delta x} (T_1^i - T_0^i) \right] + T_0^i$$

Eqn. 70

Eqn. 70 can then be re-written as:

$$\begin{aligned} T_0^{i+1} &= \frac{2k_{ins}\Delta t}{\rho_{ins}c_{p,ins}\Delta x^2} \left[\frac{\Delta x}{k_{ins}} \varepsilon_{bs}\sigma (T_s^{i4} - T_0^{i4}) + h_{cont}(T_s^i - T_0^i) + T_1^i - T_0^i \right] + T_0^i \\ &= 2Fo \left[\frac{\Delta x}{k_{ins}} \varepsilon_{bs}\sigma (T_s^{i4} - T_0^{i4}) + h_{cont}(T_s^i - T_0^i) + T_1^i - T_0^i \right] + T_0^i \end{aligned}$$

Eqn. 71

This puts the boundary condition into the typical form where the Fourier number Fo is factored out. The property values of the ceramic fibre board were obtained from the manufacturer as shown in Table 5.

The conduction correction factor was then determined to be $h_{cont} = 12 \text{ W/m}^2\text{K}$. Comparison of the calculated incident heat flux and that measured by the Schmidt-Boelter heat flux gauge showed a good agreement as shown in Figure 76.

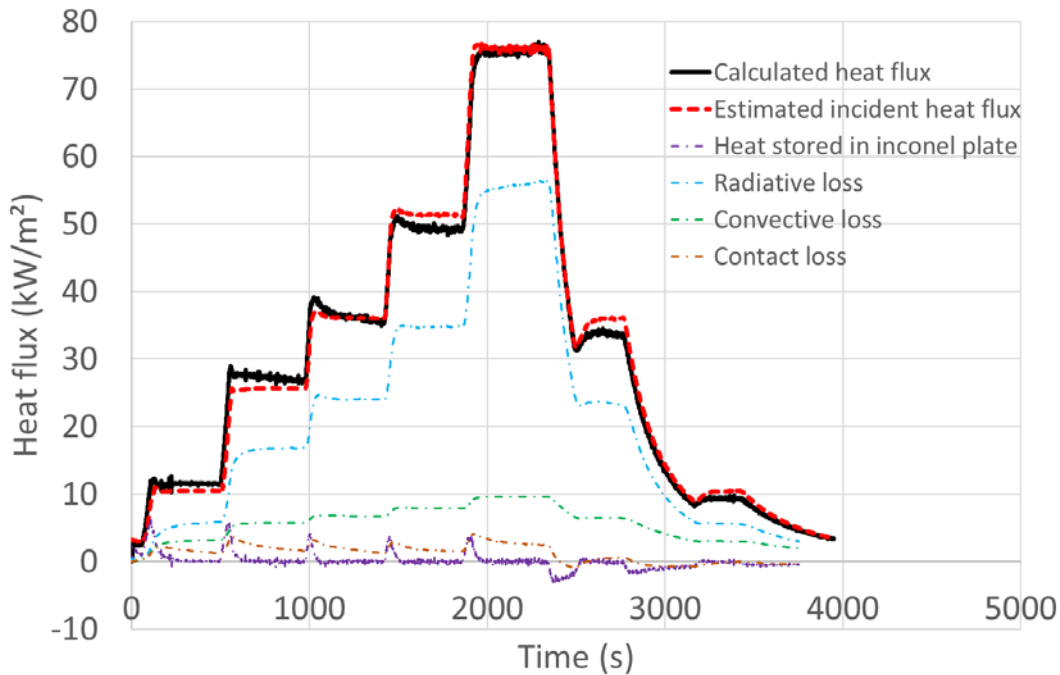


Figure 76. Incident radiative heat flux comparison with calculated heat flux components and estimated incident heat flux based on cone heater temperature.

Appendix B: Incident heat flux measurement

In fire tests, water-cooled heat flux gauges have been widely used. However, soot deposition on the gauge surface and a moderate cost with a relatively high fragility in fire conditions have been considered unfavourable. The heat flux meters used in this study are a good alternative to the commercially available water-cooled heat flux meters.

Considering the metal plate to be the control volume in the same way in Appendix A, Eqn. 61 applies and Eqn. 62 can be rewritten as:

$$\rho c_p \delta \frac{dT_s}{dt} = \varepsilon_s \dot{q}_{inc-rad}'' + h_c (T_g - T_s) - \varepsilon_s \sigma T_s^4 - [\varepsilon_{bs} \sigma (T_s^4 - T_o^4) + h_{cont} (T_s - T_o)] \quad \text{Eqn. 72}$$

Assuming a water-cooled heat flux gauge subjected to the same condition and the same surface emissivity, the heat flux reading from the gauge is calculated as (Veloo & Quintiere, 2013):

$$\dot{q}_{HFG}'' = \varepsilon_s \dot{q}_{inc-rad}'' + h_c (T_g - T_w) \quad \text{Eqn. 73}$$

Where:

T_w = cooling water temperature

Substituting Eqn. 73 into Eqn. 72 gives:

$$\rho c_p \delta \frac{dT_s}{dt} = \dot{q}_{HFG}'' - h_c (T_s - T_w) - \varepsilon_s \sigma T_s^4 - [\varepsilon_{bs} \sigma (T_s^4 - T_o^4) + h_{cont} (T_s - T_o)] \quad \text{Eqn. 74}$$

Which in turn can be rearranged as:

$$\dot{q}_{HFG}'' = \rho c_p \delta \frac{dT_s}{dt} + h_c (T_s - T_w) + \varepsilon_s \sigma T_s^4 + [\varepsilon_{bs} \sigma (T_s^4 - T_o^4) + h_{cont} (T_s - T_o)] \quad \text{Eqn. 75}$$

Here, except the convective heat transfer coefficient, h_c , other parameter values can be determined from the calibration process. The convective heat transfer coefficient is generally dependent on the flow characteristics such as the velocity and temperature of the flow as well as the configuration of the surface relative to the flow direction. The 11 heat flux meters used in the test may be largely divided into four different configurations as shown in Figure 77. Case 1 includes six heat flux meters on the vertical panel, and cases 2–4 include four heat flux meters on the walls, the ceiling and the floor of the compartment.

For case 1, $h_c = 0.03$ kW/m²K was used, calculated from the forced convection correlation of 3 m/s. The flow velocity of 3 m/s was assumed based on the previous fire experiments conducted by Wong (2012) where a similar fire size was used. For cases 2–4, $h_c = 0.01$ kW/m²K was used, calculated from the free convection correction. Although the heat transfer coefficient varies from 0.002 to 0.013 kW/m²K depending on the film temperature and the heat flux meter configurations, $h_c = 0.01$ kW/m²K is deemed to be reasonable considering that the gas temperature in the compartment is relatively uniform (see Appendix F).

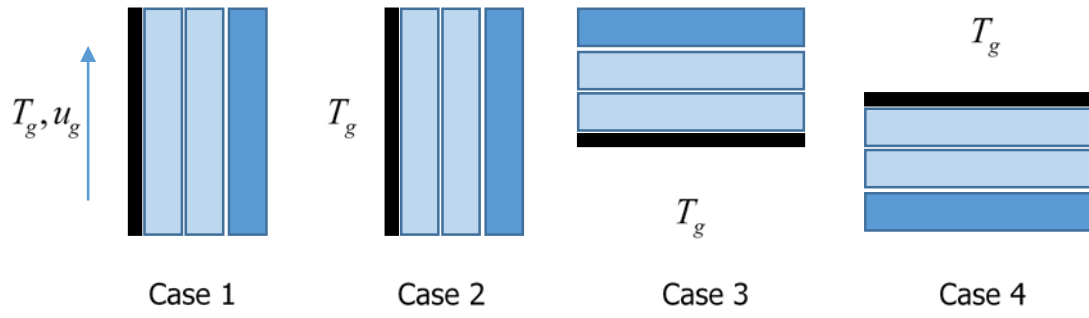
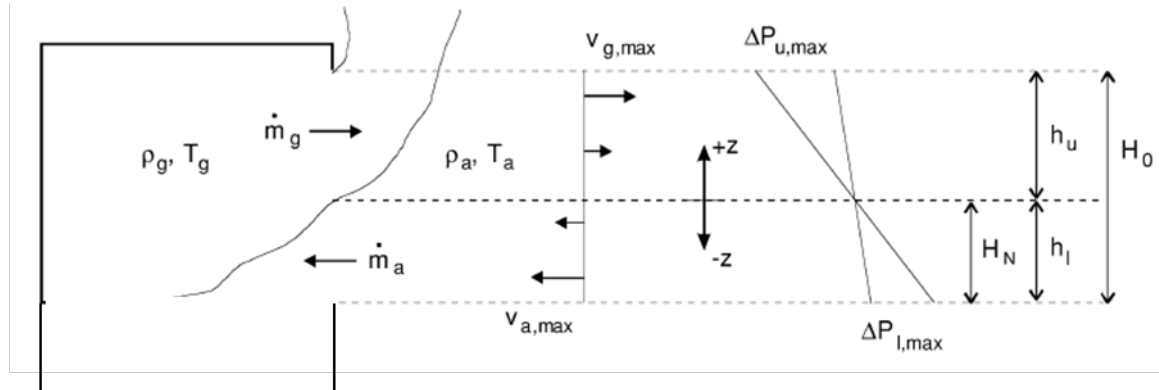


Figure 77. Various configurations of the plate heat flux meters in the test.

Appendix C: Mass flow rate calculation

Karlsson and Quintiere (2000) use the following nomenclature to describe compartment mass flows:



© CRC Press LLC. Reproduced with permission from CRC Press LLC.

Figure 78. Vent flows (Karlsson & Quintiere, 2000).

The mass flow into the compartment is:

$$\dot{m}_a = C_d W_o \rho_a \sqrt{\frac{2(\rho_a - \rho_g)g}{\rho_a}} \left(\frac{2}{3} h_l^{3/2}\right) \quad \text{Eqn. 76}$$

The mass flow out of the compartment is:

$$\dot{m}_g = C_d W_o \rho_g \sqrt{\frac{2(\rho_a - \rho_g)g}{\rho_a}} \left(\frac{2}{3} h_u^{3/2}\right) \quad \text{Eqn. 77}$$

Since $\dot{m}_a = \dot{m}_g$:

$$\sqrt{\rho_a}(h_l^{3/2}) = \sqrt{\rho_g}(h_u^{3/2}) \quad \text{Eqn. 78}$$

Or:

$$\left(\frac{h_u}{h_l}\right)^{3/2} = \left(\frac{\rho_a}{\rho_g}\right)^{1/2} \quad \text{Eqn. 79}$$

From Figure 78:

$$h_u = H_o - h_l \quad \text{Eqn. 80}$$

Substituting Eqn. 80 into Eqn. 79 and rearranging gives:

$$\frac{H_o - h_l}{h_l} = \left(\frac{\rho_a}{\rho_g}\right)^{1/3} \quad \text{Eqn. 81}$$

On this basis, the neutral plane height becomes:

$$H_N = h_l = \frac{H_o}{1 + \left(\frac{\rho_a}{\rho_g}\right)^{1/3}} \quad \text{Eqn. 82}$$

Substituting Eqn. 82 into Eqn. 76 and rearranging gives:

$$\dot{m}_a = \frac{2}{3} C_d W_o \rho_a \sqrt{\frac{2g(\rho_a - \rho_g)}{\rho_a}} \left(\frac{H_o}{1 + \left(\frac{\rho_a}{\rho_g}\right)^{1/3}} \right)^{3/2} \quad \text{Eqn. 83}$$

Since $A_o = W_o H_o$, Eqn. 83 can be represented as:

$$\dot{m}_a = \frac{2}{3} A_o \sqrt{H_o} C_d \rho_a \sqrt{2g} \frac{\left(1 - \frac{\rho_g}{\rho_a}\right)}{\left[1 + \left(\frac{\rho_a}{\rho_g}\right)^{1/3}\right]^3} \quad \text{Eqn. 84}$$

For completeness, it can be noted that from the ideal gas law, i.e.:

$$\rho \propto \frac{1}{T} \quad \text{Eqn. 85}$$

Eqn. 84 can also be expressed in terms of temperature ratios, i.e.:

$$\dot{m}_a = \frac{2}{3} A_o \sqrt{H_o} C_d \rho_a \sqrt{2g} \frac{\left(1 - \frac{T_a}{T_g}\right)}{\left[1 + \left(\frac{T_g}{T_a}\right)^{1/3}\right]^3} \quad \text{Eqn. 86}$$

Karlsson and Quintiere (2000) define the square root term on the right-hand side of Eqn. 84 as the density factor and plot this parameter against the ratio of gas to ambient temperatures, $\frac{T_g}{T_a}$ (2000, p. 100, Fig. 5.13). They note that, when the gas temperature is more than twice the ambient temperature, the density factor changes very little and has an approximately constant value of 0.214. Substituting this parameter value and constant values $C_d = 0.68$, $\rho_a = 1.2 \text{ kg/m}^3$ into Eqn. 84 gives the well-known relationship for mass flow into an opening:

$$\dot{m}_a \cong 0.5 A_o \sqrt{H_o} \quad \text{Eqn. 87}$$

Another method to calculate the airflow rate into the compartment is from the estimated neutral plane height, h_l , using the integral ratio method (He et al., 1998).

The neutral plane heights calculated based on this method are included in Appendix H, where the following correlation is used for the mass flow rate into the opening:

$$\dot{m}_a = \frac{2}{3} A_o \sqrt{H_o} C_d \rho_a \sqrt{2g \left(1 - \frac{T_a}{T_g}\right)} (h_l)^3 \quad \text{Eqn. 88}$$

In Eqn. 88, T_g becomes the average temperature above the neutral plane height at the opening. The temperature measurements at the opening are included in Appendix I.

Appendix D: Heat release rates and flame heights

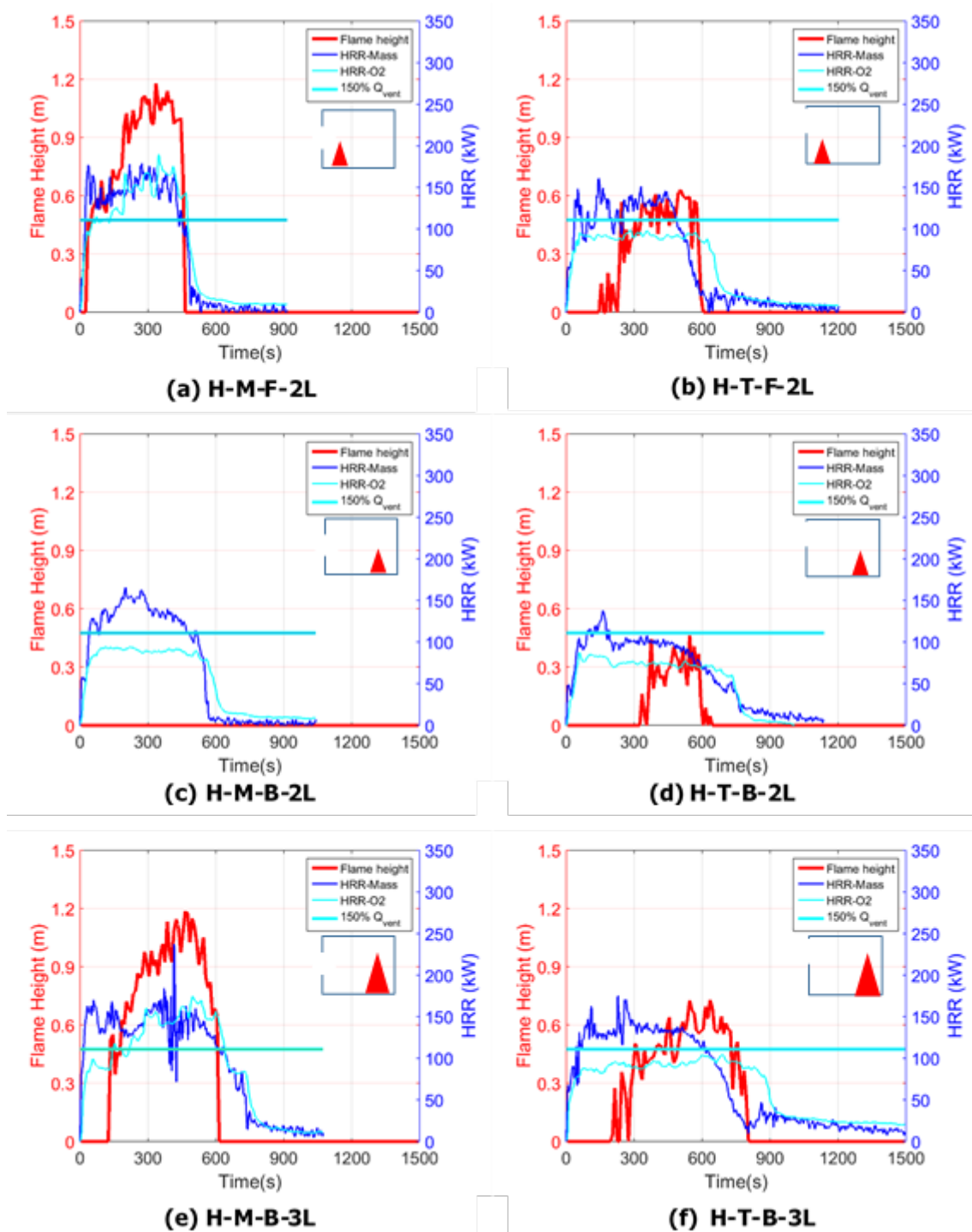


Figure 79. Heat release rates and flame heights for heptane fires with the standard 300 mm x 300 mm opening.

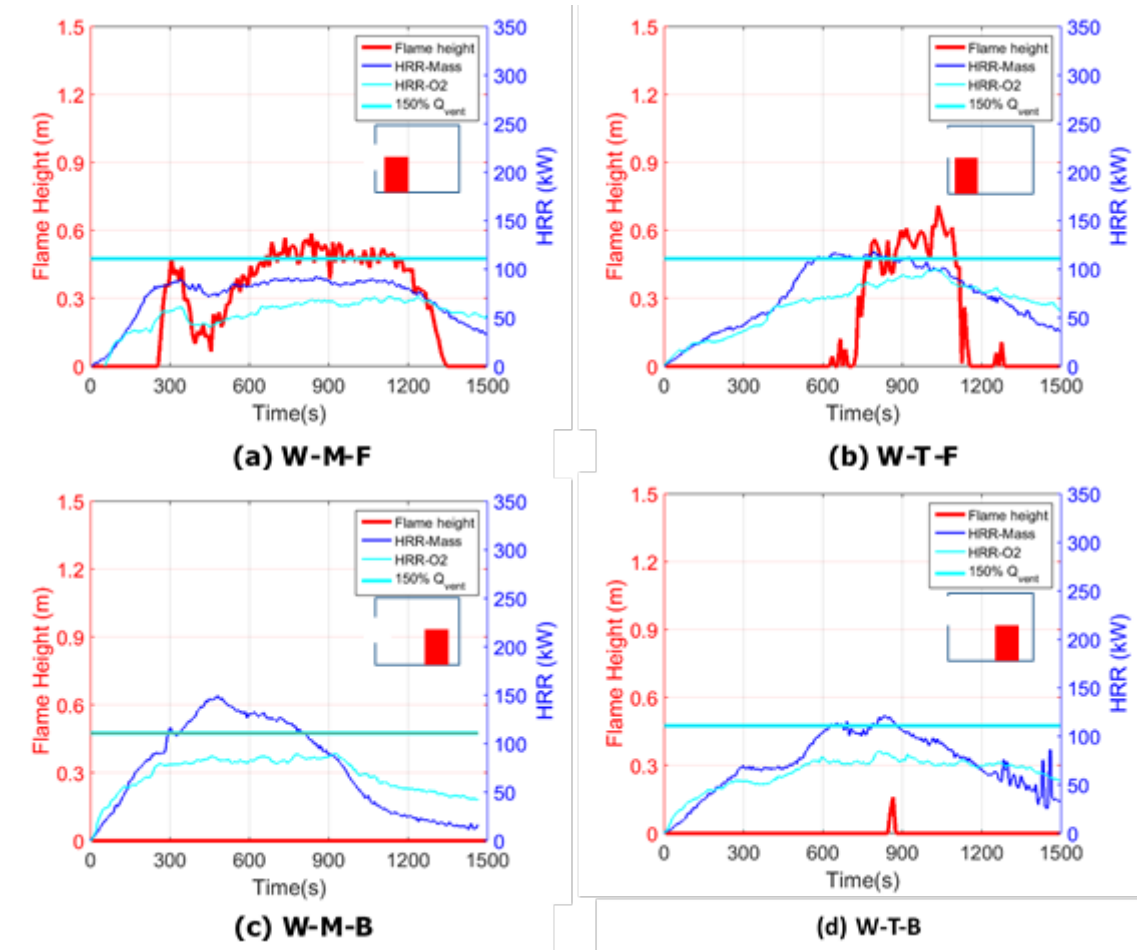


Figure 80. Heat release rates and flame heights for wood crib fires.

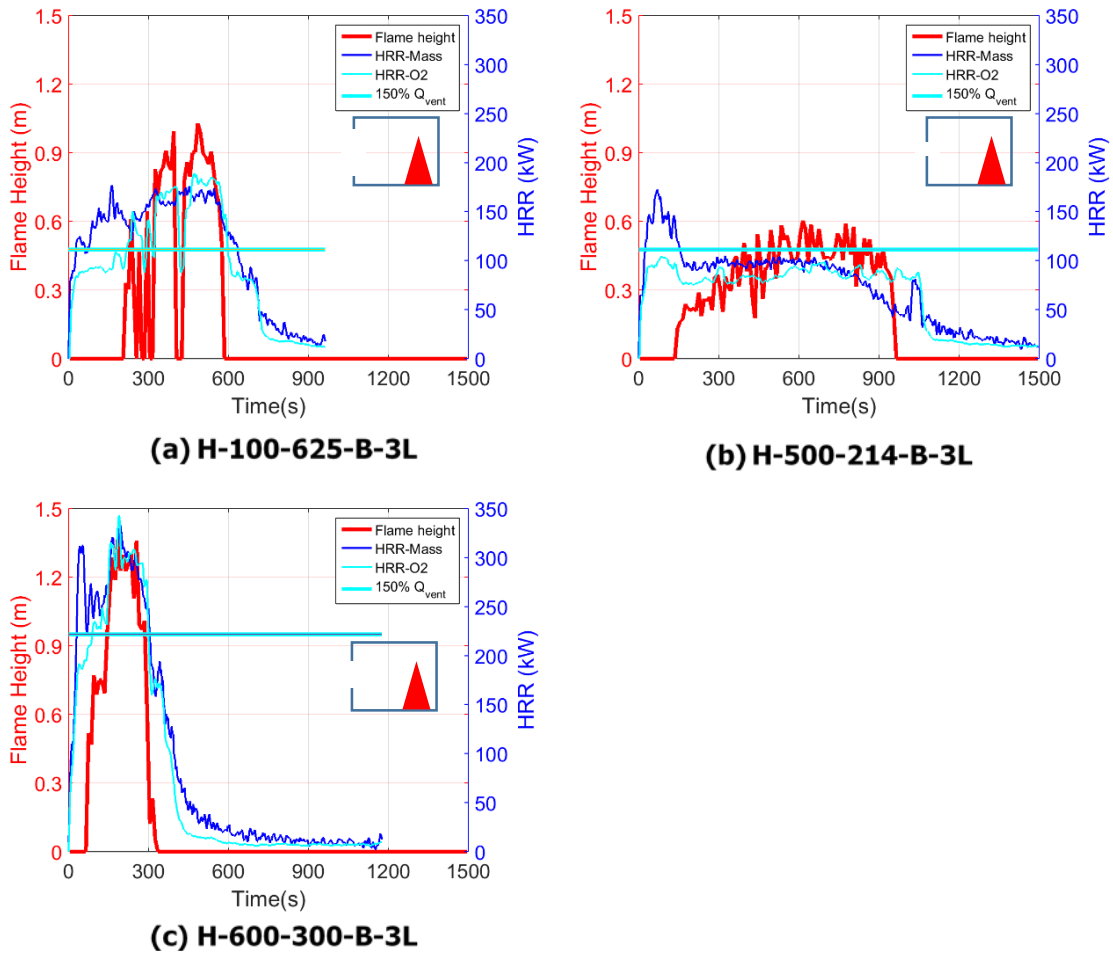


Figure 81. Heat release rates and flame heights for heptane fires with non-standard opening sizes.

Appendix E: External wall heat flux

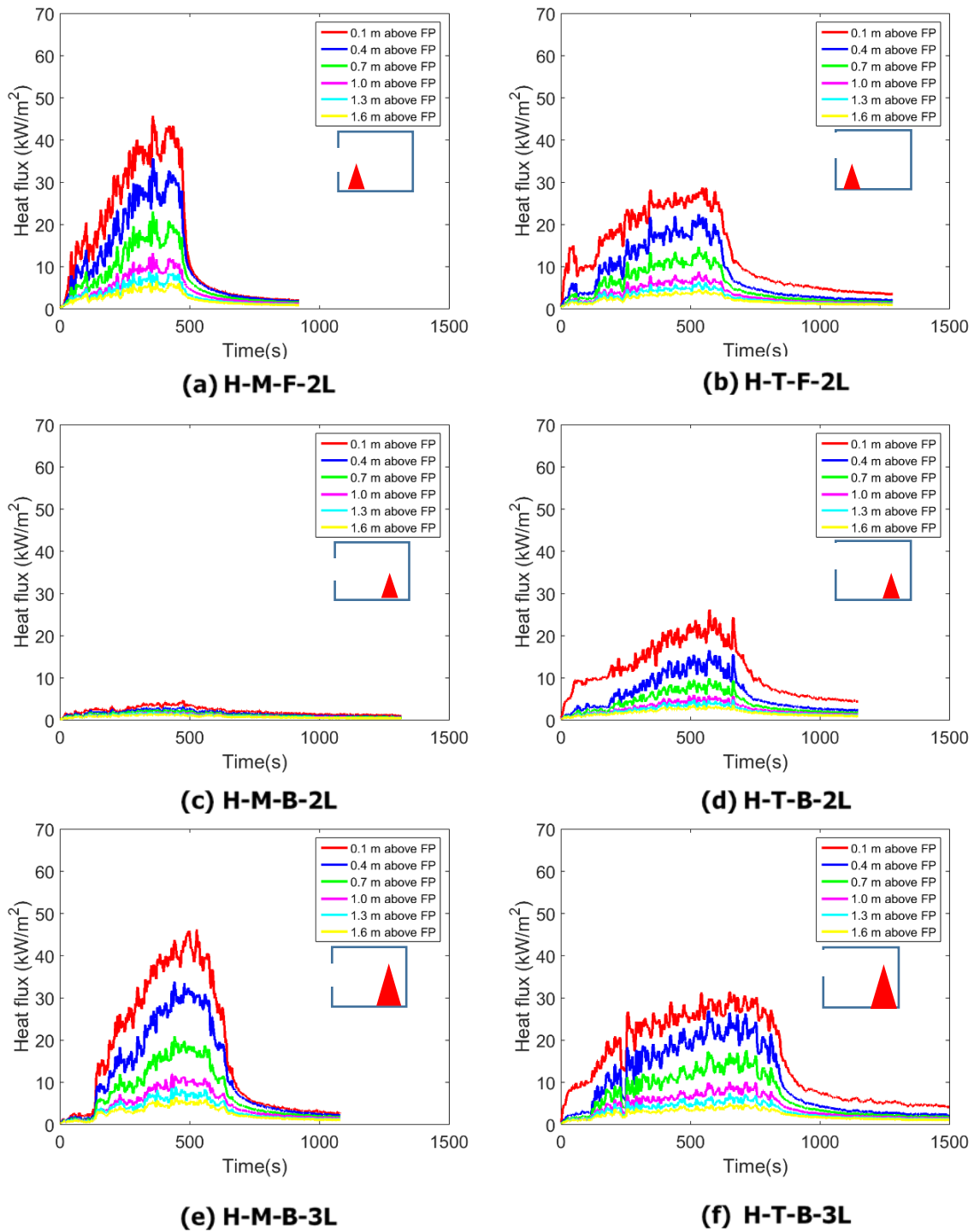


Figure 82. External wall heat flux for heptane fires with the standard 300 mm x 300 mm opening.

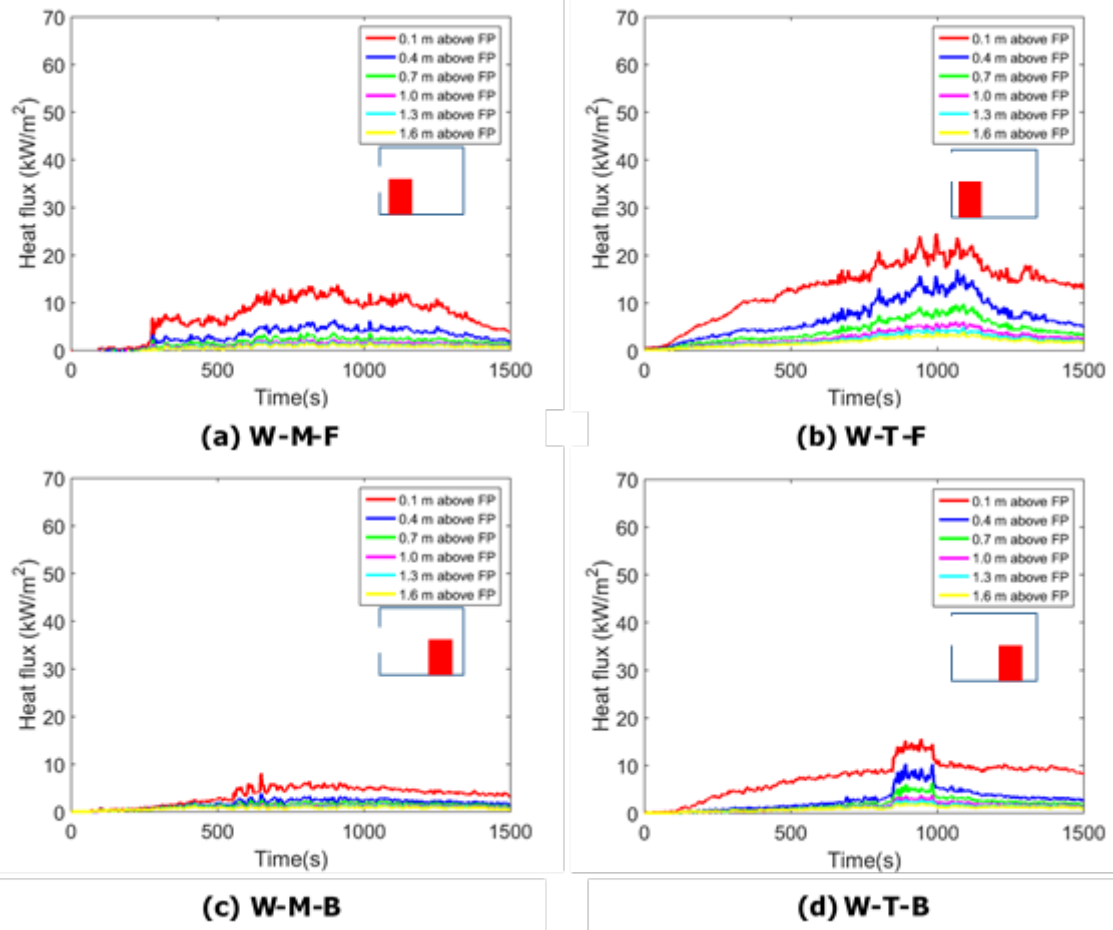


Figure 83. External heat flux for wood crib fires.

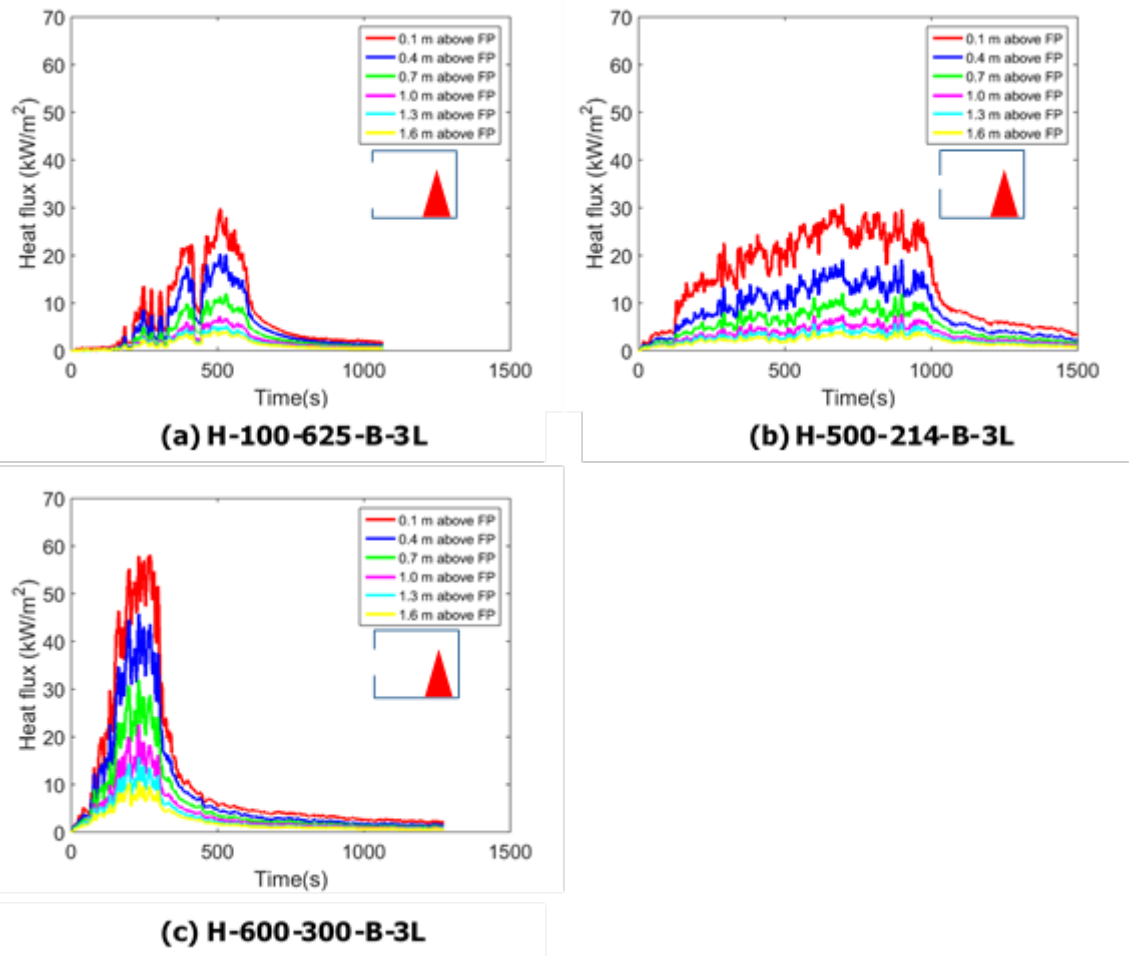


Figure 84. External heat flux for heptane fires with non-standard opening sizes.

Appendix F: Compartment temperatures

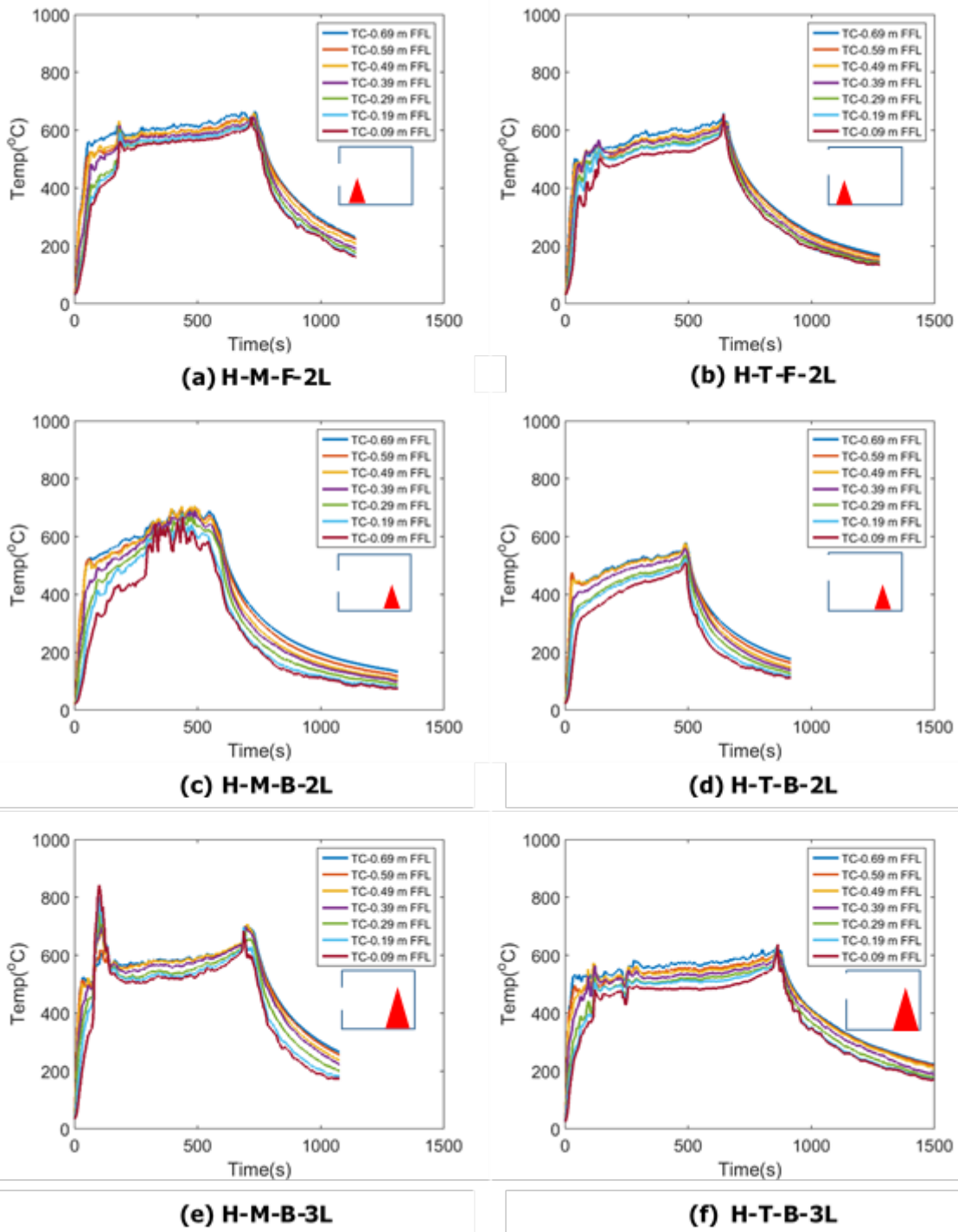


Figure 85. Front compartment temperatures for heptane fires with the standard 300 mm x 300 mm opening.

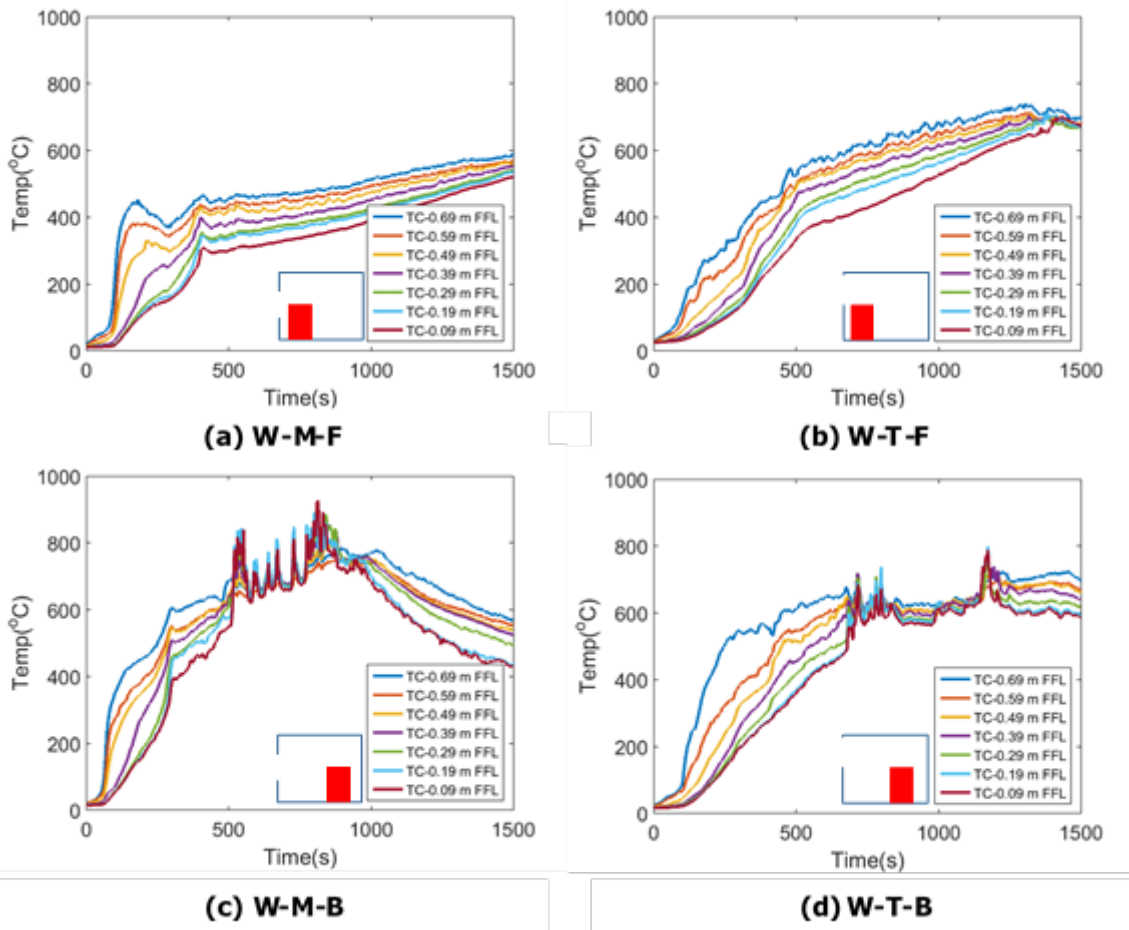


Figure 86. Front compartment temperatures for wood crib fires.

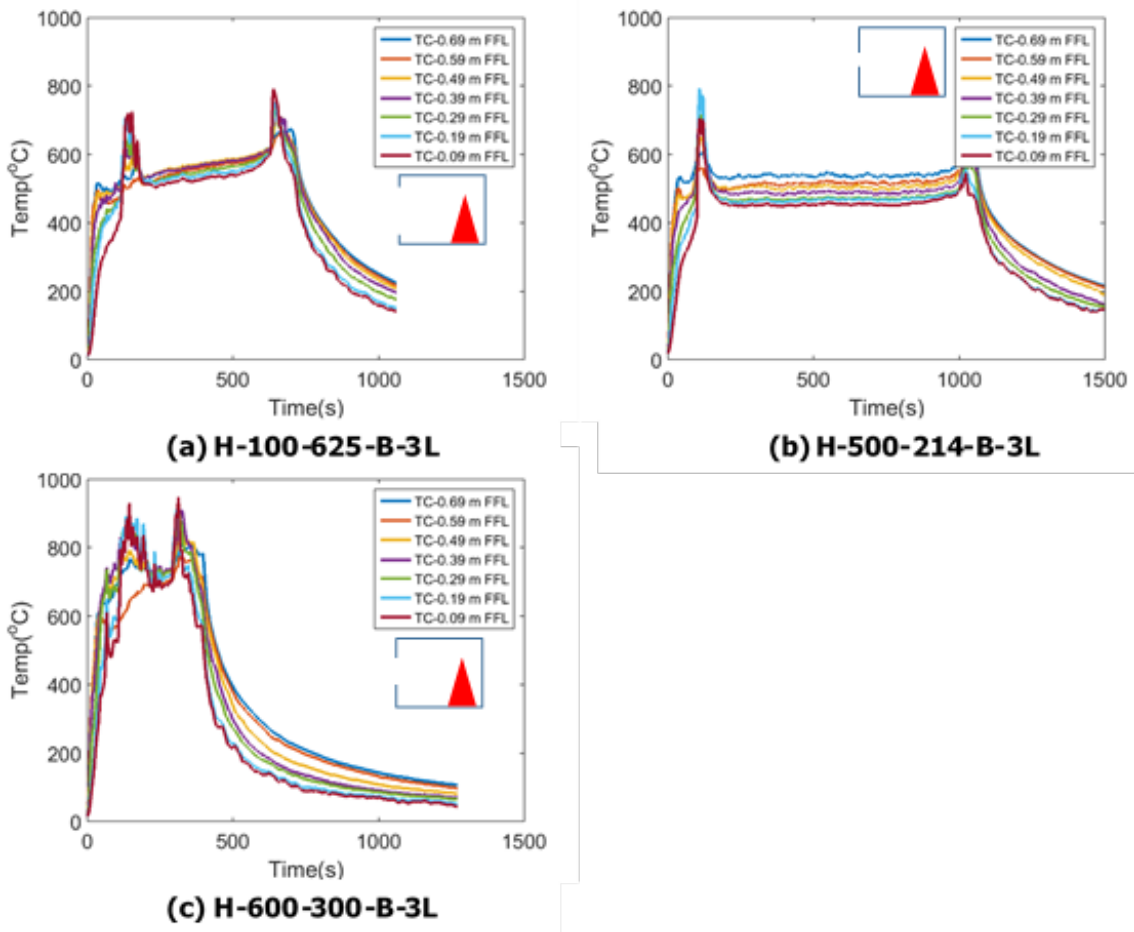


Figure 87. Front compartment temperatures for heptane fires with non-standard opening sizes.

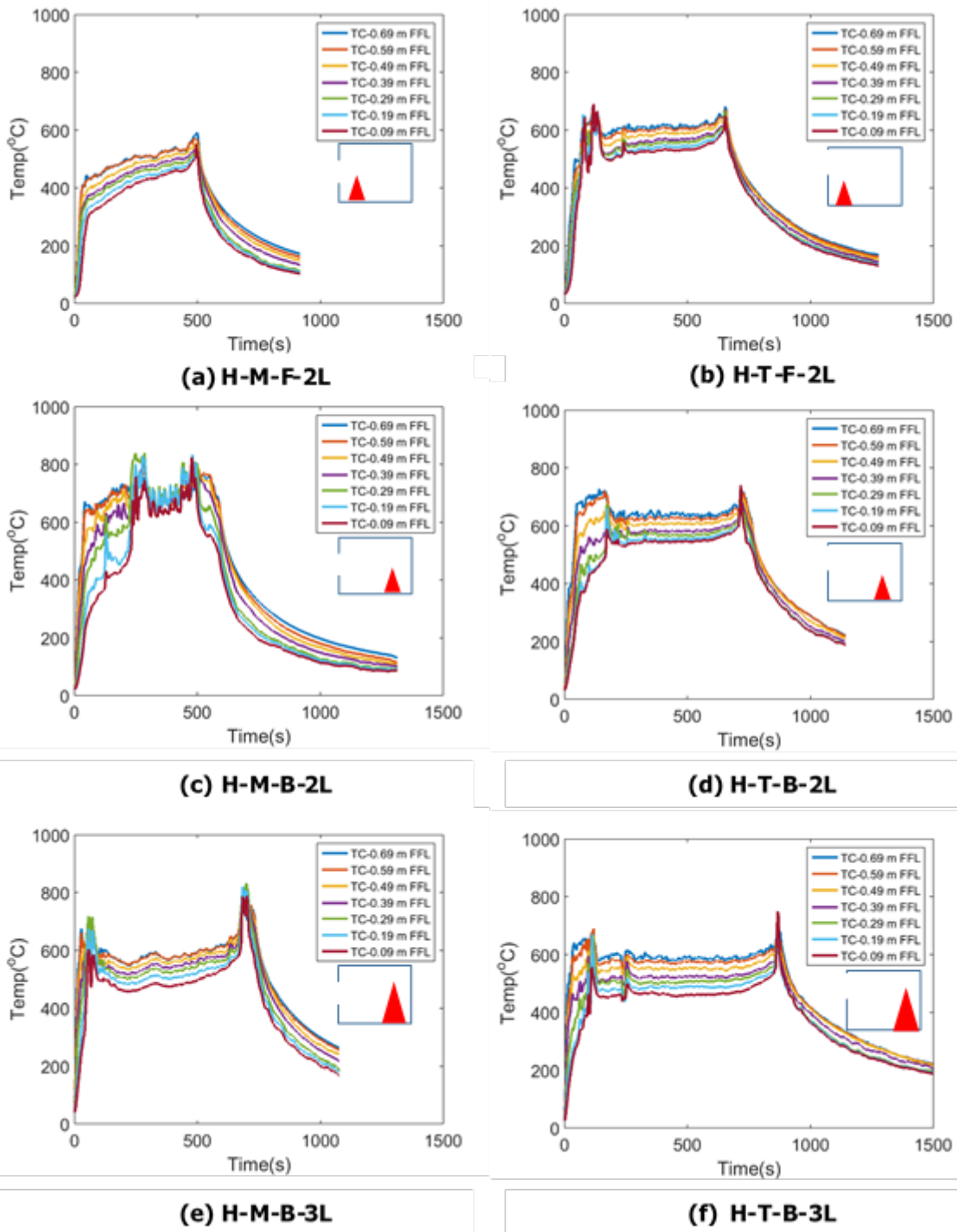


Figure 88. Rear compartment temperatures for heptane fires with the standard 300 mm x 300 mm opening.

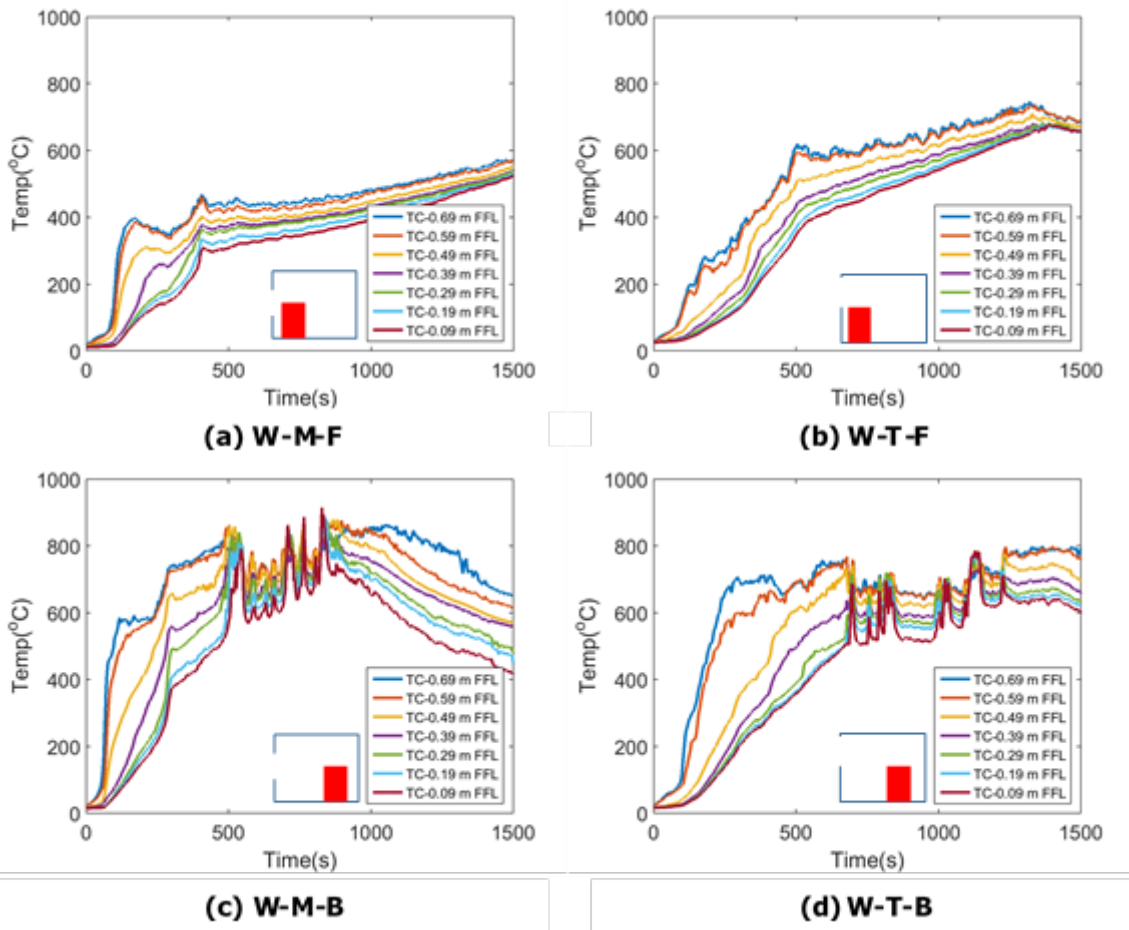


Figure 89. Rear compartment temperatures for wood crib fires.

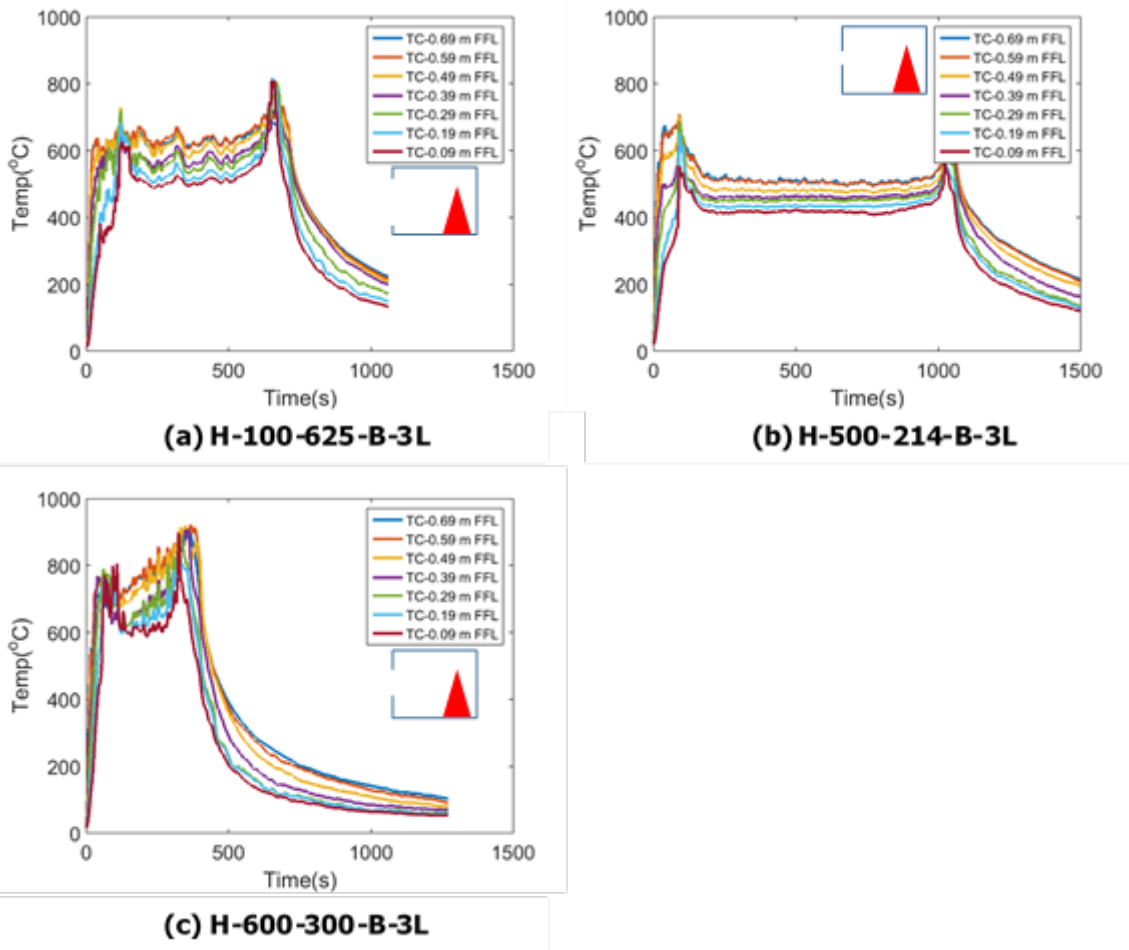


Figure 90. Rear compartment temperatures for heptane fires with non-standard opening sizes.

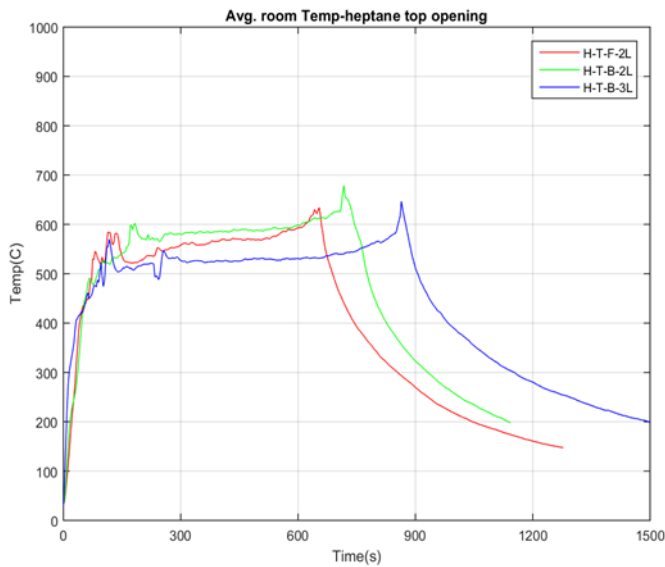


Figure 91. Average room temperature with the top opening.

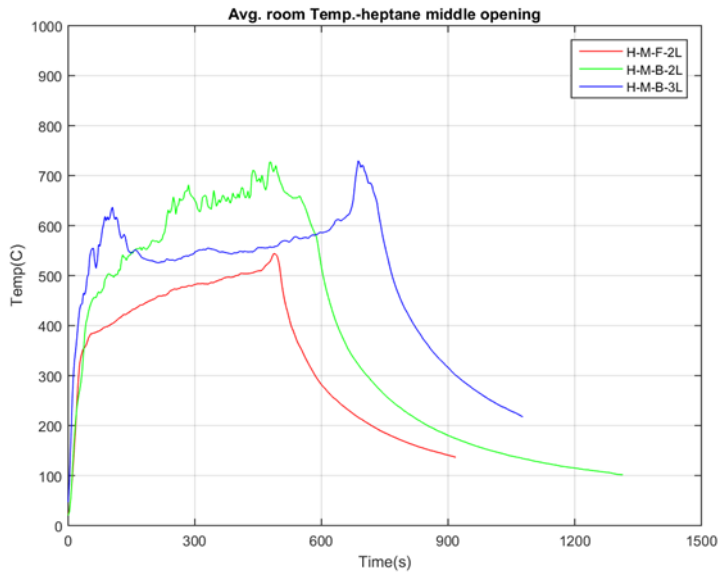


Figure 92. Average room temperature with the middle opening (heptane fires).

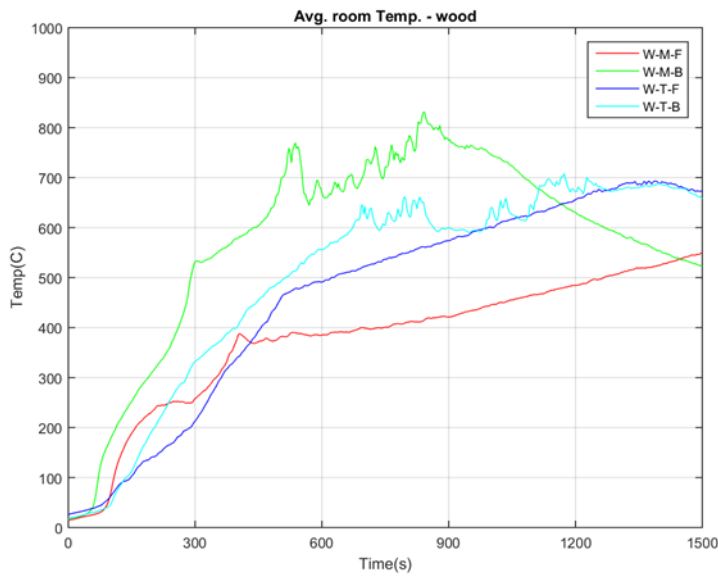


Figure 93. Average room temperature with the middle opening (wood crib fires).

Appendix G: Compartment heat flux

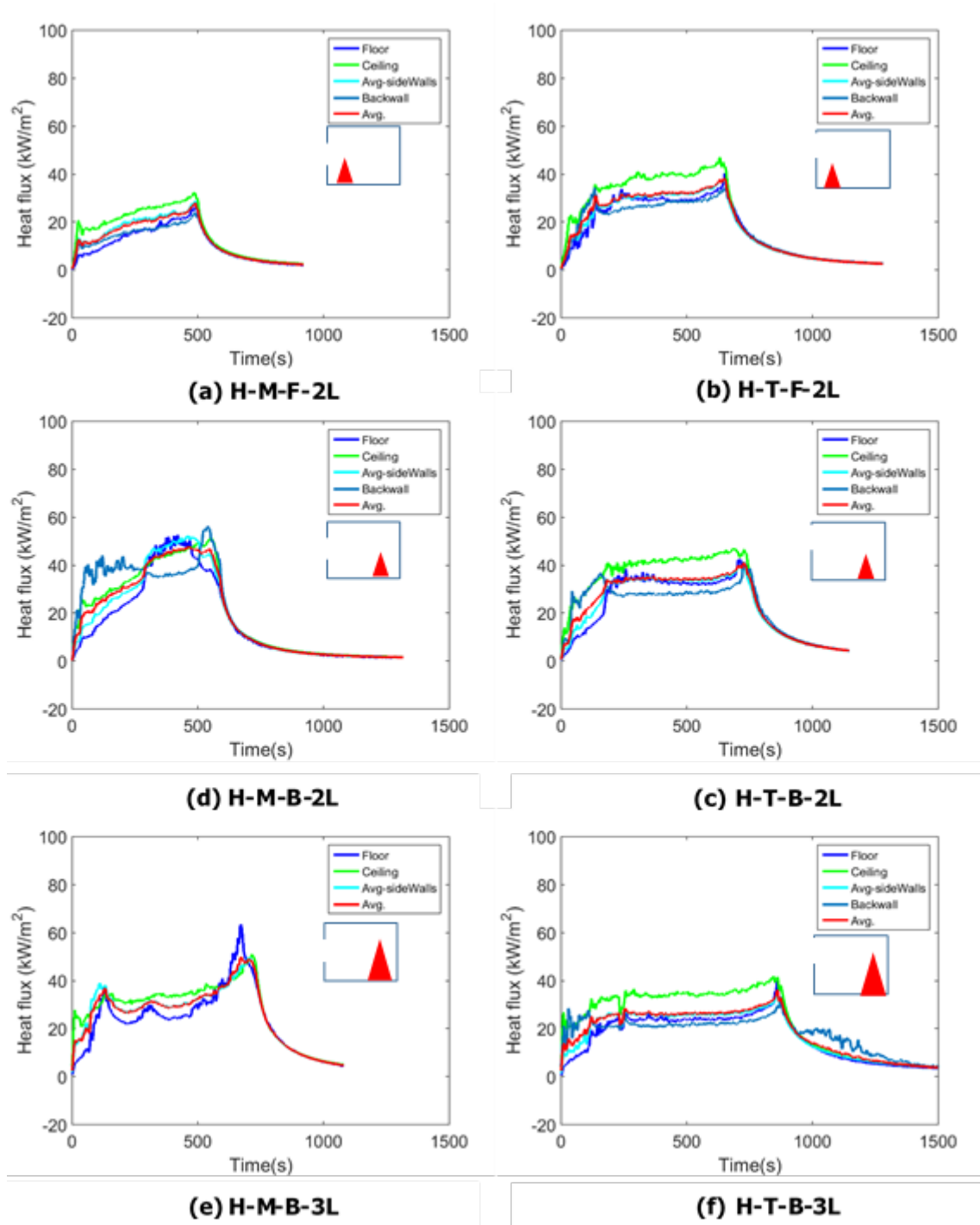


Figure 94. Compartment heat flux for heptane fires with the standard 300 mm x 300 mm opening.

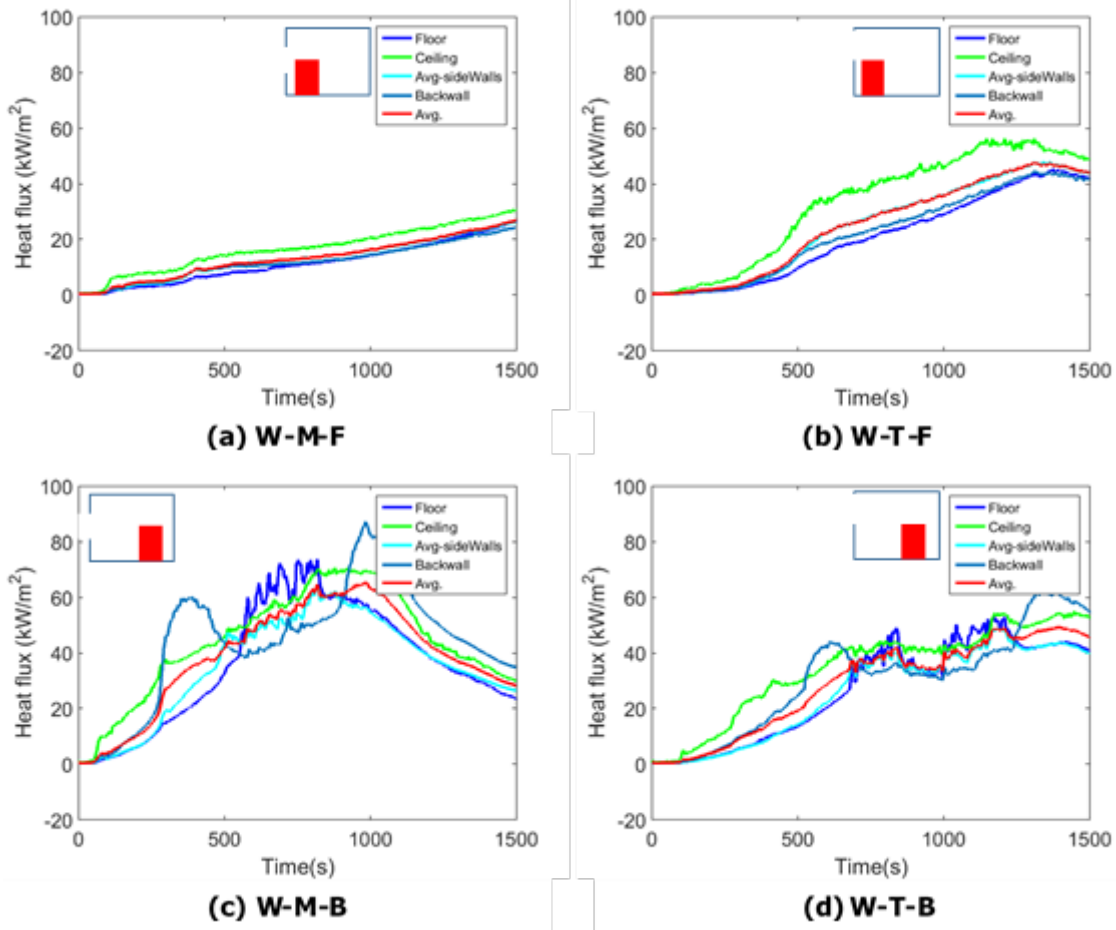


Figure 95. Compartment heat flux for wood crib fires.

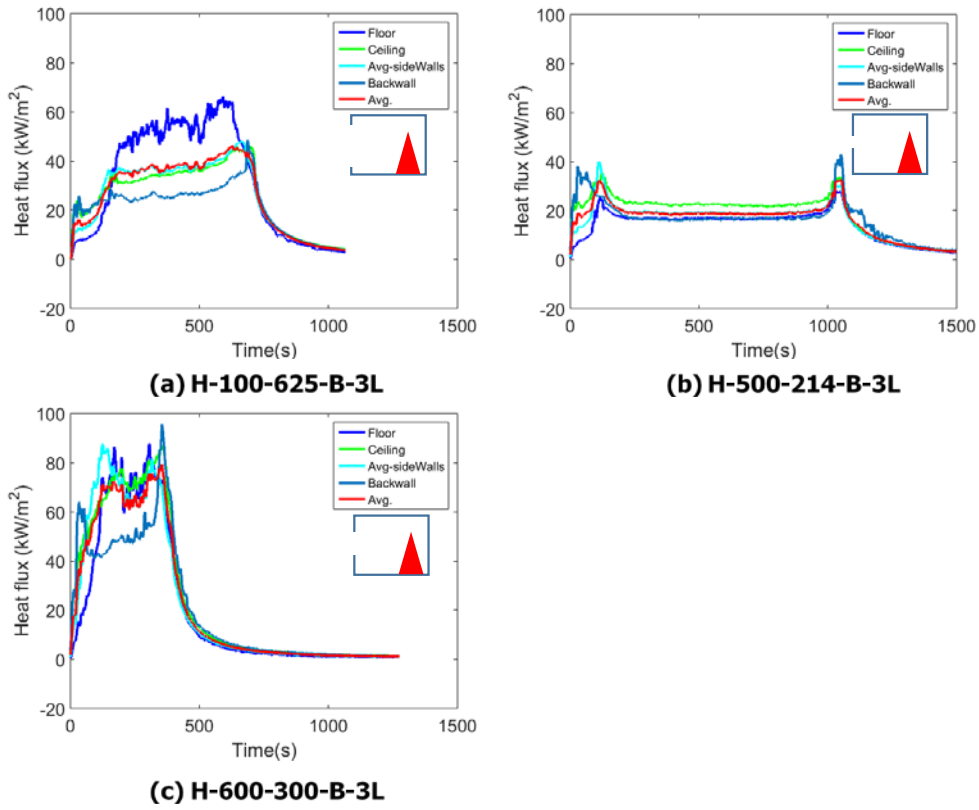


Figure 96. Compartment heat flux for heptane fires with non-standard opening sizes.

Appendix H: Neutral plane heights

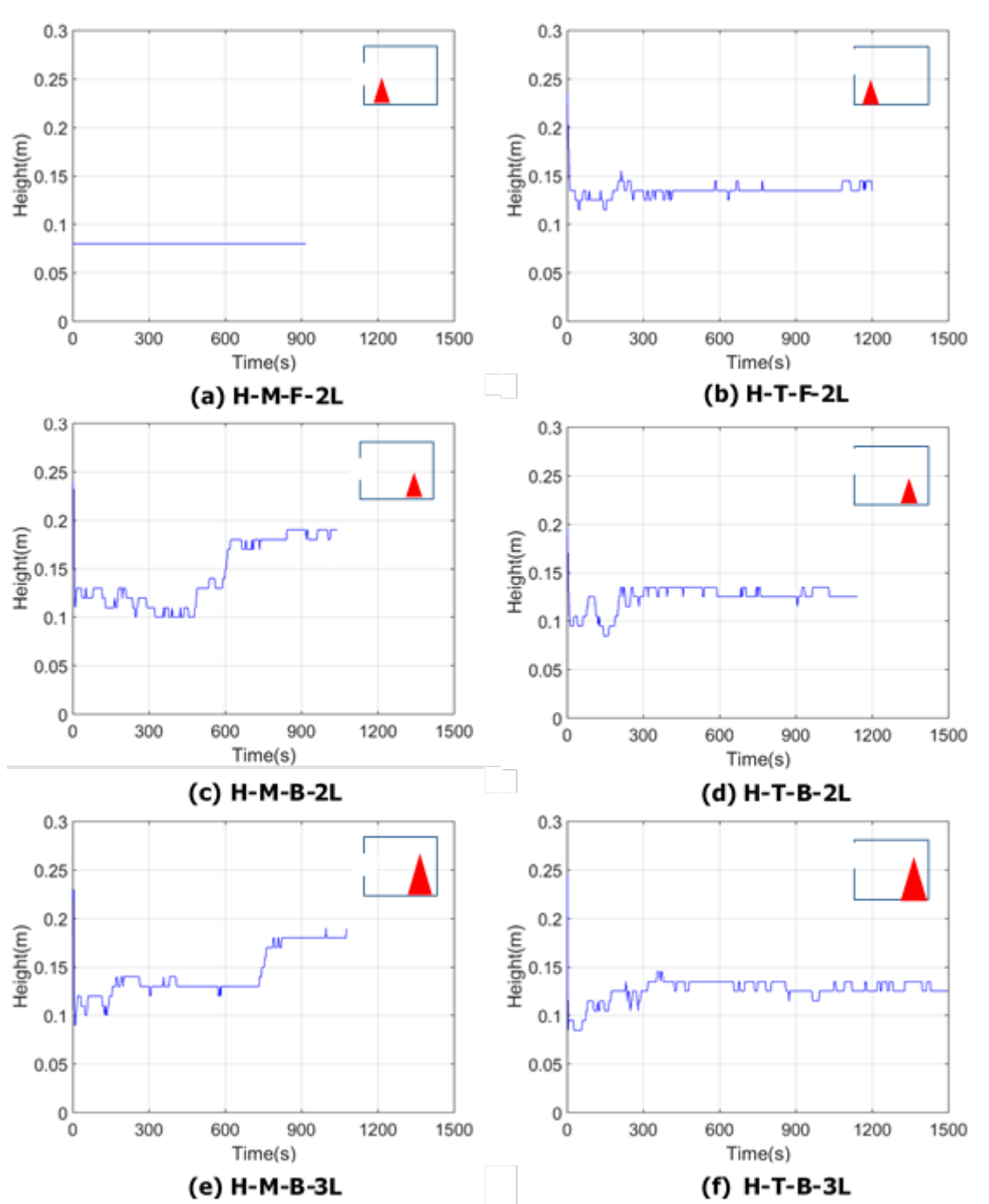


Figure 97. Neutral plane heights for heptane fires with the standard 300 mm x 300 mm opening.

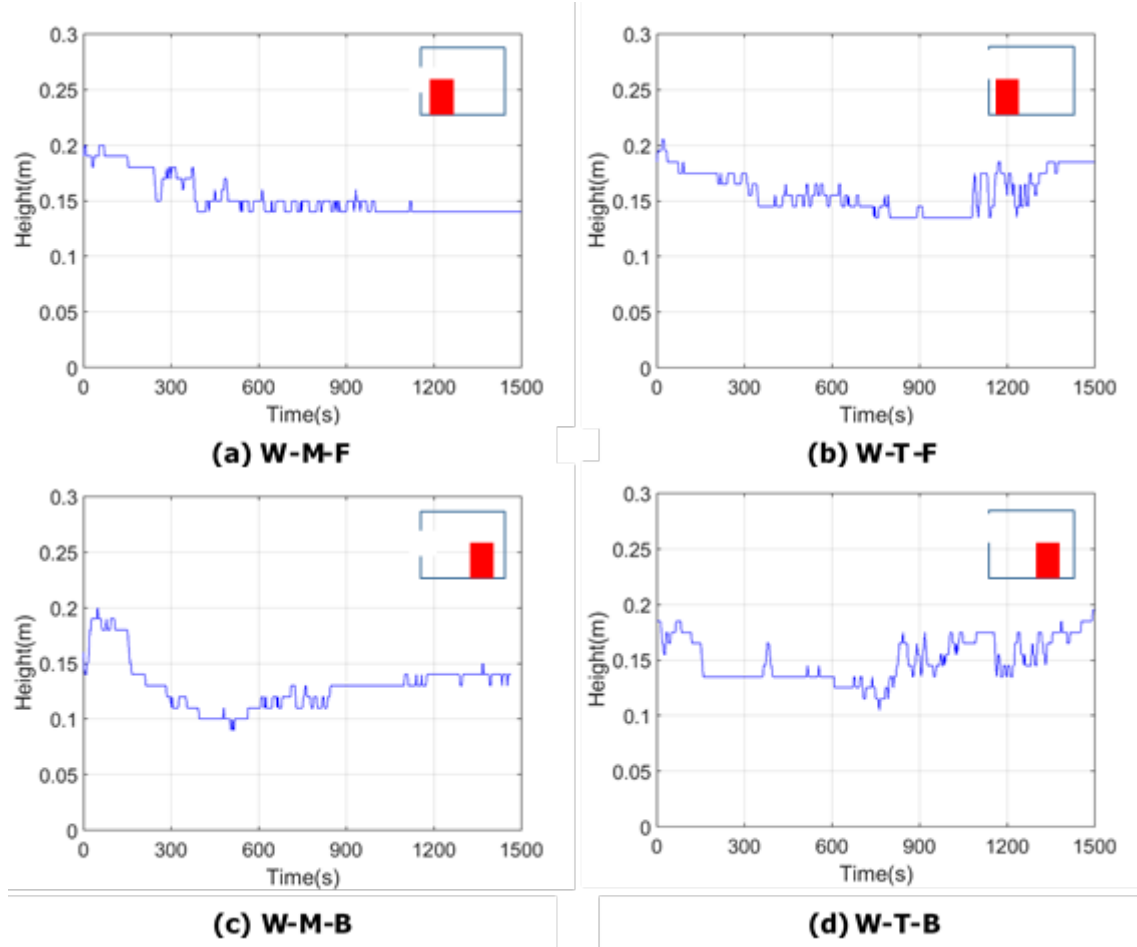
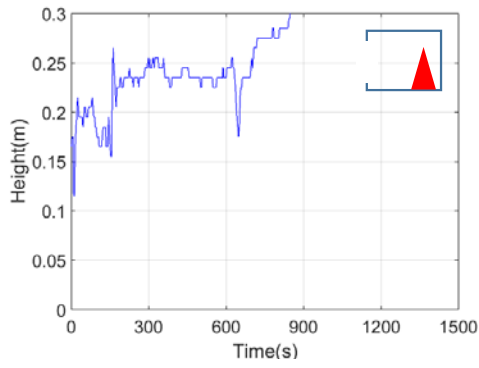
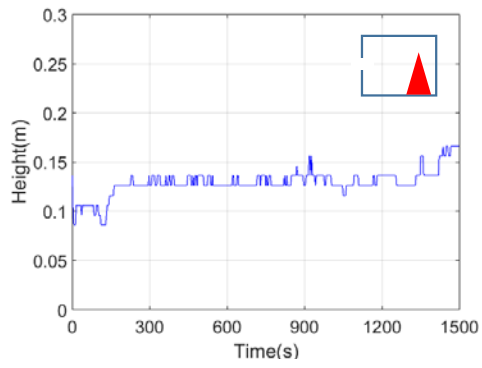


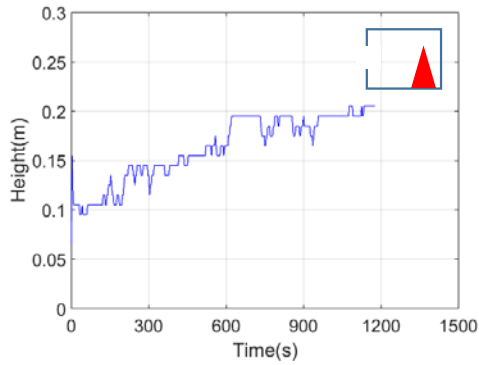
Figure 98. Neutral plane heights for wood crib fires.



(a) H-100-625-B-3L



(b) H-500-214-B-3L



(c) H-600-300-B-3L

Figure 99. Neutral plane heights for heptane fires with non-standard opening sizes.

Appendix I: Temperatures at the opening

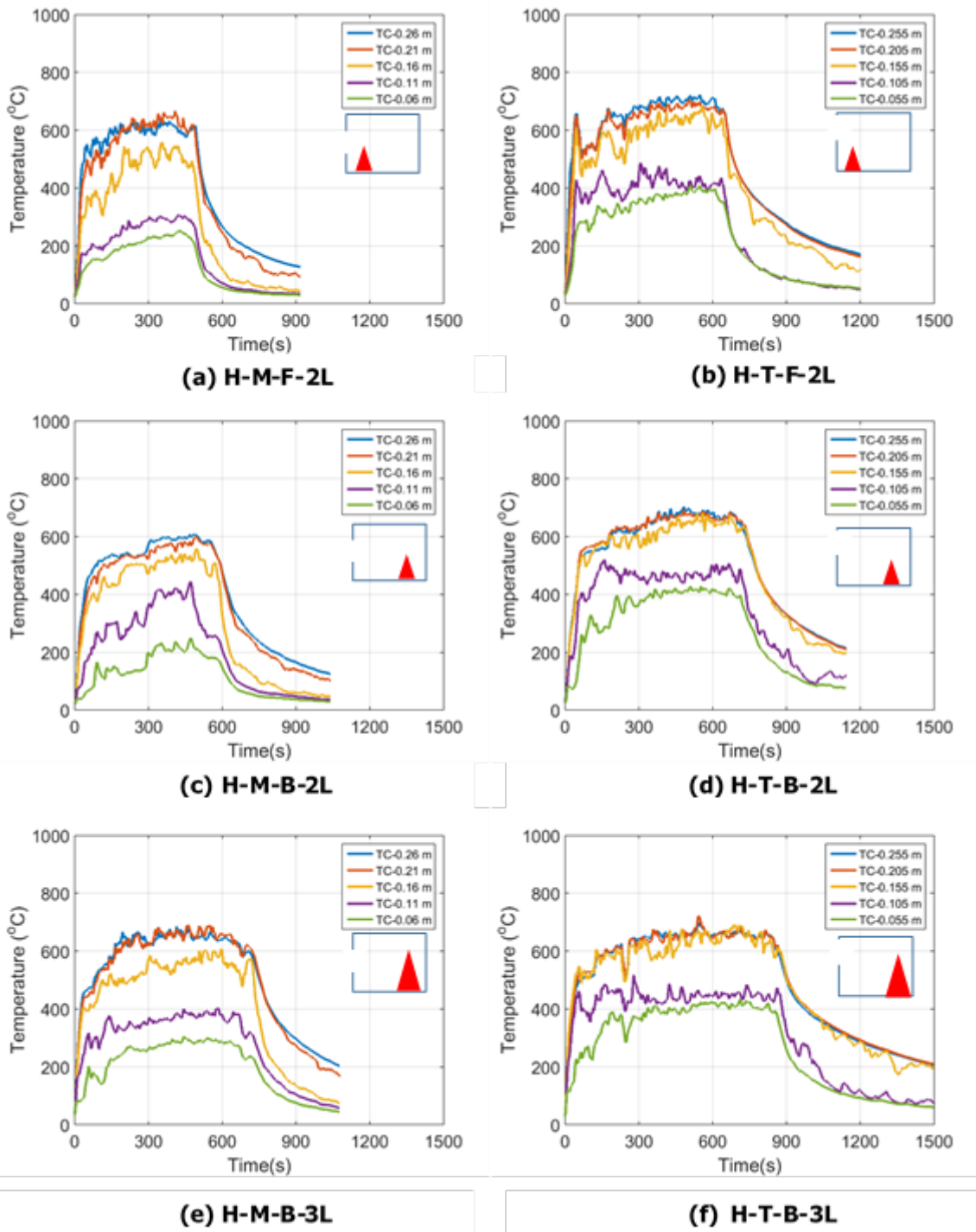


Figure 100. Opening temperatures for heptane fires with the standard 300 mm x 300 mm opening.

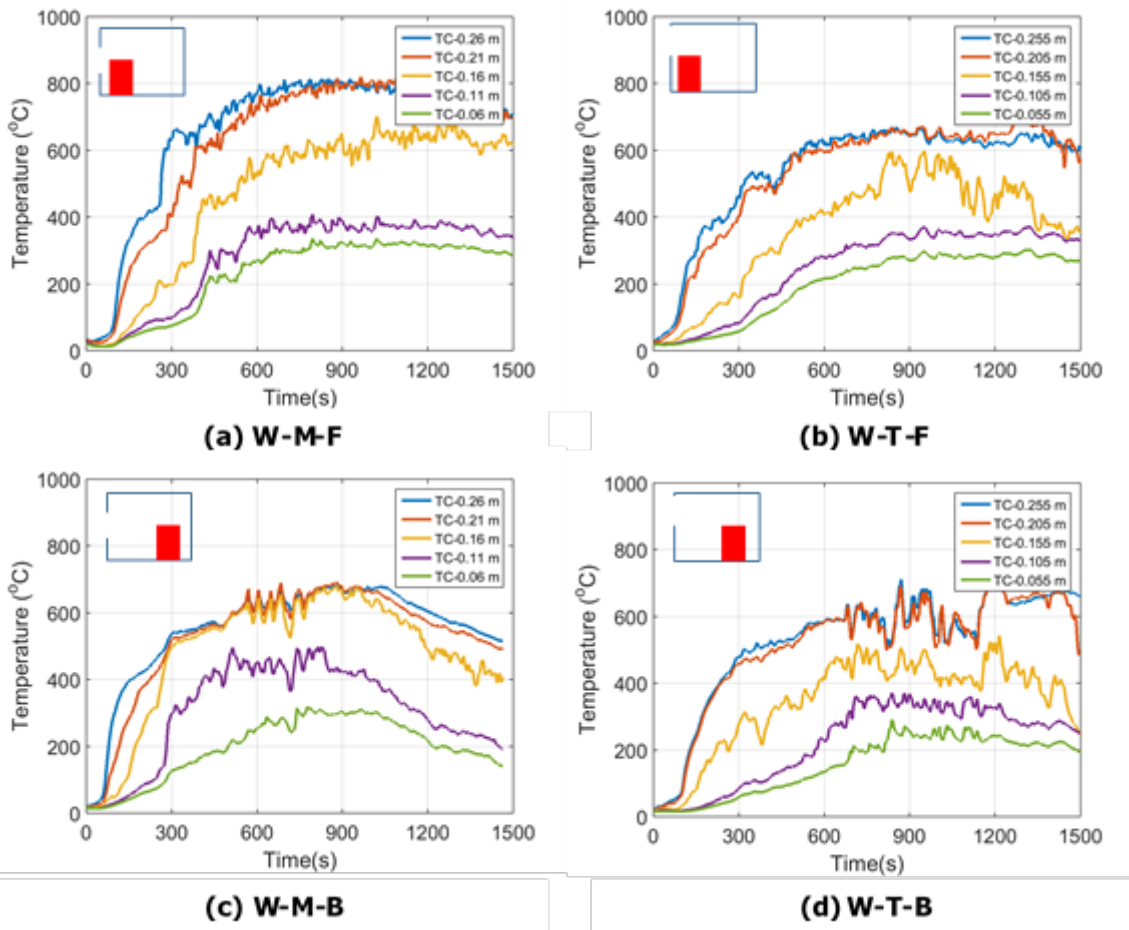
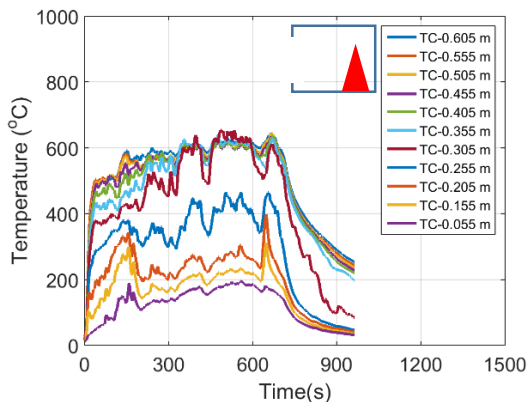
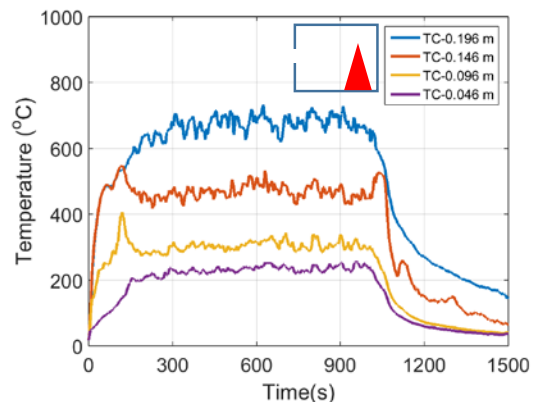


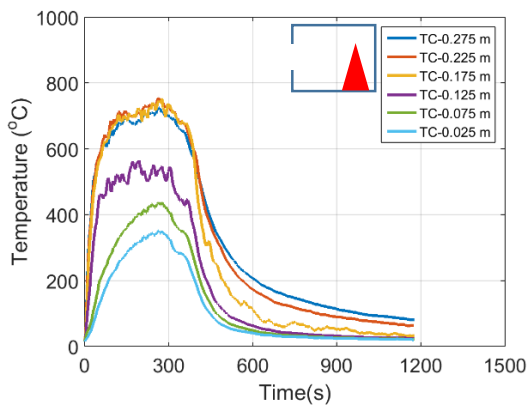
Figure 101. Opening temperatures for wood crib fires.



(a) H-100-625-B-3L



(b) H-500-214-B-3L



(c) H-600-300-B-3L

Figure 102. Opening temperatures for heptane fires with non-standard opening sizes.

Appendix J: Flame height estimation

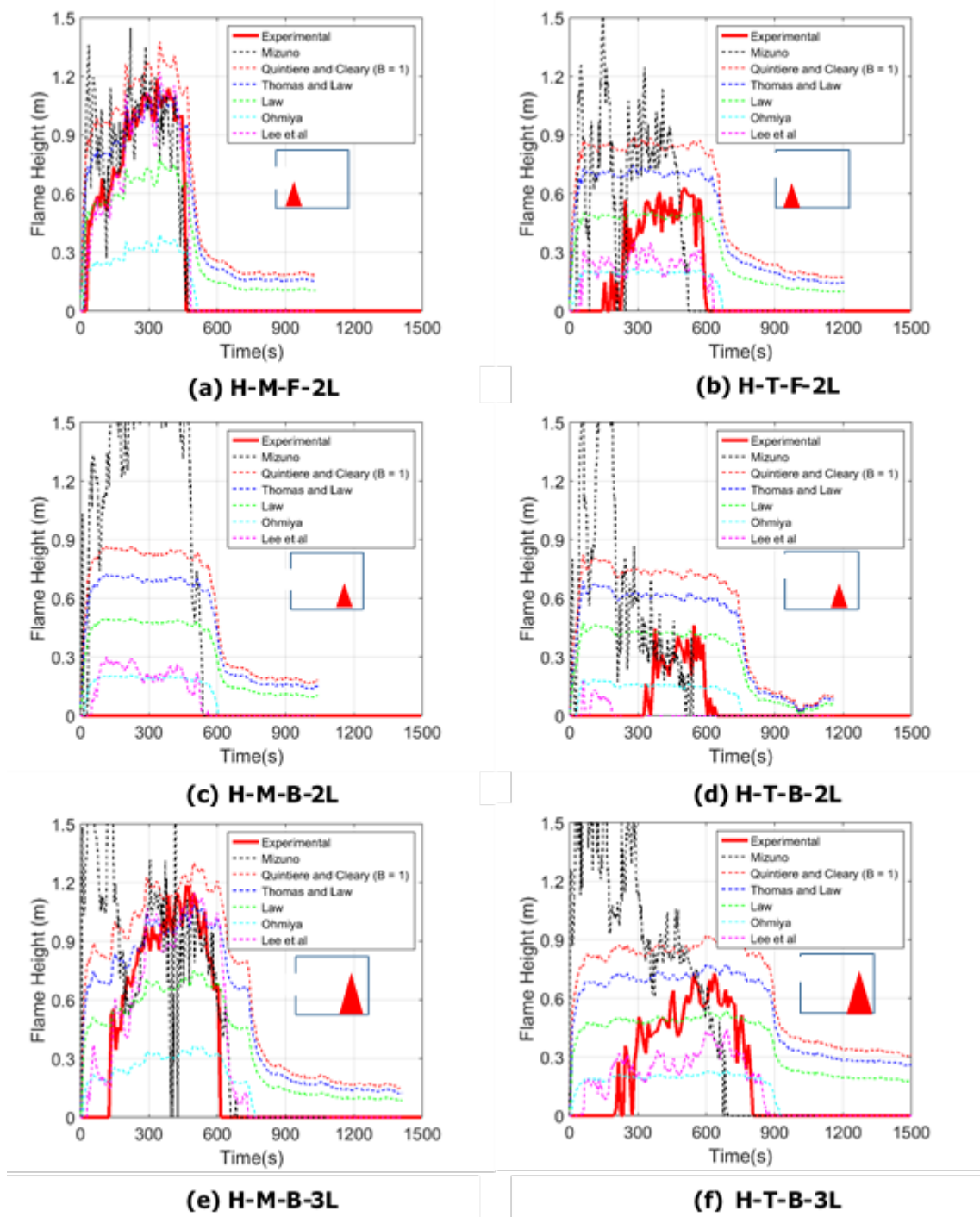


Figure 103. Flame height estimation (heptane).

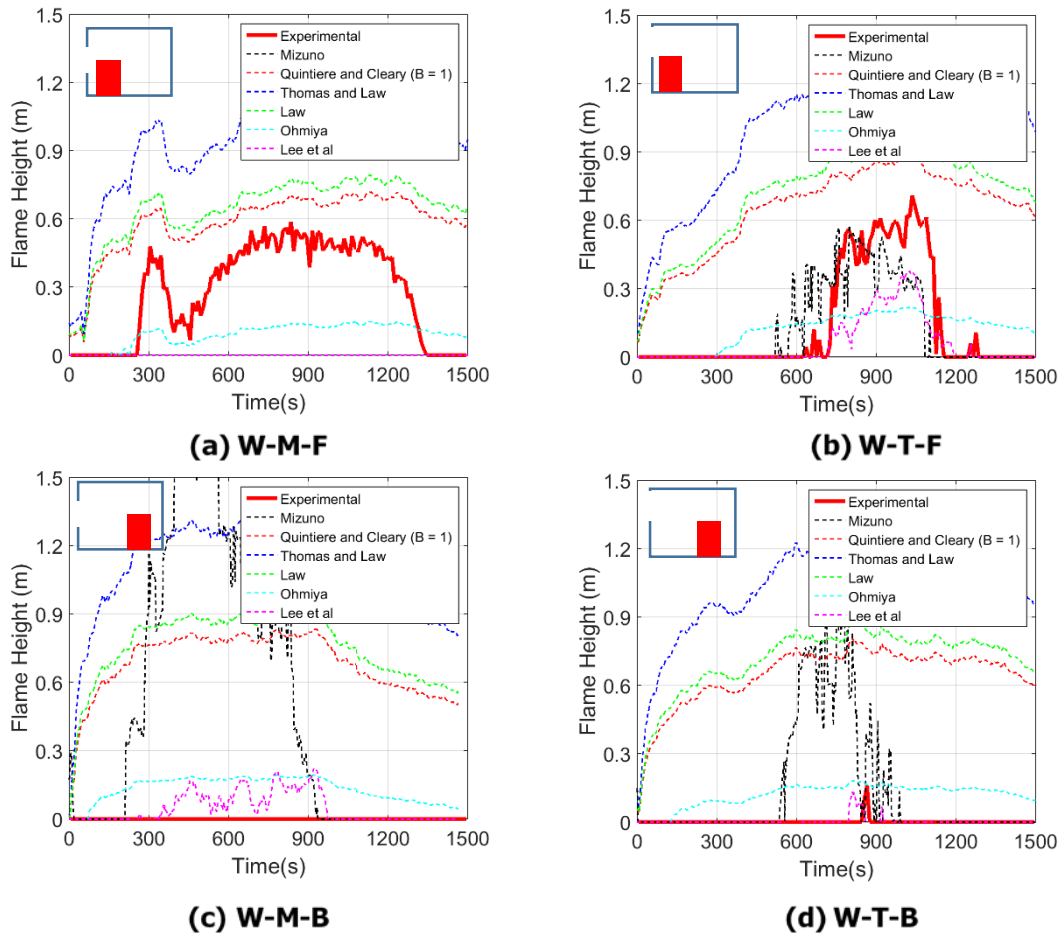
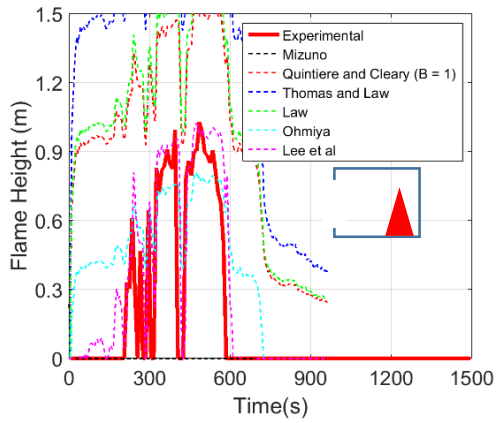
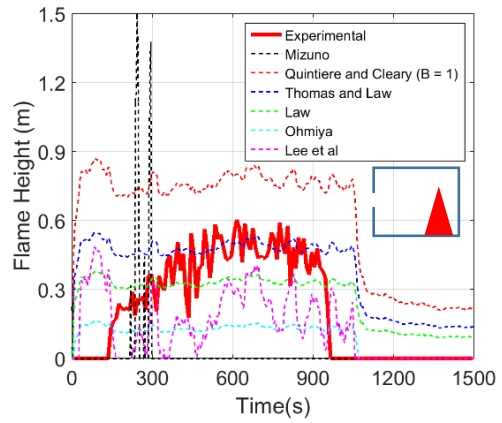


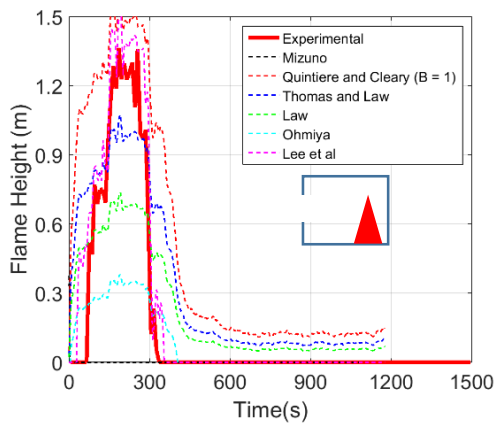
Figure 104. Flame height estimation (wood crib).



(a) H-100-625-B-3L



(b) H-500-214-B-3L



(c) H-600-300-B-3L

Figure 105. Flame height estimation for heptane fires with non-standard opening sizes.